NASA Contractor Report 179554

Analysis of Supersonic Plug Nozzle Flowfield and Heat Transfer

S.N.B. Murthy and W.H. Sheu
Purdue University
West Lafayette, Indiana

September 1988

Prepared for
Lewis Research Center
Under Grant NAG3-281

National Aeronautics and
Space Administration

PREFACE

The research was supported by the National Aeronautics and Space Administration, Lewis Research Center, under Grant No. NAG 3-281. The grant was initiated by Mr. David M. Straight and became the initial grant monitor. On his retirement, Dr. C. Spuckler became the grant monitor at NASA.

Dr. S.N.B. Murthy was the principal investigator on the project. He was assisted by Mr. (since Dr.) W.H. Sheu, Research Assistant in Mechanical Engineering. Dr. H.D. Thompson, whose work is referenced in the Report, was responsible for all of the computational effort related to gas dynamic interactions in the nozzle. Mr. (since Dr.) S.K. Hong carried out the heat transfer calculation in the film-cooled supersonic portion of the nozzle. In addition to the computational codes generated at Purdue University, a code was also obtained from the NASA Langley Research Center, and these were utilized in carrying out the project.

ABSTRACT

A number of problems pertaining to the flowfield in a plug nozzle, designed as a supersonic thruster nozzle, with provision for cooling the plug with a coolant stream admitted parallel to the plug wall surface, have been studied, based on experimental data generated at the NASA Lewis Research Center. First, an analysis has been performed of the inviscid, non-turbulent, gas dynamic interaction between the primary hot stream and the secondary coolant stream. A numerical prediction code for establishing the resulting flowfield with a dividing surface between the two streams, for various combinations of stagnation and static properties of the two streams, has been utilized for illustrating the nature of interactions. A number of illustrative cases have been worked out, for which test results have been available from the NASA Lewis Research Center data sets. The code, while not described here in detail, has been made available to the NASA Lewis Research Center for verification of its operability. Secondly, skin friction coefficient, heat transfer coefficient and heat flux to the plug wall have been analyzed under smooth-flow conditions (without shocks or separation) for various coolant flow conditions. A numerical code, obtained from NASA Langley Research Center, has been suitably modified and utilized for the determination of heat transfer parameters in a number of cases for which experimental data have been available in the NASA Lewis Research Center test results.

Thirdly and finally, an analysis has been initiated for modelling turbulence processes in transonic shock-boundary layer interaction without the appearance of flow separation. The model is based on a combination of the Reynolds stress balance equation coupled with dynamical equation for large eddy, and includes rapid distortion approximations. The model is suitable for use both under conditions of an adiabatic interaction as well as of heat transfer to the boundary wall, but in the presence of a single stream.

A discussion is presented on future possibilities for extension of each of the building block-type solutions, which in combination would be useful for the analysis of the flowfield in a plug nozzle and which can also serve individually to establish various types of interactions in wall-bounded multiple flows.

TABLE OF CONTENTS

SECTION 1

INTRODUCTION

A common method of generating thrust in aero-space propulsion systems is by the use of a nozzle for expanding high pressure gas. Such a nozzle, when it has a plug-like center body in it, is referred to as a plug nozzle. Figure 1.1 provides a schematic of such a nozzle. The "external" surface provided by the plug can be utilized as an effective additional means, along with the nozzle outer wall, for obtaining the desired gas expansion and hence thrust modulation. The geometry of the nozzle may be conical, axisymmetric or three-dimensional, and the plug shape is chosen in relation to that geometry. An extensive investigation on the flowfield of a plug nozzle and various means of cooling the nozzle wall and the plug has been undertaken at the NASA Lewis Research Center (References 1-8).

The overall flowfield of a plug nozzle involves (a) gas expansion over subsonic, transonic and supersonic speeds, (b) wall boundary layers that may be laminar, transitional, turbulent or relaminarizing over different parts of the nozzle and (c) shockwaves and concentrated expansions that may be interacting in various ways both with one another and with the wall boundary layers. Heat transfer to the boundary walls and any internal means of cooling the walls affect the flowfield in a mutually interactive fashion. Considering such aero-thermal problems, the plug nozzle provides an excellent device for their study through relatively simple variations in geometry and flow variables. Other than some direct interest in plug nozzles, one of the main motivations for the investigations at the NASA Lewis Research Center has been a general study of the problem of cooling outer and plug walls in the presence of complex flowfields.

Various methods of cooling are available for use in thrustor nozzles (Reference 9). One of them consists in injecting a stream of relatively low temperature gas at the wall to form a protective film over a length of the wall, as illustrated in Figure 1.2. The coolant fluid may be inert or reactive. In the case of air-breathing engines, in view of the availability of high pressure air from the air compression subsystem, the coolant fluid may consist of bleed air.

It may be noted that cooling, as shown in Figure 1.2, also affects the thrust generated by the nozzle.

1.1. Specific Problems

The analysis of flowfield and heat transfer in a plug nozzle with a coolant film flow requires the use of three-dimensional, compressible, Navier-Stokes equations. In view of the possible presence of turbulence, the flow variables in the Navier-Stokes equations are commonly decomposed and averaged according to Reynolds. Distinguishing the coolant flow from the primary nozzle stream, the flow interaction between the two streams needs to be taken into account.

Rather than considering such an approach to the problem of determining the flowfield and heat transfer, the analysis can be divided into a number of specific problems, each concerned with a particular aero-thermal process. This has not only the advantage of providing clarity for the process but also of yielding a predictive procedure, that can be useful in practice, for each of the flow and heat transfer processes. In the current analysis, three specific problems are identified as follows.

(1) Gas dynamic interaction between the coolant and the primary

stream of the nozzle under the assumption of inviscid, non-turbulent flows;

(2) Heat transfer and viscous losses at the wall surface in the presence of the coolant film while accounting for turbulence; and

(3) Interactions involving shockwaves, expansion regions, boundary layers and film flow, again accounting for turbulence.

The foregoing are in the nature of "building block" type of problems, the analysis of each of which provides an understanding of various aspects of the overall problem. However, some further clarification is required regarding problems (2) and (3). In problem (2), it is assumed that the flow involves no discontinuities. In problem (3), a specific interaction process is examined as an event in itself. In fact, the only interaction process that is examined in detail is a transonic shock-boundary layer interaction. Other types of interactions are referred to only in passing.

1.2. NASA Data

Throughout the discussion, experimental data provided by NASA Lewis Research Center, referred to hereafter as NASA Data, are utilized in various contexts. The data have been generated on the configuration of plug nozzle illustrated in Figure 1.2. Table 1 provides a partial listing of test conditions and data acquired. Details are provided in Appendix IV, wherein, again, only a part of all of the available data have been presented.

TABLE 1
LIST OF SELECTED TEST CONDITIONS

Nozzle pressure ratio, P_{T2}/P_0	Afterburner off		Afterburner on		
	Average hot gas total temperature, $\overline{T_7}$, °R				
	1180 Large primary	1750 Small primary	2500 Large primary	3000 Large primary	3400 Large primary
1.8	X	X	X		
2.0	X	X	X		
2.5		X	X	X	
3.0	X	X	X	X	X
3.5		X	X	X	
4.0	X	X	X	X	
4.5	X	X	X	X	X
5.0	X	X	X	X	
6.0		X	X	X	
8.0	X	X	X	X	X
10.0		X	X		
	Range of coolant flow rates, percent of W_G				
	0 to 1	0 to 5	¼ to 2	1 to 3½	2 to 5
	Engine inlet airflow, W_A, lb/sec				
	28 to 41	20 to 41	21	21	21

X represents conditions where data were obtained.

1.3. Outline of Report

Sections 2, 3 and 4 deal with the three problems discussed in Section 1.1. A summary discussion is included in Section 5.

SECTION 2

GAS DYNAMIC INTERACTIONS

Referring to Figure 2.1, the interaction between the primary and the coolant (which is also referred to as the secondary) streams may, in general, involve the following:

(1) Gas dynamic interaction, meaning nonreactive, inviscid, non-turbulent interaction;

(2) Mixing between the two streams accounting for entrainment and diffusion; and

(3) Interaction in the vicinity of the tip of the dividing wall between the two streams, when the tip is of finite thickness.

As stated earlier, it is the objective to examine (1) in the absence of (2) and (3). When mixing is neglected, one can postulate a continuous interface between the two streams each of which satisfies conservation of mass, momentum and energy separately. In neglecting (3), it is assumed that the tip of the dividing plate between the two streams is of negligible thickness. Hence, no "base" type region is formed in the vicinity of the tip, and a single, stable, continuous interface can be postulated to exist starting from the tip. Based on these assumptions, the flowfield being considered may be illustrated as in Figure 2.2. The only interaction between the two streams, then, is due to the differences in chemical composition, pressure, velocity and Mach number between the two streams.

2.1. The Coolant or the Secondary Stream

The coolant or the secondary stream may, under different conditions, be subsonic, choked or supersonic at the plane of its entry into the nozzle. The nature of the flow depends upon the geometry of the secondary flow ducting and the ratio of static pressure of the primary stream and stagnation pressure of the secondary stream at the location of secondary stream entry into the nozzle.

The coolant or the secondary stream is characterized by the mass flux, and the distributions of composition, stagnation pressure and temperature, and Mach number at the plane of entry into the nozzle. In practice, composition and stagnation pressure and temperature can be expected to be uniform across the narrow stream. It may often be adequate to assume that the Mach number is also uniform over the thin cross-section of the stream.

Noting that coolant or the secondary stream maintains its identity under nonmixing conditions, it can be expected to undergo changes in Mach number along the flow over the plug wall depending upon the pressure distribution along the primary flow. It is obvious that the values of static pressure in the two streams should be identical at each point along the interface.* In order to meet that requirement, the coolant stream, in a given case, may be subsonic or choked at entry into the nozzle, accelerate to supersonic speed and remain supersonic up to the exit plane of the nozzle. Similarly, in another case, the coolant stream may be supersonic at entry, accelerate to a higher speed,

---

* A similar requirement does not exist with respect to velocity in view of the assumption that dissipation and diffusion are neglected at the interface.

decelerate and eventually exit the nozzle as a subsonic stream.

2.2. The Primary Stream

The primary stream which starts as a subsonic flow at entry to the nozzle accelerates through transonic speeds to supersonic speeds at nozzle exit. We confine attention here to the part of the nozzle, with the plug, wherein the flow velocity is everywhere definitely supersonic. This is the part of the nozzle that is illustrated in Figure 2.2. However, the initial conditions for the supersonic flow arise in the transonic part of the nozzle. In order to establish such conditions, calculations are required in the annular throat region of the nozzle.

The primary stream is characterized by the distributions of composition, stagnation pressure and temperature, and Mach number, and the mass flux at the initial value surface of the supersonic region.

2.3. Flowfield Prediction

The details of a method of predicting the flowfield when two perfect gas streams interact under the conditions of inviscid, non-mixing flow are provided in Appendix I to this Report. Both the methodology and the building blocks of computation required are given therein.

Two illustrative examples are provided in the following to demonstrate the prediction procedure.

In both examples, one needs flow definition over an initial value surface. Such starting values may be obtained in one of two ways.

(i) Starting with a definition of flow variables in the high subsonic part of the nozzle, one can adopt the procedure described in Appendix I to this Report and carry out an axisymmetric transonic flowfield prediction up to a surface where a reasonably high enough value of Mach number is obtained. That surface is then utilized as the initial value surface for the prediction of supersonic flow.

(ii) In the alternative, one can utilize an approximation based on one-dimensional flow in the transonic region. Starting again with a definition of flow variables in the high subsonic part of the nozzle, one can establish a surface, normal to the axis of the nozzle, at which the Mach number is definitely supersonic. That surface is then utilized as the initial value surface for the prediction of supersonic flow.

In many cases, it is found that method (ii) does not yield a satisfactory solution in the supersonic part of the nozzle. Nevertheless, preliminary estimates of performance can be based upon such an initial value surface provided the throat wall curvature, or, as in the current case, the throat annulus curvature, is not too large.

In particular, in the case of the NASA nozzle configuration, the surface where the Mach number is 1.04 based on one-dimensional analysis and the iso-Mach number surface for a value of Mach number equal to 1.04 based on axisymmetric flowfield analysis may be compared. It is found that they are different. However, from the point of view of their being utilized as initial value surfaces, no substantial errors have been found in the use of the one-dimensional approximation.

2.3.1. Illustrative Case 1

The Case 1 pertains to the flowfield of a plug nozzle without any coolant or secondary stream.

Given the conditions as in Table II, the objective is to establish the flowfield along the nozzle contour in the supersonic portion of the NASA nozzle, Figure 1.2, when the coolant mass flow is turned off. The flowfield parameters of interest are static pressure, static temperature and Mach number distributions along the flow, including values at the nozzle wall and the plug wall.

The gas is assumed to be a perfect gas with constant specific heats. The geometry is axisymmetric. The flow is without any frictional loss. The initial conditions are obtained, utilizing one-dimensional approximation, over a straight (normal to axis) surface where Mach number is 1.04.

The computed solution is based on the use of method of characteristics with a second order interpolation scheme.

Figures 2.3-2.5 provide the predicted distributions of pressure, temperature and Mach number along the flow. The distribution of mass flow along the nozzle is presented in Figure 2.6, along with the local values of integrated mass flux. Figure 2.7 provides the distribution of static pressure along the plug surface.

The nozzle throat diameter is 115 sq. in., with a mass flow rate 20.97 lbs.m./sec.

2.3.2. Illustrative Case 2

The Case 2 includes the coolant or the secondary stream. In this case, the gas dynamic interactions between the primary and the secondary streams have to be

TABLE II

DATA FOR ILLUSTRATIVE EXAMPLE 1

The gas in the primary stream, treated as a perfect gas with constant specific heats, has the following properties over the surface where initial flow conditions are prescribed.

R	ft. lbs.f./lb.m.R	53.35
γ		1.3377
T_o	R	1,743.0
P_{o8}	psia	15.05

The ambient conditions are as follows.

T_o	R	550.0
P_o	psia	15.05

included and the dividing surface between the two streams established. At each point along the dividing surface between the two streams the static pressures in the two streams should be equal. Furthermore, the flow angles for the two streams should be the same at A (figure 2.2).

However, a number of features of flow become significant at A.

(1) Referring to Figure 2.2, the coolant stream may enter the nozzle at AD at subsonic, choking or supersonic conditions. It is possible to select a particular type of entry condition at AD, but it is not possible a priori to fix a value of Mach number or that of static pressure along AD.

(2) The primary flow may undergo a shock-type compression or a Prandtl-Meyer expansion at A. The extent of compression or expansion is determined by the requirement that the static pressures for the primary and the secondary streams should be equal, as also the flow angles, at A.

(3) In general, several sets of flows of the primary and the secondary streams can satisfy the requirements of static pressure and flow angle matching at A. A unique solution for the downstream flowfield may only be found based on another condition in the downstream flow itself.

The flow conditions are as given in Table III. The nature of gas, the geometry and the starting surface in the supersonic position of the nozzle remain the same as in Section 2.3.1 (case I).

TABLE III

DATA FOR ILLUSTRATIVE EXAMPLE 2

All of the data given in Table II apply, except that the ambient pressure is 1.514 psia.

In addition, the following are prescribed with respect to the coolant (secondary) stream.

R	ft. lbs.f./lb.m	53.35
γ		1.3377
T_o	R	1364.0
P_{oc}	psia	5.0

Given the foregoing, the nozzle flowfield, including the location of the dividing surface in relation to the plug wall surface, depends upon the conditions existing in the coolant or secondary stream at the plane of its entry into the nozzle. Referring to Figure 2.2, it is assumed that the coolant flow is uniform over the entry plane AD and that the flow is subsonic at that section. In view of various possible choices of Mach number along AD, the choice of a subsonic flow at that section constitutes a specific example.

It may be noted that the static pressure of the coolant stream at the point A cannot be prescribed a priori. The reason is that the static pressure, as well as the flow angle, must be the same at the point A for both the primary and the secondary streams. Thus, although one may assume a value of Mach number in the coolant stream at A, the static pressure at A is determined by the stagnation pressure of the primary stream and the expansion of that stream up to point A.

Referring to Figure 2.8, which is essentially an enlargement of the part of Figure 2.2 relevant to the current discussion, the expansion of the primary stream can be established up to the right characteristic PA. That part of the expansion process is not subject to change due to any aspect of flow downstream of PA.

At this stage, the only flow parameters that are known for proceeding further in the analysis are as follows: (1) the stagnation and the static pressures and temperatures in the primary stream at A prior to any interaction with the secondary stream, and (2) the stagnation pressure and temperature in the secondary stream at A. In addition, the Mach number at A in the coolant stream is known to be less than one by assumption. As a consequence, the static pressure at A may only be higher than the choking value of

pressure in the coolant stream. Since the static pressure values in the primary and the secondary stream must match at A, it can also be concluded that the static pressure of the primary stream at A must also be higher than the choking value of pressure in the coolant stream. However, the value of subsonic Mach number or the static pressure of the coolant stream at A is not known, as stated earlier.

We now consider the possibility of assigning a value for the static pressure of the coolant stream at A. First, we note that the primary stream can undergo either a shock-type process or a Prandtl-Meyer expansion process at A. In other words, based on the specific values of stagnation pressures in the primary and the secondary streams in any given case, the primary flow may have to undergo a compression or an expansion so as to yield the static pressure value that matches with that of the coolant stream at A. Consequently, second, we note that there must exist a series of values of static pressure in the coolant stream at A corresponding to which there is another series of static pressure values in the primary stream at A; the latter after compression or expansion should change exactly to the series of values of static pressure in the coolant stream at A. Unfortunately, such considerations do not lead to a unique solution since several pairs of static pressure values can be picked out in the afore-mentioned series that meet the imposed restrictions. It may be observed here that the condition of flow angle equality is not really restrictive since the coolant stream flow angle at A is not fixed in the problem.

Therefore, the only method of obtaining a unique solution is through the use of another flow-related constraint. Such a constraint may only arise in the flowfield downstream of PAD. To determine such a constraint, we recall that the coolant flow at

AD is subsonic and, therefore, the coolant flow, when its stagnation pressure is high enough, can accelerate to a choking condition at some location downstream from the section AD.

Meanwhile, based entirely on practical considerations, some restrictions can be imposed on the primary flow changes at A. For example, the primary stream may undergo more commonly a Prandtl-Meyer type expansion process at A rather than a shock-type process. It may be observed that such an assumption only reduces the number of possibilities and is not a contributor to obtaining a unique solution. As stated earlier, some constraint should be imposed, that arises from the downstream flow, such as choking of the coolant stream.

One can proceed as follows: based on the given geometry of the plug surface, a pseudo-wall boundary is postulated for the plug starting from A. Then the flowfield in the primary stream is calculated up to the station along the plug where the primary stream static pressure becomes equal to the choking value of static pressure in the secondary stream. That point is denoted by B in Figure 2.8, BC being the local normal from B to the given plug surface.

We now postulate that there exist (a) a value of static pressure at A in the coolant stream, (b) a value for flow angle at A, also in the coolant stream and (c) a surface AB such that (i) the two streams are matched everywhere in pressure along AB and (ii) the coolant stream chokes exactly at BC starting from AD. Obviously an iterative procedure is required for obtaining the desired unique solution. In order to simplify the iteration procedure, two other assumptions are introduced as follows:

(1) The coolant stream chokes at BC in all cases although the choked area may comprise of some element along BC. And,

(2) The nature of flow boundary between the two streams can be prescribed a priori, for example a parabola.

The first assumption implies that the static pressure of the primary stream at B is in all iterations approximately equal to the choking static pressure of the coolant stream. Regarding the second assumption, if the flow boundary is not so prescribed, one has to choose arbitrarily a matching surface between the two streams and arrive, after trial and error, at one that satisfies the imposed conditions.

In the current case, the parabola must satisfy the following conditions: (1) it must pass through the point A; (2) it must pass through a point along BC; and (3) the tangent to the parabola at A, representing the stream direction at A, should be such as to yield equal pressures in the two streams meeting at A.

One can then adopt the following procedure for determining the flowfield: A point B_1 is chosen along BC, as denoted in Figure 2.8. The static pressure at B_1 is the choking static pressure of the coolant stream. Assuming isentropic expansion of the coolant stream between AD and B_1C, the static pressure of the coolant stream at AD is determined based on one-dimensional flow approximation. At the same time, the primary stream is expanded at A to the value of static pressure of the coolant stream at A based on Prandtl-Meyer expansion rule. The resulting flow angle then is utilized as the angle which the tangent to the parabola subtends at A.

Now, a series of parabolas are selected, each of them intersecting BC at different points. Each parabola yields a value of flow angle at its intersection with BC and

another value of flow angle at A. One of the series of parabolas can be expected to yield a smooth transonic flow at BC. That parabola is chosen as the matching line between the primary and the secondary streams.

It is clear that, apart from the heuristic reasoning and the trial-and-error process involved, the choice of a parabola, rather than a general second degree curve, is arbitrary. It turns out in practice that the choice of a parabola provides a flowfield along AB that is within acceptable magnitudes of errors. Several example cases have illustrated that a parabolic shape for the dividing or matching surface yields acceptable results.

In the example under consideration, after a series of trials, a parabola that yields a flow angle of -9.9° at B was chosen. This angle should be compared with the plug surface angle, at C, of -10.0°. In an axisymmetric flow, the angle at an interior point can be expected to be smaller than at the surface.

Corresponding to that choice of the dividing surface, the flowfield in the primary stream has been determined between A and B utilizing the method of characteristics. One can then compare the static pressure distribution so obtained along AB for the primary stream with that obtained for the secondary stream under the assumption of one-dimensional isentropic flow. Such a comparison is provided in Figure 2.9 for the test case. The figure also shows the pressure distribution along the straight pseudo-boundary between the two streams. It is found that the matching of pressures along AB is acceptable for practical purposes.

Once the flow angle and the static pressure are determined at A and the matching surface between the two streams, AB, is located, it is straight forward to calculate the

entire nozzle flowfield up to nozzle exit.

2.4. Other Predicted Results

A number of flow cases corresponding to various test cases, as described in Appendix 4 of this Report, have been analyzed. They may be grouped in two parts as follows.

(1) Flowfield in the NASA nozzle in the absence of a coolant stream; and

(2) Flowfield in the NASA nozzle with the coolant stream.

Those predictions are described in the following sections.

2.4.1. Primary Flow in the Absence of the Coolant Stream

The flow cases that have been predicted and the numbers of figures wherein the results are presented are given in Table IV. Considering a particular NASA nozzle configuration, (1) the distributions of static pressure, static temperature and Mach number, (2) the distributions of mass flux and (3) the distributioin of static pressure along the plug wall are presented for various values of nozzle pressure ratios.

2.4.2. Interactions Between the Primary and the Coolant Streams

These predictions are an extension of the predictions undertaken in Section 2.3.2 for various other cases in which the stagnation pressure of the coolant stream is higher than that of the primary stream. Accordingly, in order to match the values of static pressure at A (Figure 2.8) between the primary and the coolant streams, a shockwave must be included at A in the primary stream, as shown in Figure 2.12. It will be noted that the coolant stream is choked in all cases.

TABLE IV

DATA FOR FURTHER EXAMPLES OF NOZZLE EXPANSION IN THE ABSENCE OF COOLANT FLOW

P_{08}	15.00 psia
T_{08}	1,750 R
P_o	3.75 psia; Fig. 2.10.1-2.10.5.
	1.875 psia; Fig. 2.11.1.-2.11.5.

The flow cases that have been predicted and the numbers of the figures wherein the results are presented are given in Table V. It will be observed that the various cases differ in the stagnation pressure values chosen for the coolant stream while the nozzle configuration and the stagnation conditions of the primary stream are held constant.

It is of some interest to establish the occurrence of shockwaves in the nozzle for different values of nozzle pressure ratio. Two shockwaves are of interest, one occurring at the coolant slot and the other occurring further downstream along the plume. The manner in which the location of the plume shockwave changes with nozzle pressure ratio is shown in Figure 2.15. This may also be observed in the changes in static pressure ratio along the wall, as obtained in NASA experiments given in Figure 2.16, where additional data not included in Appendix IV have been added.

TABLE V

DATA FOR FURTHER EXAMPLES OF INTERACTION BETWEEN PRIMARY AND COOLANT STREAMS

Primary Stream:	$P_{08} = 15.13$ psia
	$T_{08} = 1{,}743.0$ R
Secondary Stream:	$P_{oc} = 27.0$ psi; Fig. 2.12
	$P_{08} = 20.0$ psia; Fig. 2.13
	$P_{08} = 18.0$ psia; Fig. 2.14

SECTION 3

HEAT TRANSFER WITH FILM COOLING

The three main considerations in the analysis of heat transfer to the plug wall surface of a nozzle such as that shown in Fig. 1.1 are the following.

(1) The primary nozzle flow under consideration is a supersonic flow with large Mach number and density variations across the flow at each section along the flow.

(2) There is a coolant flow in the form of a secondary stream along the plug wall. And,

(3) The plug wall surface boundary layer can be expected to be turbulent.

References 10 and 11 provide a means of predicting the heat transfer taking account of the afore-mentioned features under various approximations. First, it is assumed that the supersonic flow does not involve shockwaves. Second, the specific momentum of the coolant stream is assumed to be lower than that of the free stream. In that case, the skin friction losses are reduced. Finally, the boundary layer over the plug wall surface is assumed to be turbulent everywhere. A modified turbulent mixing length model is employed for eddy viscosity in the boundary layer.

A slightly different model for a turbulent boundary layer, that is also in the nature of a mixing length model, has been presented in Ref. 12. A more elaborate model is discussed in Ref. 13. A second order closure model has been outlined in Appendix II of this Report.

One important consideration in the case of boundary layers is the nature of modelling to be employed in the vicinity of the wall surface. A brief description of some possible approaches to this problem is presented in Appendix III of this Report.

In certain problems it may not be appropriate to introduce the assumption of zero normal pressure gradient in the vicinity of the wall. Reference 12 permits imposition of arbitrary pressure gradients both along and across the flow during heat transfer and skin friction calculations.

When there is a coolant stream at the plug wall surface, one has to account for the mixing layer between the primary and the secondary streams. A turbulent mixing length model is suggested in Ref. 11 for the mixing layer also.

In order to take into account heat and mass transfer processes, non-unity turbulent Prandtl and Schmidt numbers are introduced in Ref. 11, while assuming that the Lewis number is unity.

3.1. Prediction Procedure

A computational scheme, generated at the NASA Langley Research Center, namely Program D2630 (referred to as LANG hereafter), has been described in part in Refs. 10 and 11. The computational scheme was obtained for use in connection with the current investigation.

3.1.1. Outline of the Code LANG

The code has been developed for the prediction of compressible, turbulent boundary layers in high Mach number flows, with heat transfer to the wall. The code is also suitable for heat transfer to the wall when a coolant stream is injected into the free

stream to form a film of cold fluid along the wall.

The code solves coupled, nonlinear equations of conservation of mass, mean momentum and mean total enthalpy by an iterative, finite-difference procedure. The flow geometry can be two-dimensional or axisymmetric.

In the formulation, the governing equations are transformed from (x,y) space to (ζ,η) space as follows.

$$\zeta = R_s \int_o^{x/L} \frac{(\rho\mu)_e}{(\rho\mu)_s} \cdot \frac{u_e}{\sqrt{2H_e}} \cdot r^{2j}\, d\left(\frac{x}{L}\right)$$

$$\eta = R_s \frac{u_e/\sqrt{He_e}}{(2\zeta)^{0.8}} r^j \int_o^{y/L} \frac{\rho}{\rho_s} \cdot d\left(\frac{u}{L}\right)$$

Here, ρ, μ, u, H, r, R, and L denote density, viscosity, velocity, enthalphy, radius of streamline, radius of nozzle and length of nozzle, respectively. The subscripts e and s denote external and stagnation conditions and j = 0 or 1 for two-dimensional or axisymmetric flow. It is clear that the solutions obtained in the (ζ,η) space are thus in the nature of similarity solutions.

The following assumptions are then introduced.

(1) The mean static pressure is uniform across the boundary layer. Accordingly, the density ratio, ρ/ρ_e, is related to the ratio of static enthalpy, the fluid being treated as a perfect gas with constant specific heats.

(2) Turbulent transport of momentum in the boundary layer is based on the concept of eddy viscosity with prescribed distributions of length

scale. Turbulent heat conductivity is defined by analogy to eddy viscosity.

(3) Turbulent transport of momentum and heat in the presence of a coolant stream is modeled by assuming piecewise linear functions for the turbulent length scale with respect to the normal coordinate.

The basic equations and the assumptions underlying the problem formulation are the same as in the code commonly referred to as STAN5 (Reference 13). However, STAN5 involves linearizing the system of equations by treating the counterpart in the nonlinear terms, for instance u in $u \frac{\partial u}{\partial x}$, as known coefficients. This removes the necessity for an iterative procedure in obtaining the solution for the set of equations.

Further details on the turbulence modelling in the NASA Langley codes are given in Appendix V to this Report.

3.2. Predicted Cases with Results

Four flow cases are presented in the following. The principal parameters pertaining to them are given in Table VI and VII.

Based on those input variables, predicted results are presented in each of the four cases for the following: external velocity, wall static pressure, wall and external flow static temperature, Mach number, initial velocity profile, boundary layer thickness, skin friction, Stanton number, heat flux, velocity profile and temperature profile. The results are presented in a series of figures as listed in Table VIII.

TABLE VI

FLOW CASES SELECTED FOR HEAT TRANSFER PREDICTIONS

Case No.	A_t sq. in.	NPR	P_{TG} lb/sq. in.	T_{TG} °R	P_{TC} lb/sq. in.	T_{TC} °R	Notes
I	175.0	8.08	13.0	2,593	4.69	1,365	A
II	175.0	7.98	15.57	1,135	-	-	B
III	175.0	7.98	15.57	1,135	-	-	C
IV	115.0	8.0	15.16	1,752	-	-	D

NOTES

(A) Pertaining to Case I

The primary stream consisted of products of combustion treated as a perfect gas with R = 52.8 ft lbm/lb°R and $\gamma = 1.3377$.

The coolant stream consisted of air treated as a perfect gas with R = 57.8 ft. lbs./°R and $\gamma = 1.40$.

The boundary conditions were obtained form NASA data. The nozzle discharge coefficient was assumed to be 0.97 and the wall recovery factor to be 0.930.

(B) Pertaining to Case II

The primary stream is the same as in Case I. The boundary conditions were obtained as in Case I.

(C) Pertaining to Case III

The primary stream is the same as in Case I. The boundary conditions were obtained from predictions, as described in Section 2, under the assumption of isentropic flow and setting the static temperature value at the wall equal to that at the edge of the boundary layer in the free stream.

(D) Pertaining to Case IV

The assumptions with respect to the primary stream and the boundary conditions are the same as in Case I.

TABLE VII. FLOW CONDITIONS ALONG THE WALL FOR CASE III

x (inch)	T_w (°R)	P_w/P_{Te}	$P_w = P_e$ (psia)	$M = M_e$	Te(x) (°R)	$a_e = \sqrt{\gamma R T_e}$ (fps)	$u_e = a_e M_e$ (fps)	$\sqrt{2He}$ (fps)
0.5	1505	.19	2.88	1.742	1090	1619	2820	4589
2.0	1485	.11	1.67	2.096	933	1498	3139	4590
4.0	1432	.075	1.14	2.341	836	1418	3319	4590
6.0	1395	.075	1.14	2.341	836	1418	3319	4590
8.0	1395	.095	1.44	2.19	894	1467	3212	4590
10.0	1380	.10	1.52	2.16	906	1476	3189	4590
12.0	1390	.10	1.52	2.16	906	1476	3189	4590
14.0	1425	.10	1.52	2.16	906	1476	3189	4590
16.0	1475	.125	1.90	2.01	969	1527	3068	4590
18.0	1510	.15	2.27	1.90	1017	1564	2972	4590
20.0	1507	.16	2.43	1.85	1040	1582	2926	4590
22.0	1490	.145	2.20	1.92	1008	1557	2990	4590

NOTE: He represents the total enthalpy in the external stream.

TABLE VIII

RESULTS FOR THE FOUR SELECTED CASES

Parameter	Figure Number			
	Case I	Case II	Case III	Case IV
1. External velocity	3.1	3.12	3.12	
2. Wall static pressure	3.2	3.13	3.13	
3. Wall and external static temperature	3.3	3.14	3.14	
4. Mach number	3.4			
5. Initial velocity profile	3.5			
6. Boundary layer thickness	3.6	3.15	3.15	3.21
7. Skin friction	3.7	3.16	3.16	3.22
8. Stanton number	3.8	3.17	3.17	3.22
9. Heat flux	3.9	3.18	3.18	3.23
10. Velocity profile	3.10	3.19	3.19	3.24
11. Temperature profile	3.11	3.20	3.20	3.24

NOTES: Cases II and III are compared in one set of figures as indicated.

It may be observed that the results for Cases II and III are provided in the same figures to permit comparison. There is substantial difference between the input data, between Cases II and III. As a result, the predictions also differ substantially. It will be recalled that Case III uses predicted values from inviscid calculations to deduce the boundary conditions for the heat transfer calculation. At the same time, it may be pointed out that experimental data on the measurements of static pressures in the free stream and of temperature along the plug wall may be subject to unknown errors.

The main conclusion form the predictions is that the NASA Langley code, as adapted by us for use in the current predictions, is suitable for use in continuously expanding flows under supersonic conditions.

More specifically, there are considerable differences between Cases II and III in the predicted values of distributions of boundary layer thickness, δ, and heat flux, q_w.

SECTION 4

SHOCK-BOUNDARY LAYER INTERACTION UNDER NON-ADIABATIC CONDITIONS

In a plug nozzle, such as that illustrated in Figures 1.1 and 2.2, a shock-boundary layer interaction process (Figure 4.1) may occur in several ways as follows.

a) Under transonic or supersonic conditions, without or with separation;

b) With the plug surface exposed to the gas stream or covered by a coolant; and

c) With the uninteracted or original boundary layer being laminar or turbulent, while the freestream is inhomogeneously turbulent.

A shockwave produces across itself an increase in static pressure and static temperature and a decrease in velocity and Mach number. When a shockwave arises at a wall or impinges over a wall after being generated by an external source, it cannot extend up to the wall on account of the slow-moving, subsonic fluid present near the wall. A real fluid satisfies the no slip condition at the wall on account of its viscosity. The shockwave itself has a finite thickness on account of fluid viscosity. These factors cause a finite extent of the flow in the wall region to be affected by the presence of the shockwave. The processes occuring in that region constitute the interaction. The region of interaction extends both upstream and downstream of the nominal location of the shockwave.

Both the shockwave and the relevant wall region may be three-dimensional and the interaction region then is complex in geometry. The extent of the interaction region is, of course, three-dimensional, and generally unsteady, even when a plane shockwave impinges or arises on a plane wall with a laminar boundary layer, whether or not a flow

separation occurs in the interaction region.

In the interaction of a shockwave with a boundary layer, there may arise packets of compression and expansion waves and, also, a reflected shockwave. Under any given set of flow conditions, the entire system of waves should be considered together in order to analyze the flow structure. In early experimental studies of H.W. Liepmann (Reference 14) on shock-boundary layer interaction over the suction surface of an airfoil under transonic flow conditions, it was found that a shockwave may be inclined towards the on-coming flow (Figure 4.2) when the boundary layer was expected to be laminar. Such a flow configuration may be understood only by taking into account the entire combination of waves that arise in the interaction region. A similar observation may be made concerning the occurrence of a second shockwave in certain flows involving flow separation, which itself is the results of the "original" interaction between a shockwave and a wall boundary region (Figure 4.3).

The flow processes in the interaction region must depend in a complex fashion on a nonlinear combination of the following parameters unless the flow does not involve any of them:

1) Density of fluid: At sufficiently low densities, the fluid may have to be considered as a rarefied gas. The molecular mean free path and the Knudsen number are the characteristic parameters.

2) Mach number of the flow: Transonic conditions must be distinguished from supersonic flow conditions.

3) Reynolds number of the flow: The free stream may be turbulent with inhomogeneities.

4) Presence of pressure gradient in the flow: Zero, favorable (as in a nozzle flow) or adverse (as in a diffusing flow) pressure gradient may exist.

5) Presence of rotation in the flow: The flow may include finite vorticity which can couple variously with the ambient turbulence and the vorticity of the shockwave and of the wall region.

6) Velocity and enthalpy profiles in the boundary layer at the location where interaction with the shockwave may be recognizable: The characteristic parameters are various Reynolds numbers (based on boundary layer, displacement and momentum thicknesses), Prandtl number and wall recovery factor. The profiles may correspond to laminar, transitional or turbulent conditions. The characteristic parameters related to the profiles are the shape factors, H based on momentum thickness and H* based on energy thickness (Reference 15). The magnitudes of H and H* may be understood in terms of the extent to which the boundary layer profiles are "filled", and therefore, in terms of the ability of the boundary layer to "resist" changes occuring either at the wall or in the free stream. Reference may be made to Figure 4.4.

7) Nature of shockwave: The shockwave may be externally generated and impinging on the wall or locally generated.

8) Velocity and temperature profiles "within" the shockwave: The characteristic parameter is the thickness of the shockwave which may be appreciably different in the interaction region compared to that in the free stream. The shockwave thickness is, in general, small compared to the boundary layer thickness.

9) Boundary condition pertaining to temperature at the wall surface: The wall may be in equilibrium with respect to the temperature of the flow or, it may be heated or

cooled. Both the viscous sublayer and, at least, a part of the turbulent layer become affected by the wall temperature.

10) Roughness of wall surface: This is especially significant in the case of transitional flow.

11) Presence of wall curvature

12) Presence of injection or suction at the wall; and

13) Presence of a film of fluid that may be undergoing modification or mixing over the wall: There arise several characteristic parameters related to the film in determining the interaction between the flow, the shockwave and the film. In the case of a film of gas, such as the coolant stream utilized in the case of the NASA plug nozzle configuration, a number of fluid and geometrical parameters have to be taken into account.

The foregoing list is formidable. A background to the nature of related investigations may be found in Reference 15. No substantial body of experimental data or analysis are available on interaction in the presence of wall heat transfer. In practice, as in the case of the NASA plug nozzle, wall cooling is of greater interest than wall heating. Cooling seems to cause a boundary layer to become more "filled" and generally less susceptible to changes such as separation.

One of the main uncertainties in the interaction region is the extent to which the wall region retains its identity as a classical boundary layer upstream of the interaction region. The boundary layer, whether laminar or turbulent, is in part subsonic. The shockwave can penetrate the boundary layer only up to the outer vicinity of the surface

where the Mach number, M, is equal to one. In the upstream (relative to the nominal location of the shockwave) part of the interaction, the subsonic part of the boundary layer is affected by propagation of simple pressure waves, and that change may also cause other changes to occur in the outer part of the boundary layer. The resulting flow in the wall region may depart substantially from the characteristics of the initial boundary layer. The initial boundary layer may be laminar or turbulent, and transitional conditions may arise in the interaction region. In all cases, there arises a need to establish what part of the initial boundary layer retains its classical features over the length of the interaction region. For example, one needs to know in what part of the flow the assumption of negligible normal pressure gradient continues to be meaningful or that pertaining to viscosity-dominated flow is appropriate.

In the case of turbulent flow, basic questions arise concerning the production of Reynolds stresses and its relation to dissipation and also redistribution in different directions through the action of pressure fluctuations. The concept of equilibrium (Reference 16) in any part of the initial boundary layer becomes questionable in the interaction region. In general, there is an increase in the thickness of the "boundary layer" but the increased entrainment has not been explained on the basis of modifications to the structural features of any part of the layer (Reference 17).

4.1. Problems Considered

In view of the foregoing, only two problems are selected for further analysis in the current effort. Both of them are related to shockwave-boundary layer interaction over the plug surface of the NASA nozzle configuration, Figure 1.2. The problems selected are (1) shockwave in the transonic flow region and (2) shockwave in the supersonic flow

region. In both cases, it is assumed that the free stream is non-turbulent while the initial boundary layer is fully turbulent. The wall is assumed to be cooled but exposed directly to the gas stream, that is, without a coolant as in backside cooling. The flow is not expected to tend to separate from the wall in either case.

It may be noted that the main practical considerations in both cases are : the changes in skin friction coefficient and heat transfer in the interaction region.

A hierarchy of selected methods for predicting the flowfield in the two cases is described in the next Section. The methods are selected either on the basis of some developments presented here or on the basis of promise of future development.

4.2. Prediction Schemes

The main prediction schemes of interest in non-adiabatic shock-boundary layer interaction are as follows.

(1) Non-asymptotic multi-deck theory (Reference 18); and

(2) Reynolds-averaged Navier-Stokes equations applied to the problem (Reference 19).

They are discussed in the following.

4.2.1. Multi-Deck Perturbation Theory

The multi-deck theory of Inger for a turbulent boundary layer is referred to as a non-asymptotic theory, in comparison with Lighthill's original theory (Reference 20), as is the theory developed by Tu and Weinbaum (Reference 21) for the case of a laminar boundary layer interacting with a shockwave. In both cases, the inner deck is governed

by the complete boundary layer equations. For the cases of a turbulent boundary layer, Inger postulates that the entire inner layer obeys the law of the wall throughout the interaction region.

The triple-deck then consists (Figure 4.5) of (1) the outer inviscid and irrotational flow of moderate rise in entropy, (2) the thin shear-disturbance sublayer governed by the law of the wall and (3) an intermediate layer that is in the nature of a boundary layer with the total (viscous as well as turbulent) shear stress "frozen" or "unaffected" along each streamline. The shear stress, of course, remains a function of distance normal to the wall.

Inger develops a prediction procedure based on the foregoing model for, necessarily, weak transonic shocks. The disturbance produced by the shockwave is in the nature of a perturbation. The perturbed equations are deduced assuming that (a) a reference temperature, due to Eckert (Reference 22) can be employed for the boundary layer and, hence, density is constant and (b) density perturbation in the case of a non-adiabatic wall can be modeled in the inner layer. A ratio of actual temperature of wall (T_W) to the adiabatic value of wall temperature (T_{WAD}) in the range 0.5 - 2.0 has been assumed in illustrative problems.

If the perturbation procedure is assumed to be valid for the problem of interaction between the three decks, it turns out that only two changes seem feasible: (a) any change in the outer layer may only be a consequence of changes in the inner layer and (b) the entire boundary layer structure becomes affected. Since the change in (a) is essentially the interaction between the three decks, Inger argues that an appropriate change should be introduced in the overall boundary layer structure. The parameters

chosen are the form factors H and H*.

Details of the calculation procedure can be found in References 23-24.

Several questions arise regarding the basis of the method. They are discussed in the following.

The main question regarding the method is the use of a form factor as an initial value and its subsequent impact on the developing structure of the triple deck. It should be noted that the shock-boundary layer interaction problem is "closed" without the need for choosing a value for the form factor. However, the form factor is a means of taking into account, in a parametric form, the combined effect of shock strength (or, equivalently, the upstream Mach number), the displacement thickness Reynolds number, the wall temperature ratio and the initial incompressible form factor. Its use depends upon the assumption of a boundary layer velocity profile for compressible flow (for example, such as that given in Reference 25) and a condition linking the Cole's wake function, skin friction coefficient and displacement thickness Reynolds number. Thus, the prescription of the form factor is equivalent to providing an additional parameter by means of which the three decks are integrated for given initial conditions.

The method is successful in predictions of global quantities related to the flowfield so long as (a) the flow is attached everywhere, (b) the extent of the interaction region is small both upstream and downstream of the shockwave, (c) the shock strength is small and (d) the wall temperature ratio is not too far different from unity.

No analysis is, of course, possible within the framework of the theory to deduce any of the turbulence quantities. Thus all of the quantities deduced are either mean values or integral quantities, other than skin friction and heat transfer at the wall. It should

be noted that, based on the perturbation procedure, the streamwise distribution of normal disturbance velocity is determined in the inner deck, but that velocity disturbance, although assumed to be affected by turbulence directly, is not of the nature of turbulence fluctuations. The eddy viscosity is assumed to be changed; however, no details are established for the change.

A method that is comparable, in several respects, for the interaction of a normal shockwave with a boundary layer is due to Bohning and Zierep (Reference 26). In this model, the triple deck consists of (1) the inner viscous layer treated as a parallel stream governed by boundary layer flow equations and retained in the interaction region in the undisturbed incoming state; (2) the outer deck treated as a transonic inviscid flow; and (3) the main, intermediate deck treated as a perturbed parallel and inviscid rotational stream. The set of describing equations is solved under the boundary conditions, namely (a) prescribed pressure distribution at the outer boundary of the main deck as equal to the pressure distribution in the external stream; (b) vanishing of vertical disturbance at upstream and downstream infinity; and (c) zero vertical velocity at the outer edge of the inner layer. Velocity distribution in the in-coming boundary layer is taken in power law form.

It is clear that the method of Bohning and Zierep is also based on mean flow approximations. The turbulence in the flow produces its effect, if any, through the selection of the mean flow profile and its development in the interaction region.

The second major question pertains to the use of the Crocco velocity-temperature relationship. Both the use of the relationship and its interaction with the logarithmic law of the wall are questionable even considering the low Reynolds number of the

region. In addition, the presence of wall cooling and pressure gradients (both streamwise and normal) affects the relationship. It has been found (Reference 27) in analysis of experimental data that neither the temperature distribution according to the Crocco relationship nor the experimentally-measured density distribution yield the "norm" of incompressible flow for the shear velocity, for example.

The success of the methods in providing reasonable predictions of mean values in the interaction region, including the location of the sonic line, is difficult to rationalize on the basis of individual processes.

4.2.2. Multi-Deck Asymptotic Expansion Method

The method, primarily initiated by Adamson and Melnik, is again based on the central ideal of Lighthill (Reference 20) and utilizes a matched asymptotic expansion method for a three-zone interaction region. Details on the method can be found in References 28-29. The method can be utilized for transonic normal shock cases and also for finite oblique shocks. In the latter case, the method is applicable so long as the flow is everywhere supersonic except below the sonic line.

The asymptotic expansion is based on the use of a small parameters, namely ϵ defined by

$$\bar{U}_e = \bar{a}_e^* (1 + \epsilon)$$

where $\bar{U}_e$ and $\bar{a}_e^*$ represent the external uniform velocity and the acoustic velocity, respectively. In addition, it is assumed that the shear stress and density (for the case of the insulated wall) are constant at the values at the beginning of the interaction. Furthermore, the shear velocity is considered to be small compared to the acoustic velocity.

The flow is considered in terms of (1) external transonic flow region, (2) velocity defect region, and (3) two inner regions, namely the Reynolds stress sublayer and the wall layer, the latter affected only by viscous shear stress. Modeling is required for the normal and shear stresses due to turbulence.

In the model of Adamson, the structure of the inner layers (two of them) is dependent upon the model employed for the Reynolds stresses and the manner of introducing perturbations in those stresses. Both the model and the order of perturbations affect the structure.

Now, in the undisturbed boundary layer, that is in the region upstream of the interaction, it can be shown that the stagnation enthalpy, H, is equal to the following.

$$H = \frac{T}{(\gamma - 1)} + \frac{U_e^2}{2} + f$$

where f is given by

$$f = u_\tau^2 \, (Pr_T - 1) \ ,$$

noting that $(Pr_T - 1)$ can be very much less than unity in a given case. Here u_τ represents the shear velocity and Pr_T, the turbulent Prandtl number. When the Reynolds number is large H is a constant in the external inviscid flow. In the boundary layer region, it is suggested by Adamson that H can be expanded in the same manner as T and U. However, it is not necessary to change H in the case of an insulated wall. On the other hand, in cases where wall heat transfer needs to be taken into account, a distribution of H must be introduced in the thermal boundary layer that is compatible with the given wall temperature distribution in the interaction region. The wall temperature distribution affects the density distribution at the wall. Hence no simple assumptions are admissible for the distribution of ρ_w and $u_{\tau w}$ so long as $T_w \neq T_e$, the

subscript w indicating condition at the wall. If $(T_w - T_e)$ or $(Pr_T - 1)$ is considered a small parameter, then a two-parameter expansion procedure can be adopted. However, it is clear that no significant case of practical importance can be covered by that procedure.

4.3. Use of Reynolds-Averaged Navier-Stokes Equations

The objective, as stated earlier, has been to model shock-boundary layer interaction in a near-transonic Mach number regime, without separation of flow, in the presence of heat transfer to the wall. However, the main emphasis, in the short duration of the project, has become restricted to the analysis of turbulence processes in the interaction region.

The Reynolds-averaged Navier-Stokes equations of interest can be found in Reference 28. A further development of those along with a consistent procedure for treating the wall region have been presented in Appendices II and III of this Report. The evolution of Reynolds stresses is discussed in the following with specific application to shock-boundary layer interaction processes.

4.3.1. Reynolds Stress Evolution

The interaction processes may be grouped, for purposes of discussion under (a) mean flow deformation changes and (b) turbulence changes, although they are interactive also. Volumetric changes due to density changes are also included in (a) and thus, (a) represents the total geometry effects. The problem then is to determine the changes in the Reynolds stresses along the flow, given the stress distribution at a sufficiently far upstream station. In particular, the initial Reynolds stresses are to be considered as

being anisotropic.

It may be observed that cooling the wall is expected to reduce the upstream interaction length (Reference 29). Some contrary experimental results have been published (Reference 30), but boundary layers are generally expected to become "stiff" and "more full" when the boundary wall is cooled. On the other hand, the anisotropy of Reynolds stresses and turbulent intensities depends also very strongly on wall cooling. In the case of an adiabatic wall, the largest changes across a shockwave arise with respect to intensity in the streamwise direction. The extent of changes in the normal component of intensity is determined by streamline curvature and redistribution of total turbulent kinetic energy by the action of pressure fluctuations. When the boundary wall is cooled, the $v'T'$ correlation is altered considerably. Then similarity between the normal stress intensity and variance of temperature fluctuations requires substantial additional changes in the normal stress component.

The major consideration in analyzing changes in turbulence is the relation between the flow time scales and the time intervals required for adjustment of turbulence to local conditions. It has been suggested that the latter time intervals are rather large compared to the flow time scales and therefore, some of the turbulence processes, for example dissipation, may be "frozen" at the "upstream" level. This can be understood by noting that the main interaction length is comparable to the linear dimension of turbulent eddies. Both the mixing length model, however improved, and the standard Reynolds stress model can be expected to fail (Reference 31) in various ways.

4.3.2. Recommended Solution Procedure

The solution procedure, it is suggested, should include the following considerations.

(1) A means of determining the changes in turbulence structure in the interaction region.

(2) A means of including the disparity in time and length scales through a form of rapid distortion.

(3) A means of modifying the profiles of mean velocity and mean temperature.

The building blocks of the model can be expressed in terms of the following.

(1) The mean momentum and energy balance equations.

(2) The Reynolds stress balance equations.

(3) A representation of local large eddies that can be incorporated into the large eddy interaction model (LEIM) (Reference 32).

And

(4) Rapid distortion approximations in different parts of the wall layer.

A discussion on incorporating those into a model is presented in the following.

4.3.3. Interaction Region Layers

The initial boundary layer is divided into the subsonic and the supersonic layer portions. The viscous sublayer is identified as a part of the subsonic portion of the boundary layer. The interaction region is considered in the same two parts. Equations are set up for describing mean flow properties in the two regions.

4.3.4. Reynolds Stress Balance Equations

The balance equations for Reynolds stress are presented in Appendix II.

4.3.5. Large Eddy Interaction Model

The genesis of large eddy interaction model is given in Reference 32, and the application of the model to adiabatic boundary layers with wall curvature is illustrated in Reference 33, when the fluid is incompressible.

The model is based on (a) orthogonal decomposition of velocity and temperature fluctuations, (b) identification of the first mode as the large eddy, (c) setting up of dynamical equations for velocity and temperature, in which the eddy-eddy interactions are appropriately modelled, and (d) determination of velocity and temperature fluctuation intensity and other correlations in spectral space.

At the current stage of development, the following have been accomplished, namely:

(1) The setting up of the dynamical equations for velocity and temperature under incompressible flow approximations and

(2) The general basis for modelling eddy-eddy interactions.

The latter consists in dividing the influence of eddy-eddy interactions into (a) a skewness factor associated with each of the velocity and velocity-temperature correlations and (b) pseudo turbulent viscosity and conductivity, which are in the nature of damping factors in the dynamical equations. The skewness factor is physically related to the skewness of the probability density function. It is suggested that (a) the two factors are necessary (in order to account for nonlinearity of interactions) and sufficient for closing the dynamical equations and (b) there is appreciable flexibility in the choice of the magnitude of the two factors in application to a given flowfield.

The suggested procedure for solution is as follows.

(1) The Reynolds stress equations are written as in Appendix II and also in the rapid distortion approximation.

(2) The large eddy interaction model for incompressible flow is utilized in conjunction with the compressible mean flow equations to determine the mean flow and the closure parameters, namely the skewness factor and the pseudo eddy coefficients.

(3) The rapid distortion equations are then solved utilizing the information generated in (2) above.

(4) The procedures in (2) and (3) are repeated iteratively until the Reynolds stress balance equations are satisfied.

SECTION 5

DISCUSSION

A plug nozzle with turbulent flow and with a secondary coolant stream admitted parallel to the plug wall has been the subject of the investigation. Attention has been focussed on flows that do not involve separation. Thus, although both weak and strong shockwaves are expected to be generated during the interaction between the primary hot gas stream and the coolant cold gas stream, only shockwaves in near-transonic flow Mach number regime, such as those occurring close to the coolant admission station, are considered. However, such separationless interactions may also arise in the region of impingement of shocks that may be generated immediately downstream of the throat section due to the strong turning of the flow.

5.1. Status

(1) The establishment of interaction between the coolant stream and the primary stream has been limited by the assumption of inviscid flow in both streams and further by considering the tip of the dividing wall between the two streams as being sharp and without a "base". However, the inviscid interaction code does permit the main features of the flowfield, including the possible occurence of shockwaves, to be determined for given sets of initial conditions in the two streams.

The numerical codes for the foregoing prediction are suitable for use in the subsonic, transonic and supersonic regions.

The inviscid interactions are particularly of interest in determining the nature of flowfield changes that arise on account of the coolant stream, which is admitted

generally in a region with transonic or slightly supersonic velocity, and may be subsonic, choked or supersonic. The manner in which the two streams develop with a dividing surface between them depends upon the coolant stream initial conditions relative to the local primary stream conditions. For example, it is shown that a coolant stream which enters the nozzle at a subsonic speed, determined by the local static pressure of the primary stream, may accelerate to sonic speed along the nozzle plug wall and may further accelerate to supersonic speed towards the nozzle exit. It is clear that a turbulent mixing layer between the two streams can be expected to modify the acceleration process. However, the inviscid, non-diffusing flow prediction can serve as a basis for further refinements.

(2) A numerical code received from NASA Langley Research Center has been modified for use in the case of a plug nozzle with a coolant gas stream flow along the plug. Account is taken of the pressure gradient along the flow and of the mixing between the two streams, but the flow is assumed to be continuous without shockwaves or separation.

Calculations have been performed with the free stream conditions as determined from selected NASA experimental data and also as determined from calculations of inviscid flow interactions as discussed in (1) above. Although heat flux to the wall was established in both cases, it was not found feasible to compare the predictions with experimental data, principally due to the uncertainty of the latter.

The free stream boundary conditions obtained from experimental data are also subject to uncertainty. However, the skin friction coefficient, Stanton number and heat flux values obtained with such free stream boundary conditions differ from those based

on inviscid interaction between the primary and the secondary streams.

The experimental data indicate the occurence of shockwaves. This is reflected in predictions through inclusion of a discontinuity in free stream velocity and static pressure distributions. In view of changes in those quantities across the nozzle, some ambiguity exists in the selection of free stream conditions corresponding to the edge of the thermal boundary layer.

The greatest uncertainty in these predictions, both in the continuous flow regime and in the shock-occurring regime is in accounting for turbulence. Both mixing and the wall boundary regions are affected by turbulence. The turbulence model has been retained in the modified code in the same form as originally incorporated into the NASA Langley Research Center code: namely, the use of a mixing length model both in the mixing layer and in the boundary layer.

(3) The shockwave-boundary layer interaction has been examined only in the case of a transonic shock with no flow separation. However, even in that case, no overall prediction scheme has been set up. The main emphasis has been on the analysis of changes in turbulence in the interaction region.

The main feature of shockwave-boundary layer interaction in a case such as the plug nozzle is the influence of heat transfer, for example to the plug surface. Unfortunately, no experimental data are available on mean flow and turbulence quantities in self-consistent experimental configurations with (nearly) adiabatic walls and variously cooled walls. The overall effects of wall cooling on mean flow distribution have been known for some time. However, it is rather unsatisfactory to utilize correlations of such data in a case with a secondary coolant stream. In any case, very

few data are available to determine the influence of heat transfer on turbulence quantities.

Predictions of mean flow and such quantities as shear stress and other turbulence quantities have been shown to be unsatisfactory by other investigators even in the case of uncooled walls whether based on two-equation or Reynolds stress modelling. The uncertainties in the latter have been made clear in Appendices II and III of this Report, wherein a detailed development has been presented for the Reynolds-averaged Navier-Stokes equations and the use of wall functions for wall-bounded flows.

Two procedures have been elaborated in the current report, largely as providing opportunities for extension. Both procedures deal with methods for determining turbulence development in regimes with rapid changes in mean flow. In a sense they may be considered to be complementary. At the current level of development, they both require a definition of mean flow development.

In the large eddy interaction model, two major uncertainties are (1) the influence of presure fluctuations and (2) the matching between subsonic and supersonic portions of the boundary layer.

5.2. Future Developments

Based on the current status, one can conclude the following.

(1) The flow interaction prediction code needs to be extended so as to take into account (a) a mixing layer between the two streams and (b) a finite thickness tip at the point of admission of the coolant stream.

A zonal approach that permits interaction between the coolant stream and the primary stream can be developed: The coolant stream is then considered as a wall jet, in turn as a combination of a jet and a boundary layer; the mixing layer between them is modelled insofar as mean flow and growth are concerned; finally, the three zones are matched entirely on the basis of gas dynamic interactions.

(2) The problem of turbulence modelling is common to both adiabatic and cooled wall configurations. The most urgent need here is for a set of test data on a single configuration that consists of a simple flat plate with a weak shockwave impinging on it and in which a number of wall temperature boundary conditions can be set up. The flow details required are distributions of mean flow, turbulence quantities, spectra and various probability density functions. Both attached and separated flows are of interest.

One major question to be answered pertains to the extent to which rapid distortion approximations are valid in different parts of the developing interaction region. For an example, a division of the interaction region into initiation, upstream, most dominant, downstream and relaxing zones will be helpful. For another example, any relation between outer and inner portions of a wall layer in the interaction region without and with wall cooing will be helpful.

(3) A prediction code needs to be developed, calibrated and validated for a model based on a combination of rapid distribution and large eddy interaction principles. Such a prediction code will serve also to calibrate other models such as two-equation and Reynolds stress models on selected term-by-term basis.

REFERENCES

1. Straight, D.M., Effect of Shocks on Film Cooling of a Full Scale Turbojet Exhaust Nozzle Having an External Expansion Surface," *AIAA* 79-1170, June 1979.

2. Nosek, S.M. and Straight, D.M., "Heat Transfer Characteristics of Partially Film Cooled Plug Nozzle on a J-85 After-burning Turbojet Engine," NASA TM X-3367, March, 1976.

3. Nosek, S.M. and Straight, D.M., "Heat Transfer Characteristics of Partially Film Cooled Plug Nozzle on a J-85 Afterburning Turbojet Engine," NASA TM X-3362, March 1976.

4. Straight, D.M., Harrington, D.E. and Nosek, S.M., "Experimental Cold-Flow Evaluation of a Ram-Cooled Plug Nozzle Concept for Afterburning Turbojet Engines," NASA TMX-2811, June 1973.

5. Jeracki, R.J. and Chenoweth, F.C., "Coolant Flow Effects on the Performance of a Conical Plug Nozzle at Mach Numbers from 0 to 20," NASA TM X-2076, September 1970.

6. Clark, J.S. and Liebermann, A., "Thermal Design Study of an Air-Cooled Plug Nozzle System for a Supersonic-Cruise Aircraft," NASA TM X-2475, January 1972.

7. Graber, E.J. and Clark, J.S., "Comparison of Predicted and Experimental Heat Transfer and Pressure-Drop Results for an Air-Cooled Plug Nozzle and Supporting Struts," NASA TN D-6764, 1972.

8. Straight, D.M., "Test Data on Air-Cooled Plug Nozzle," private communications.

9. Goldstein, R.J., *Advances in Heat Transfer*, Vol. 7, Academic Press, 1971.

10. Beckwith, I.E. and Bushnell, D.M., "Calculation by a Finite-Difference Method of Supersonic Turbulent Boundary Layers with Tangential Slot Injection", NASA Langley Research Center Report, March 1971.

11. Hixon, B.A., Beckwith, I.E., and Bushnell, D.M., "Computer Program for Compressible Laminar or Turbulent Nonsimilar Boundary Layers", NASA Technical Memorandum No. NASA TMX-2140, April 1971.

12. Cebeci, T. and Smith, A.M.O., "Calculation of Compressible Adiabatic Turbulent Boundary Layers," *AIAA* 69-087, 1969.

13. Herring, J.H. and Mellor, G.L., "A Method of Calculating Compressible Turbulent Boundary Layers," NASA CR-1144, 1968.

14. Liepmann, H.W., "The Interaction Between Boundary Layer and Shock Waves in Transonic Flow," *J. Aero. Sci.*, December, 1946.

15. Walz, A., Stromungs- and Temperatur-grenzshiechten, *Verlag G Brawn*, Karlsruhe.

16. Hinze, J.O., "*Turbulence*", second edition, McGraw Hill Book Co., New York, 1976.

17. Delery, J. and Marvin, J.G., "Shock Wave Boundary Layer Interactions," AGARD-AG-280, February, 1986.

18. Inger, G.R., "Application of a Shock-Turbulent Boundary Layer Interaction Theory in Transonic Flowfield Analysis," Ch. 17 in *Transonic Aerodynamics*, Vol. 81, Progress in Astronautics and Aeronautics, *AIAA*, 1982.

19. Vandromme, D. and Hamin, H., "Numerical Study of Reynolds Stress in Compressible Flows," *Physico Chemical Hydrodynamics*, Vol. 6, Nos. 5/6, 1986.

20. Lighthill, M.J., "On Boundary Layers and Upstream Influence, II. Supersonic Flow with Separation," *Proc. Roy. Soc. A.*, Vol. 217, 1953.

21. Tu, K.M. and Weinbaum, S., "A Non-Asymptotic Triple-Deck Model for Supersonic Boundary Layer Interaction," *AIAA Journal*, Vol. 14, 1976.

22. Inger, G.R., "Analysis of Transonic Shock Interaction with Nonadiabatic Turbulent Boundary Layers," *AIAA* 76-463, July 1963.

23. Inger, G.R., Lynch, F.T., and Fancher, M.F., "A Theoretical and Experimental Study of Non-Adiabatic Wall Effects on Transonic Shock/Boundary Layer Interaction," Paper 83-1421, 1983.

24. Lynch, F.T., Fancher, M.F., and Patel, D.R., and Inger, G.R., "Nonadiabatic Model Wall Effects on Transonic Airfoil Performance in a Cryogenic Wind Tunnel," AGARD CP 283, September 1983.

25. Coles, D.E., "The Law of the Wake in Turbulent Boundary Layers," *J. Fluid Mech.*, Vol. 1, 1966.

26. Bohning, R. and Zierep, J., "Normal Shock Turbulent Boundary Layer Interaction," AGARD-CP-291, 1981.

27. Hankey, W.L., and Holden, M.S., "Two-Dimensional Shockwave-Boundary Layer Interactions in High Speed Flows," AGARDograph AGARD-AG-203, 1979.

28. Messiter, A.F., and Adamson, T.C., "On the Flow Near a Weak Shock Wave Downstream of a Nozzle Throat," *J. Fluid Mech.*, Vol. 69, 1975.

29. Agarwal, S. and Messiter, A.F., "Turbulent Boundary-Layer Interaction with a Shockwave at a Comparison Corner," *J. Fluid Mech.*, Vol. 143, 1984.

30. Padova, C., Falk, T.J. and Wittliff, C.E., "Experimental Investigation of Similitude Parameters Governing Shockwave Boundary Layer Interaction," *AIAA* 80-0158, 1980.

31. Andonceau, P.L., "The Structure of Turbulence in a Supersonic Shockwave/Boundary Layer Interaction," *AIAA J.*, Vol. 22, No. 9, Sept. 1984.

32. Hong, S.K., "Large Eddy Interactions in Curved Wall Boundary Layers," Ph.D. Thesis, Purdue University, Aug. 1983.

33. Hong, S.K. and Murthy, S.N.B., "On Effective Velocity of Transport in Curved Wall Boundary Layers," *AIAA J.*, Vol. 24, March 1986.

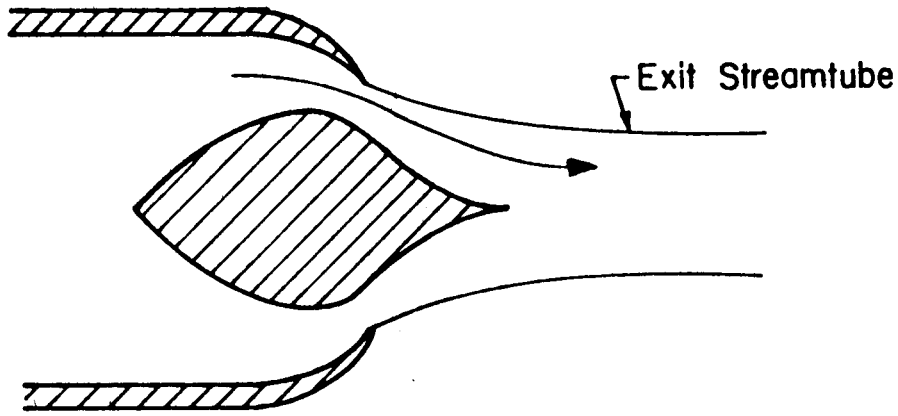

a) Overexpanded nozzle (pressure ratio below design)

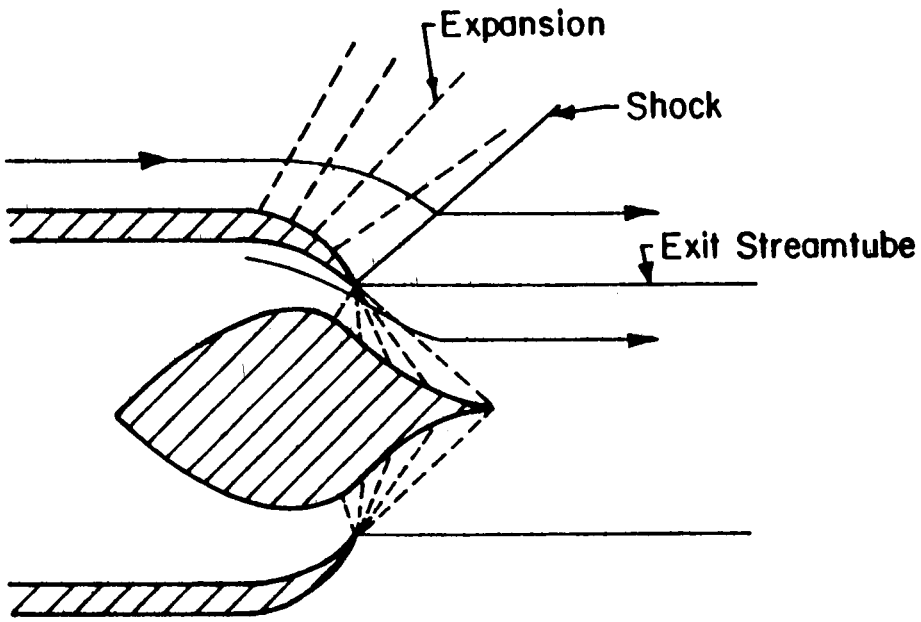

b) Ideally expanded nozzle

Figure 1.1. Schematic of a plug nozzle.

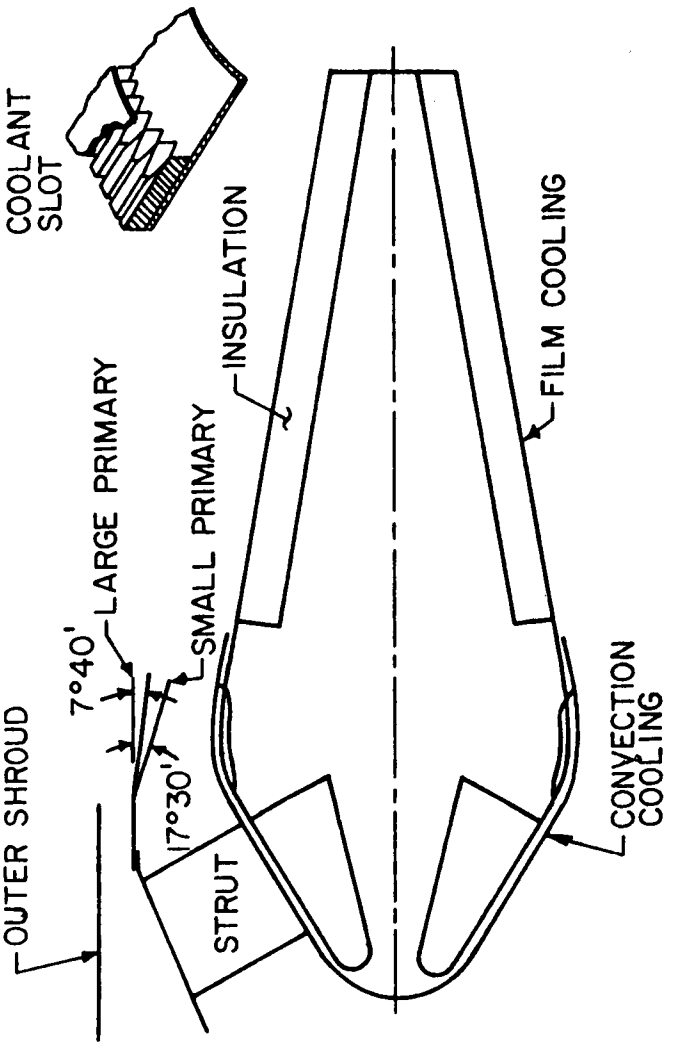

Figure 1.2. NASA nozzle configuration (continued)

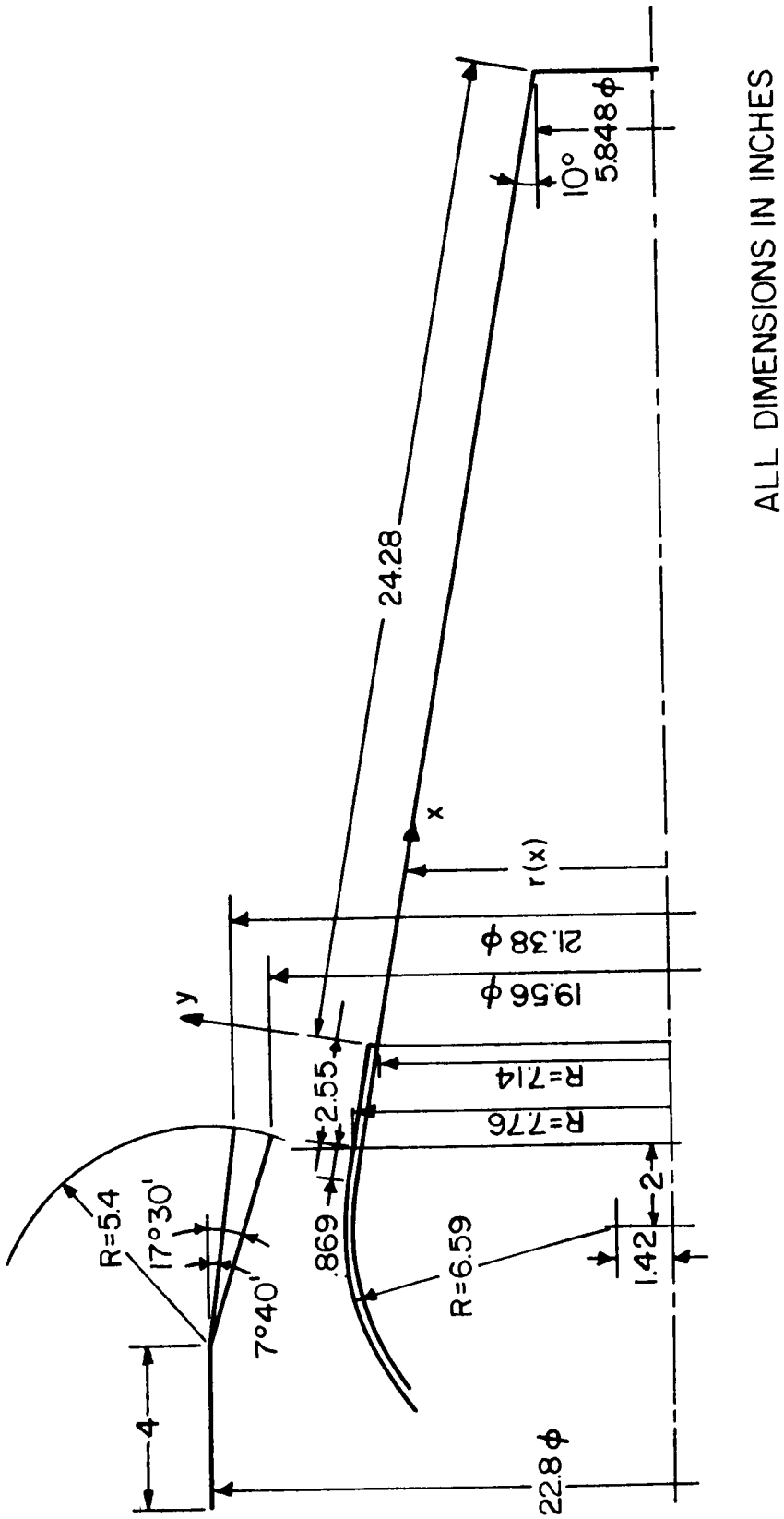

Figure 1.2. NASA nozzle configuration (concluded)

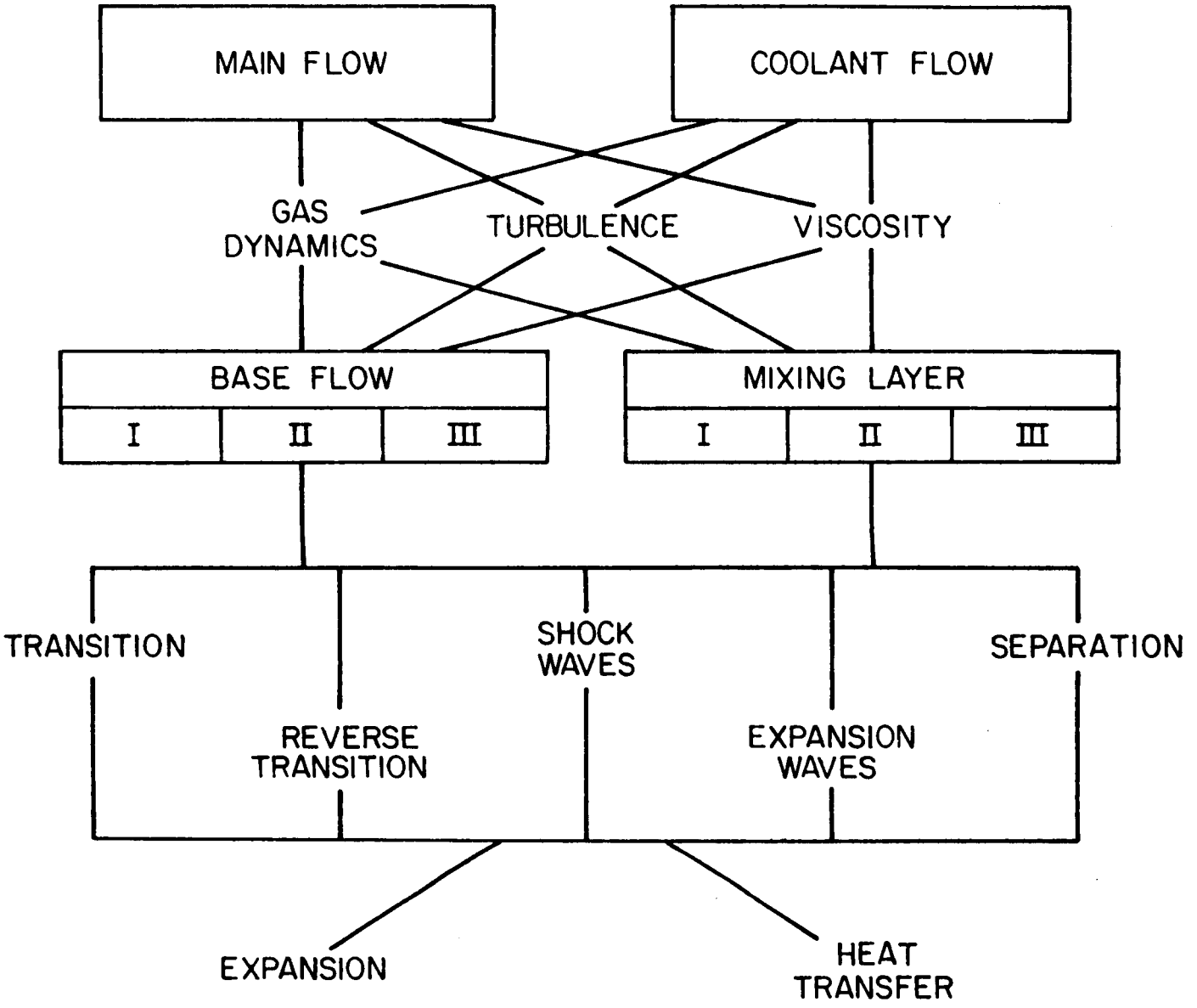

Figure 2.1. Flow interactions in a plug nozzle. I at nozzle outer wall; II at coolant stream wall; and III at end of plug.

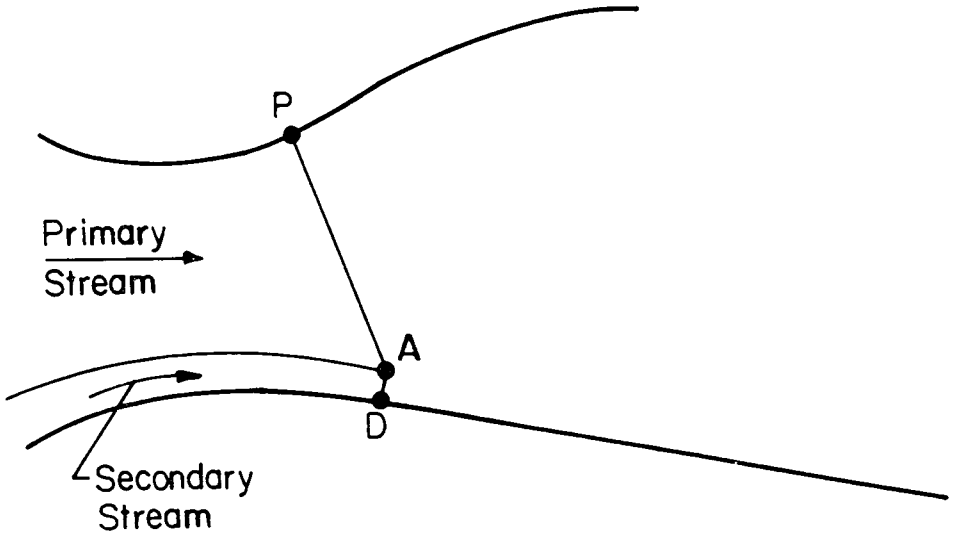

Figure 2.2. Flowfield analyzed

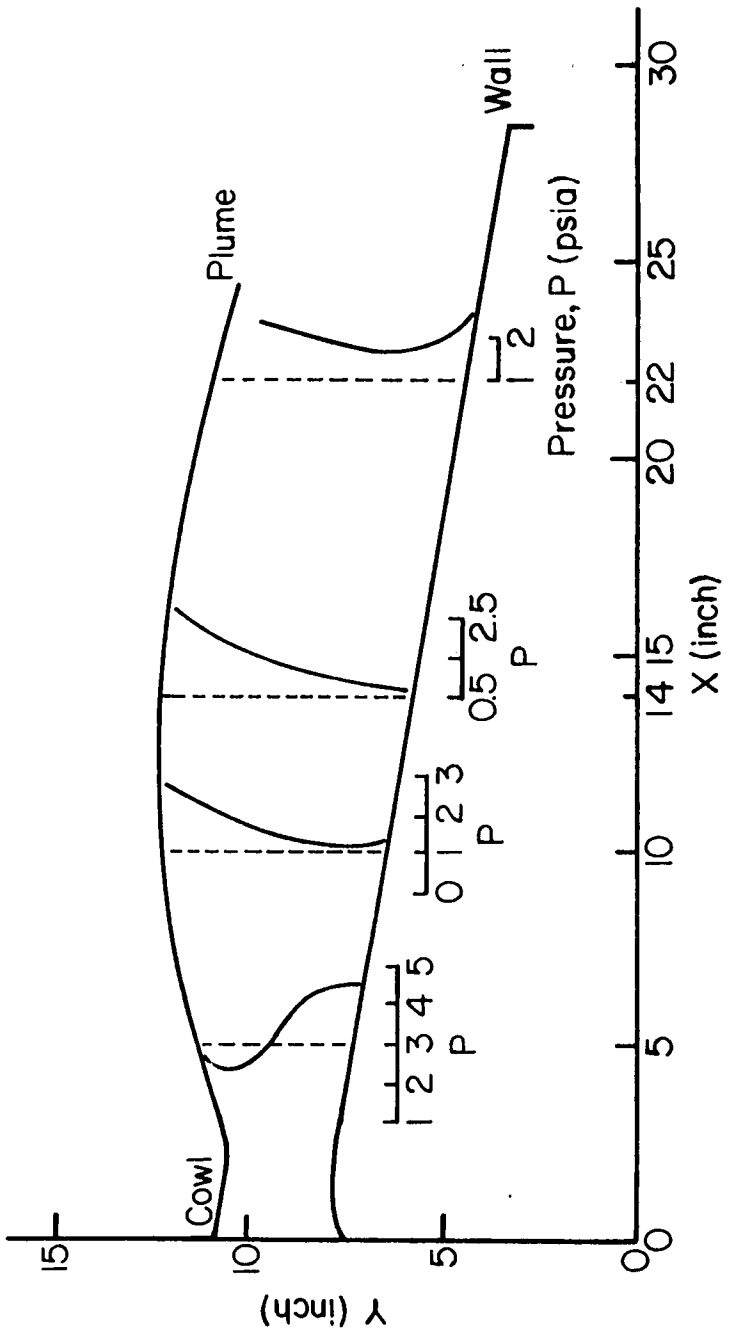

Figure 2.3. Prediction for Case 1: Distribution of static pressure along the flow

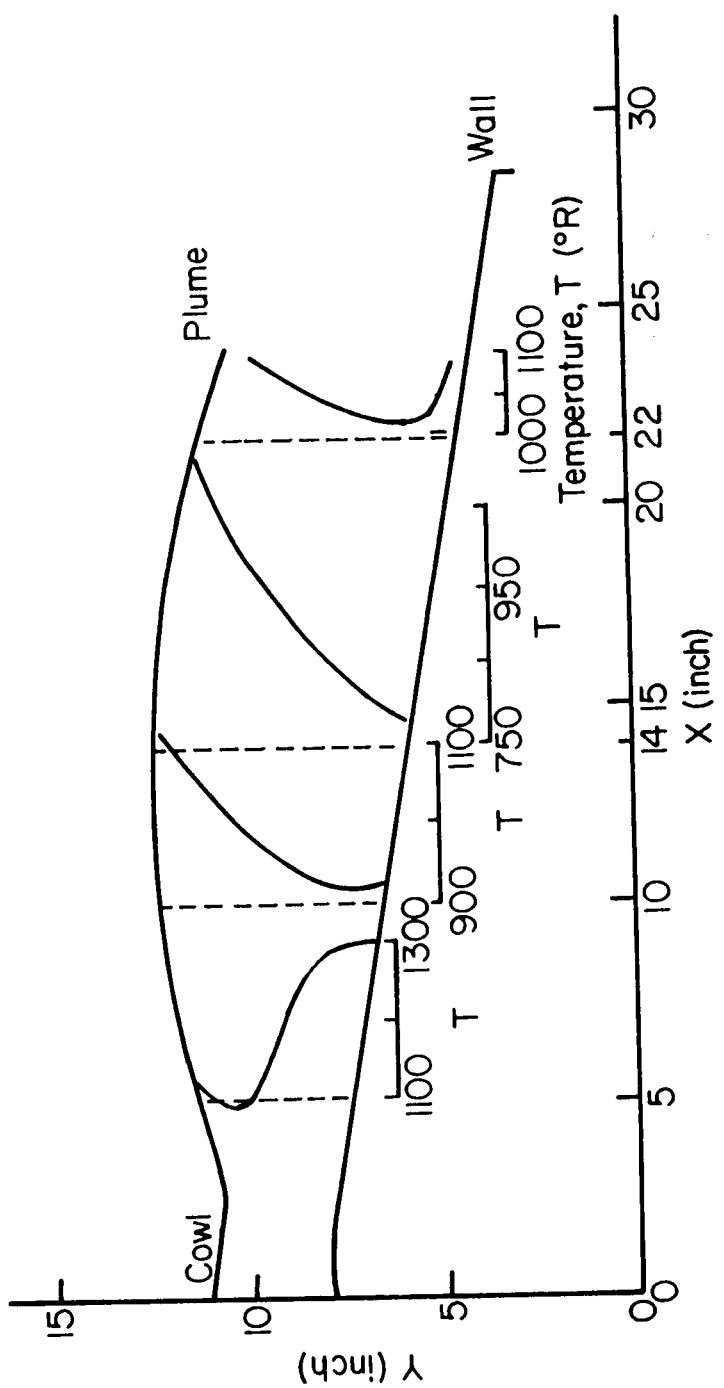

Figure 2.4. Prediction for Case 1: Distribution of static temperature along the flow

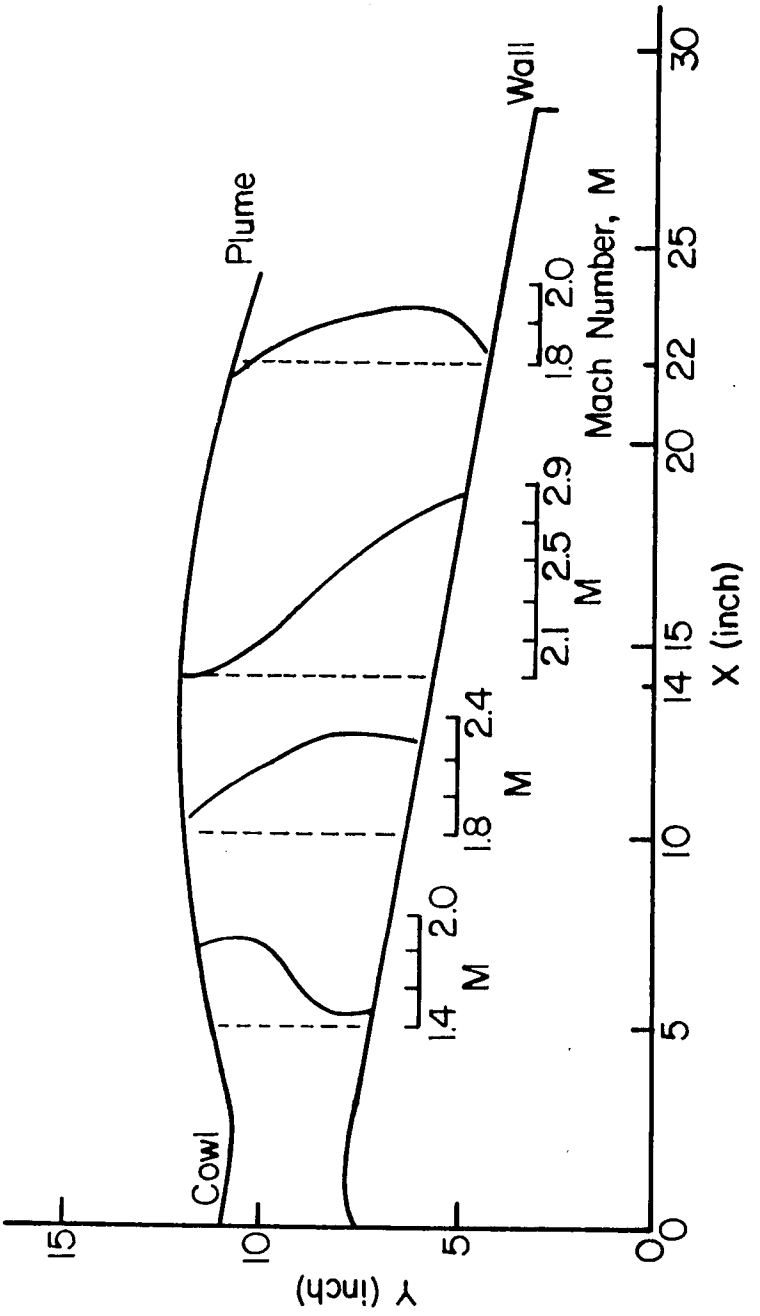

Figure 2.5. Prediction for Case 1: Distribution of Mach number along the flow

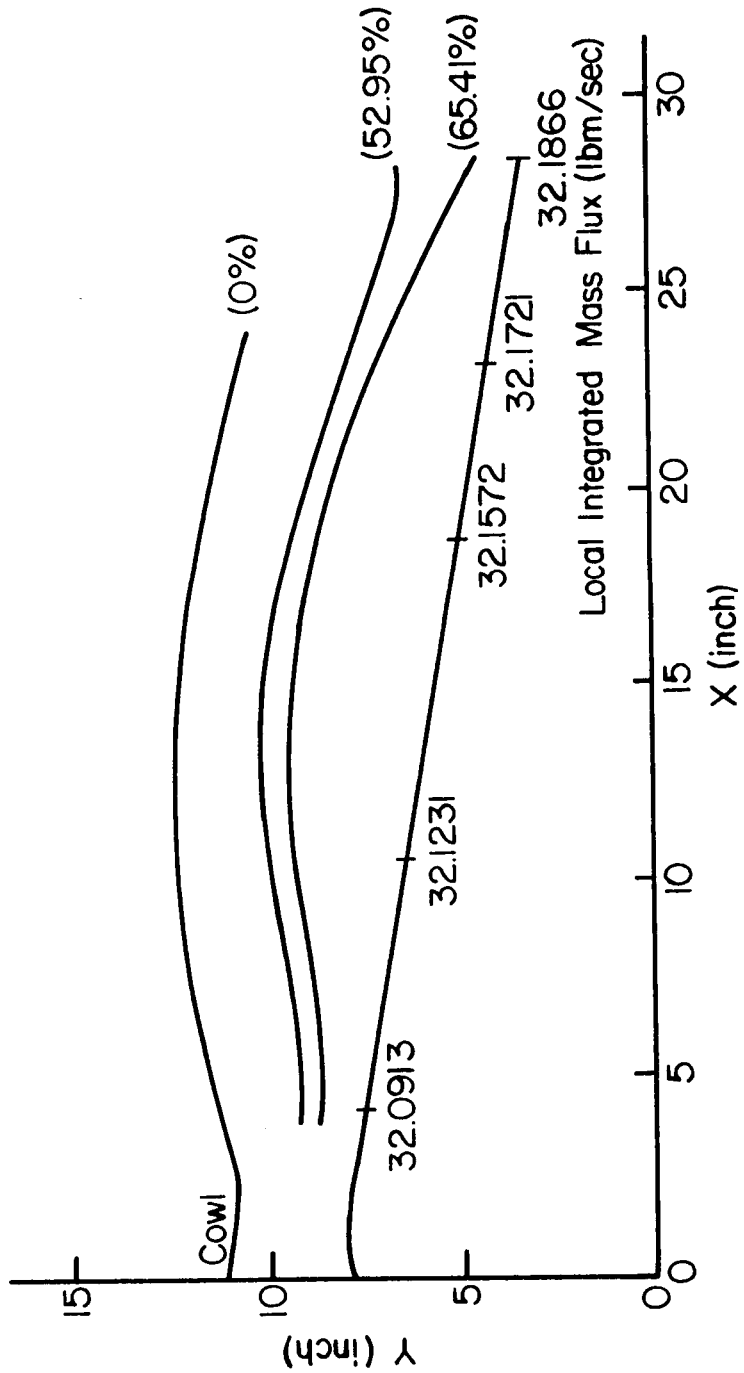

Figure 2.6. Prediction for Case 1: Distribution of mass flux along the flow

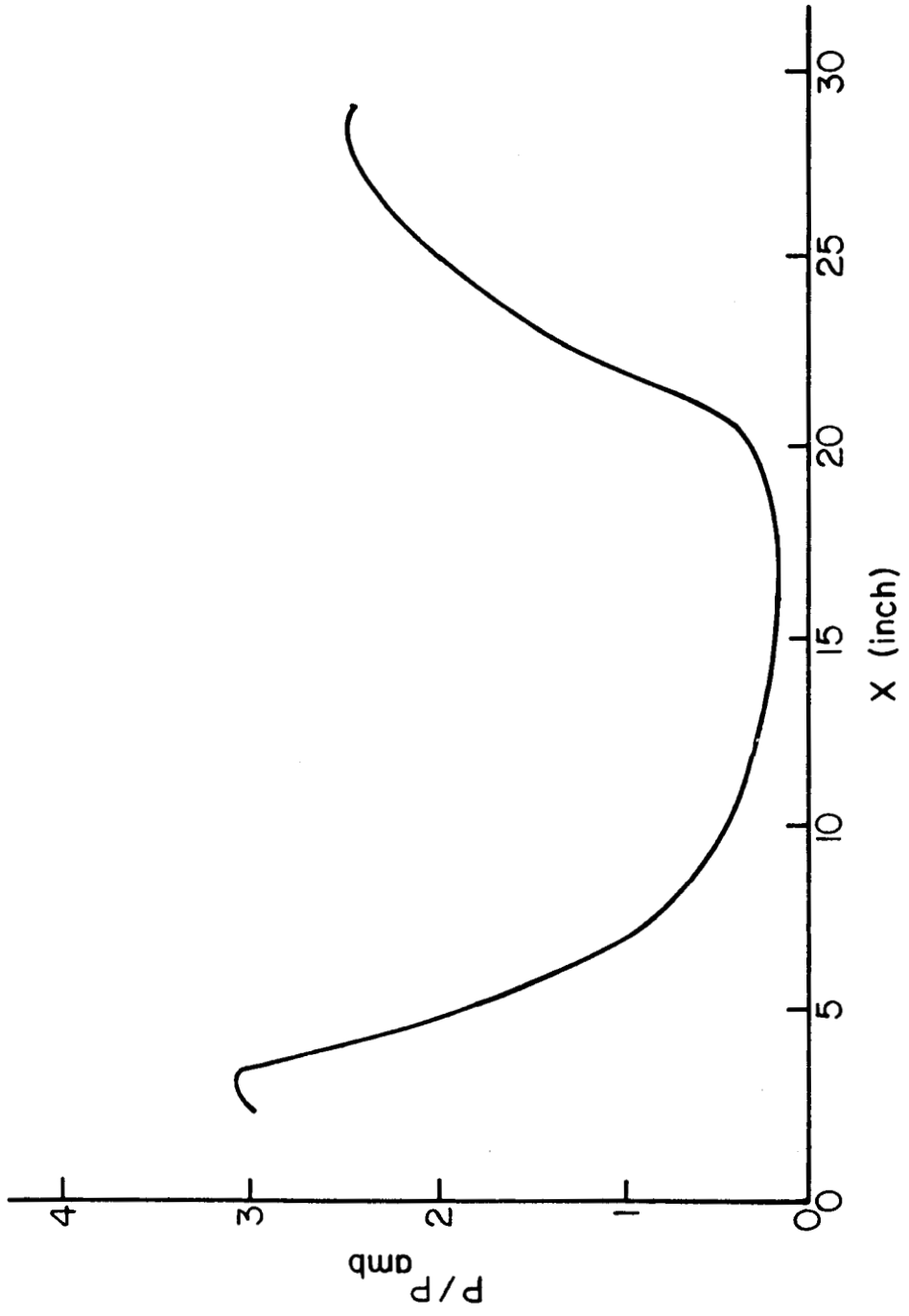

Figure 2.7. Prediction for Case 1: Distribution of static pressure along the plug wall

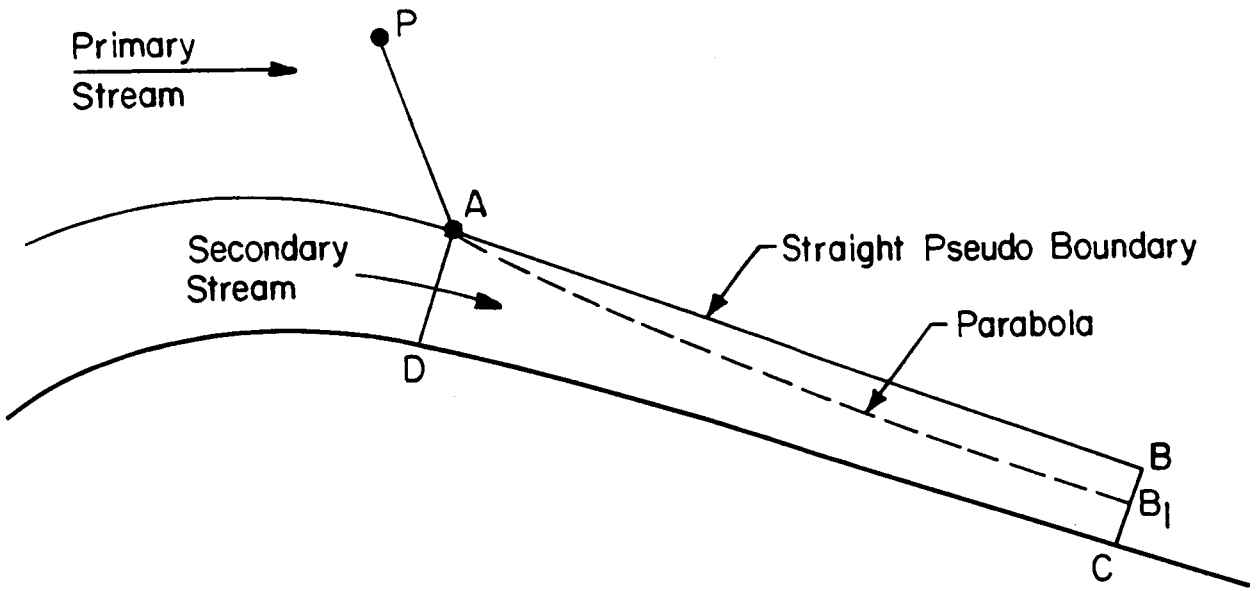

Figure 2.8. Flowfield interaction in Case 2

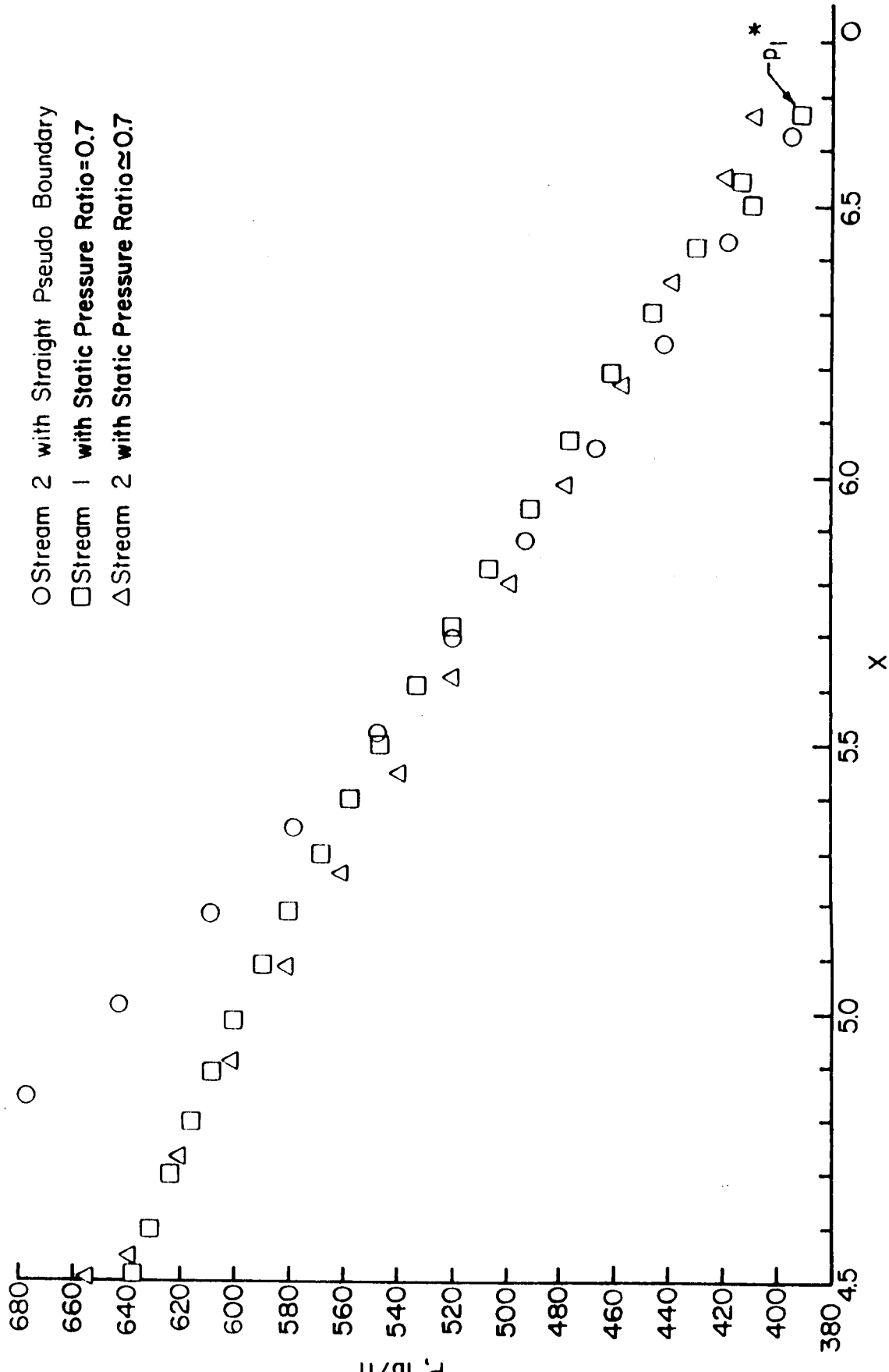

Figure 2.9. Static pressure distributions along joining surface between primary and coolant streams in Case 2. p_1* is choking value of static pressure

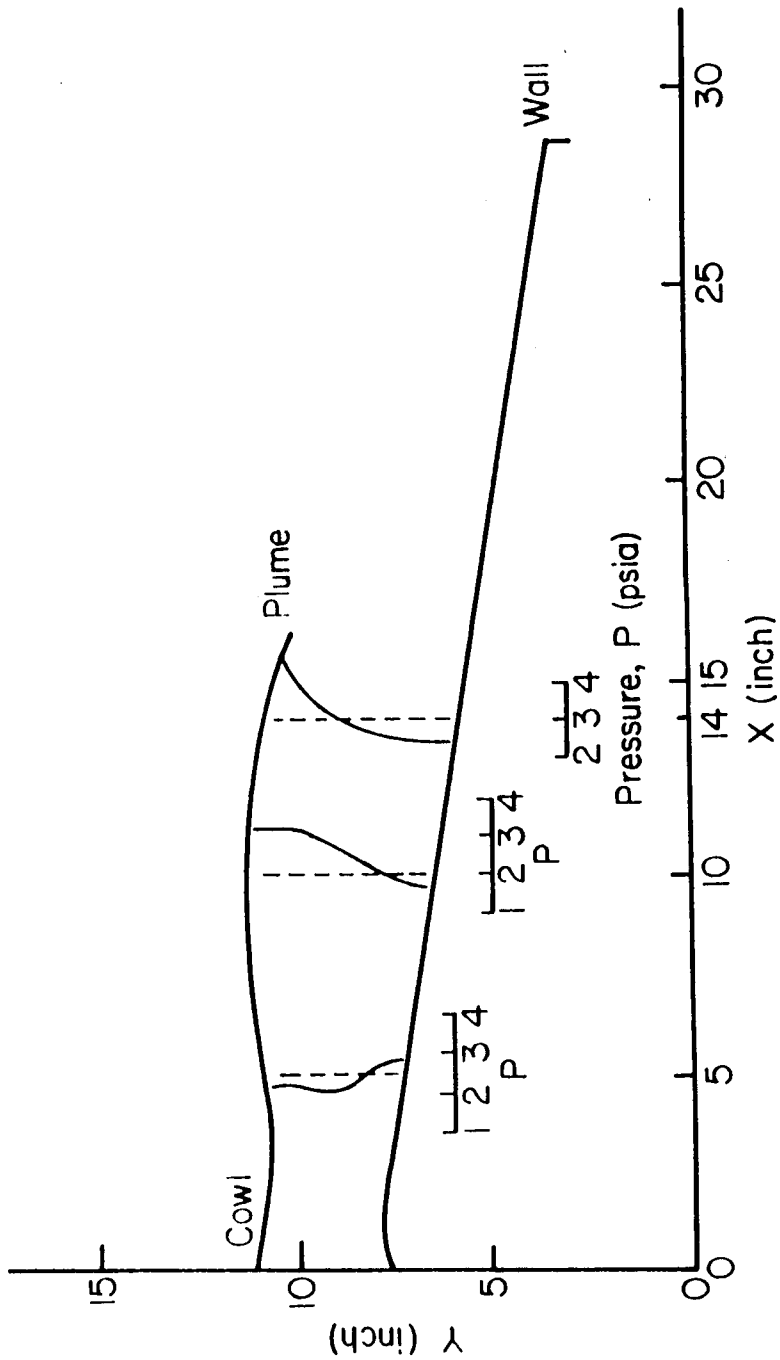

Figure 2.10.1. Case 2: Nozzle pressure ratio = 4.0. Static pressure distribution along flow

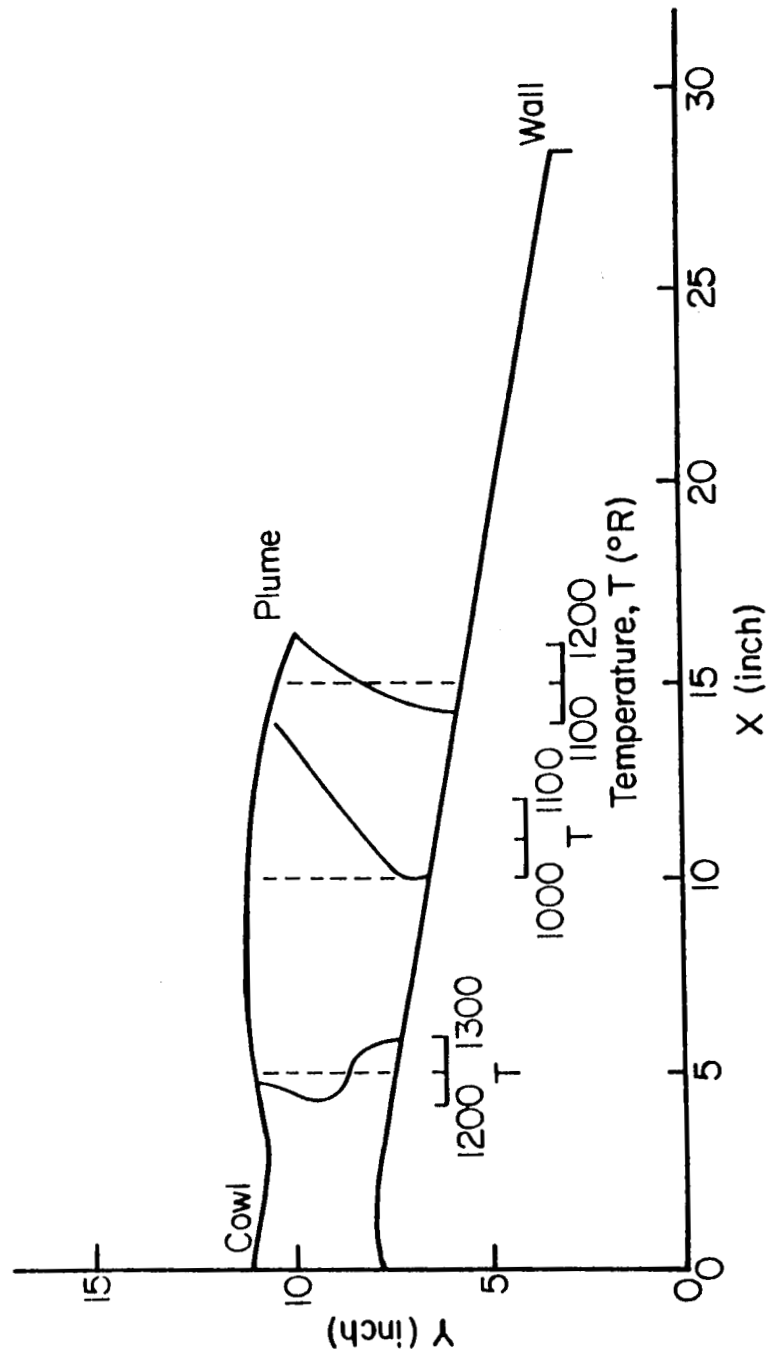

Figure 2.10.2. Case 2: Nozzle pressure ratio = 4.0. Static temperature distribution along flow

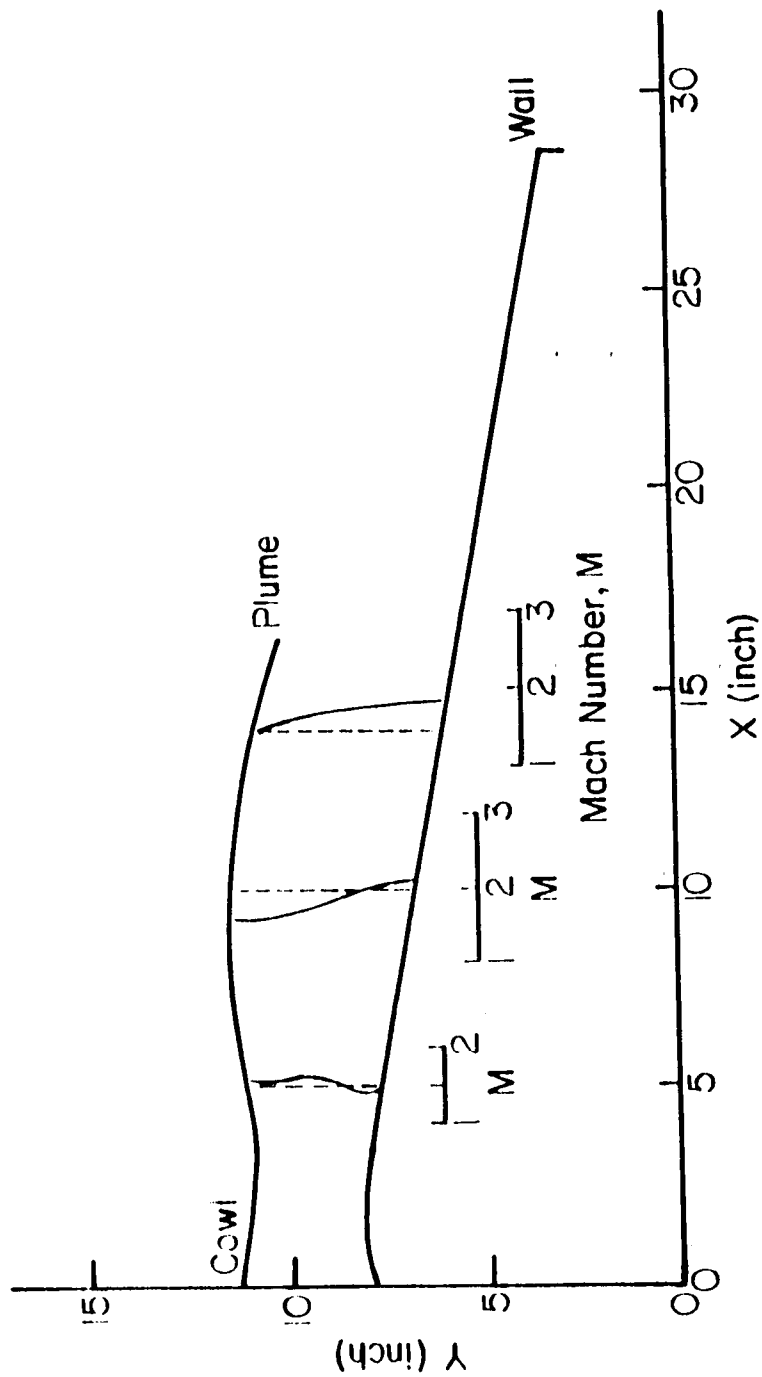

Figure 2.10.3. Case 2: Nozzle pressure ratio = 4.0. Mach number distribution along flow

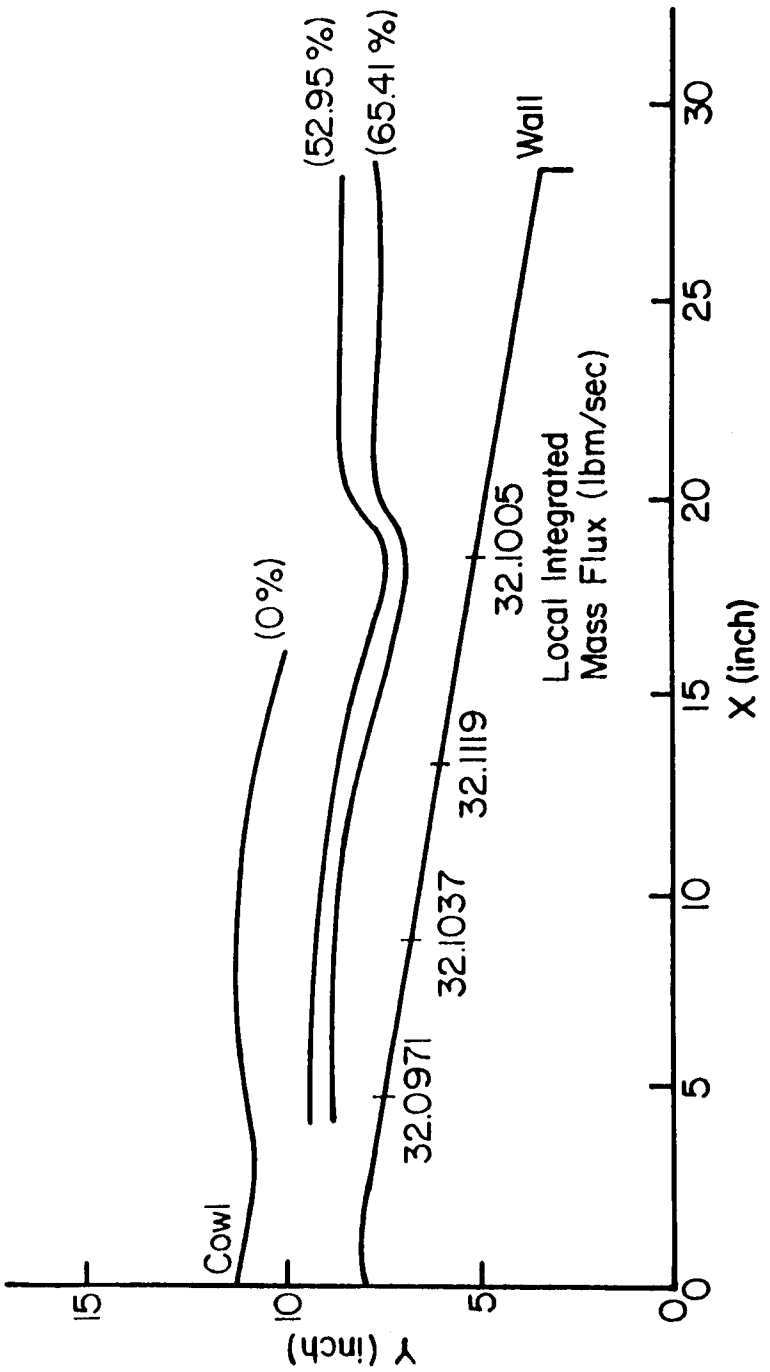

Figure 2.10.4. Case 2: Nozzle pressure ratio = 4.0. Mass flux distributions along flow

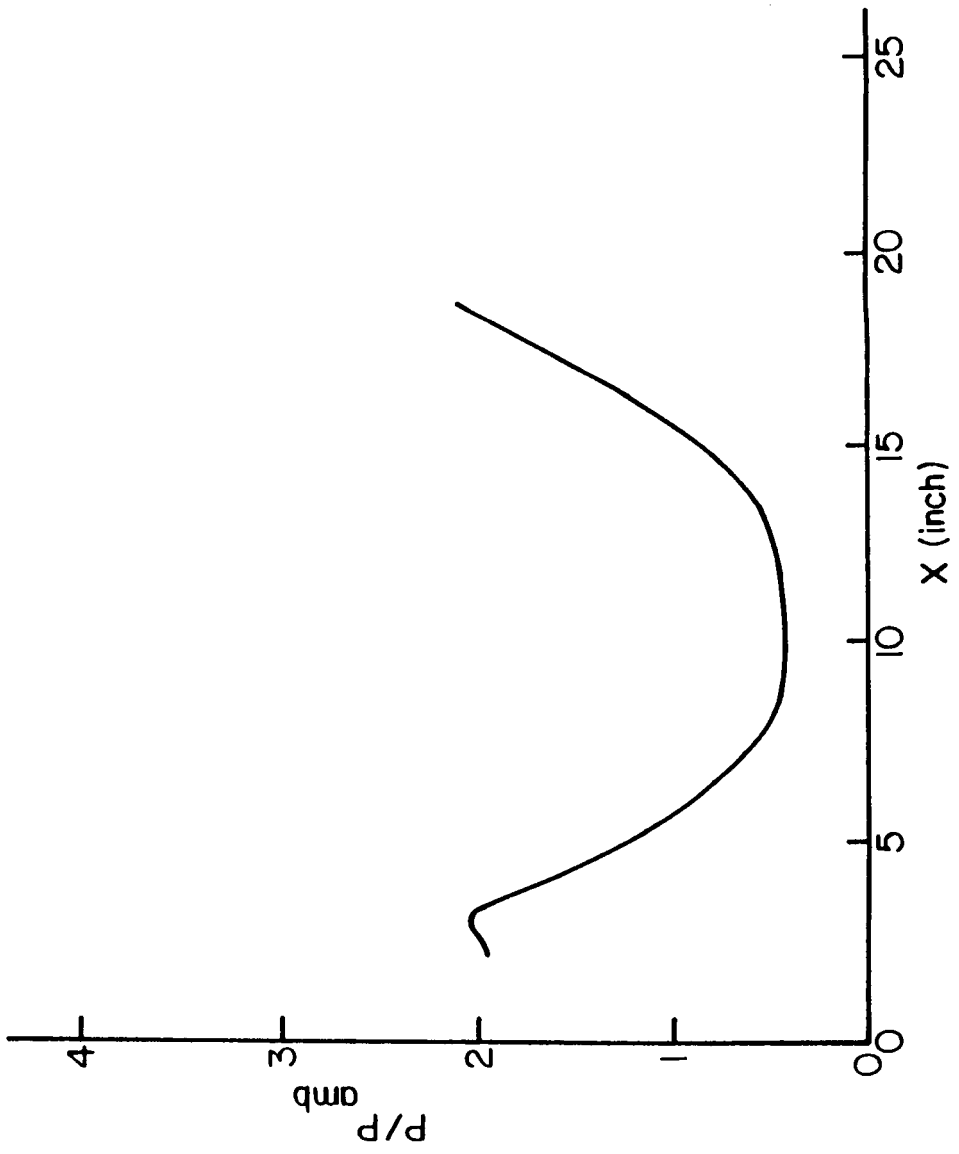

Figure 2.10.5. Case 2: Nozzle pressure ratio = 4.0. Static pressure distribution along plug wall

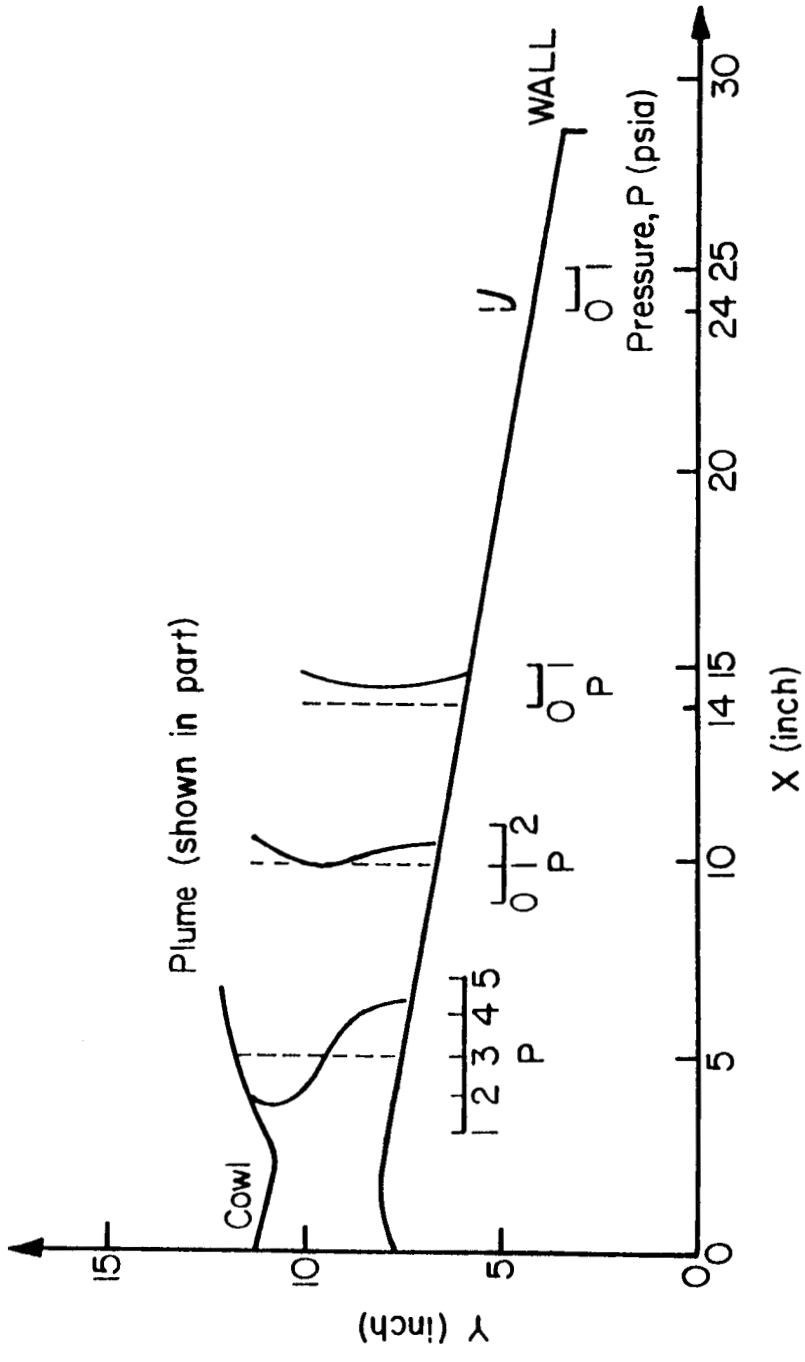

Figure 2.11.1. Case 2: Nozzle pressure ratio = 8. Static pressure distributions along plug wall

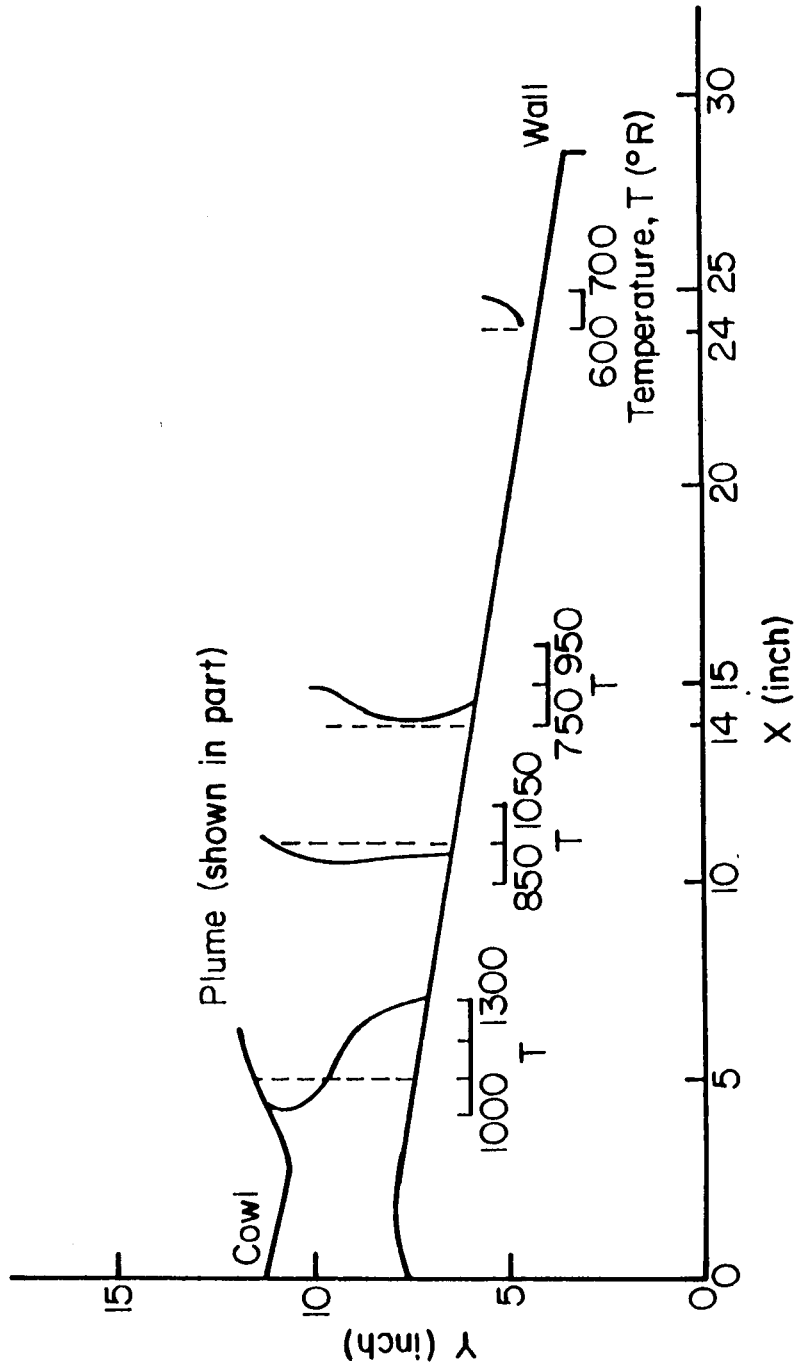

Figure 2.11.2. Case 2: Nozzle pressure ratio = 8. Static temperature distribution along flow

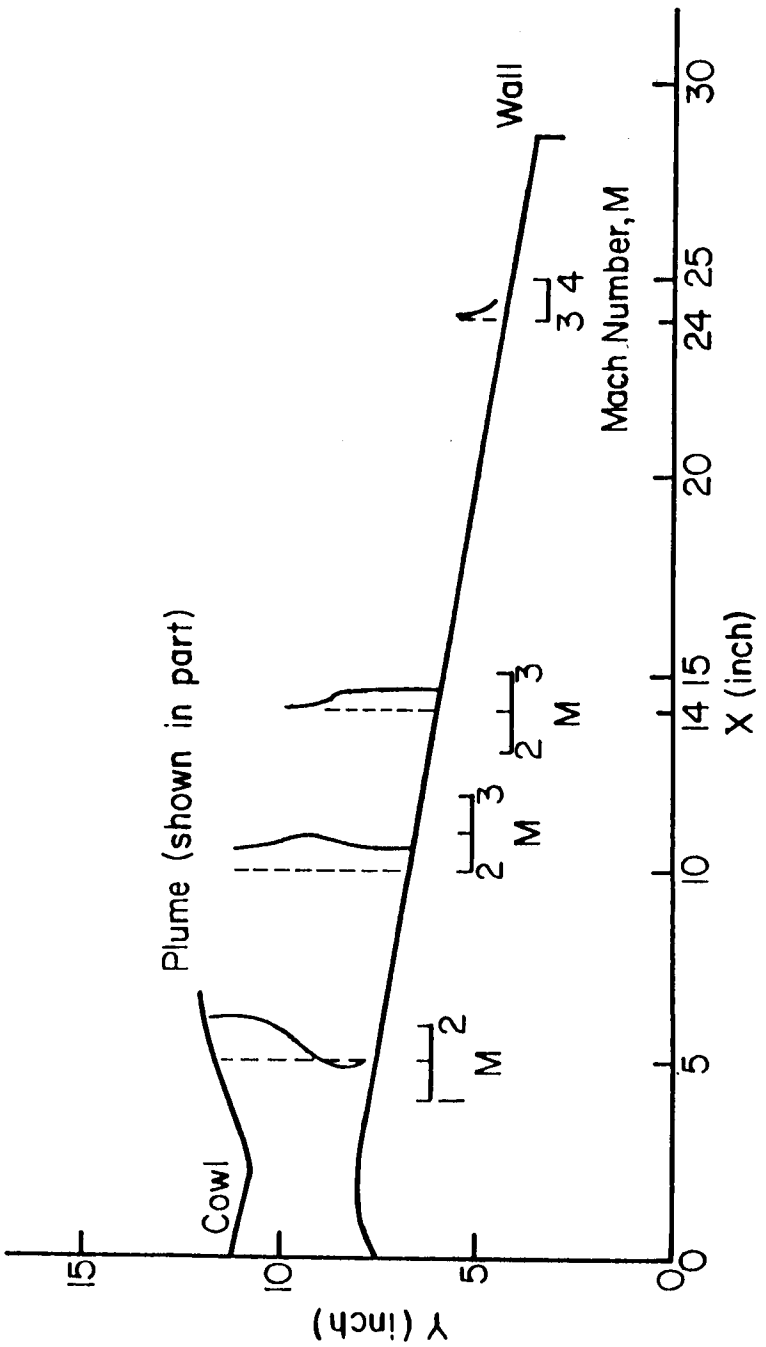

Figure 2.11.3. Case 2: Nozzle pressure ratio = 8. Mach number distribution along flow

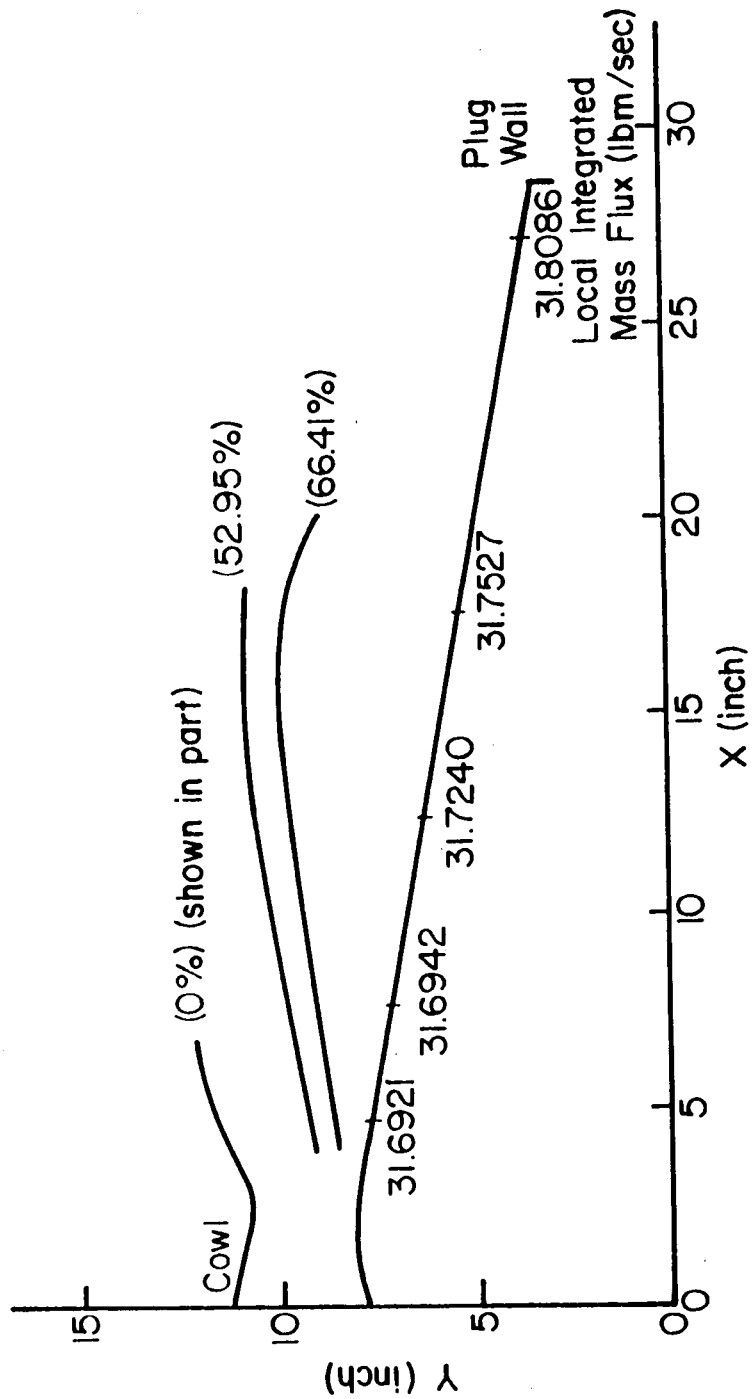

Figure 2.11.4. Case 2: Nozzle pressure ratio = 8. Mass flow distributions along flow

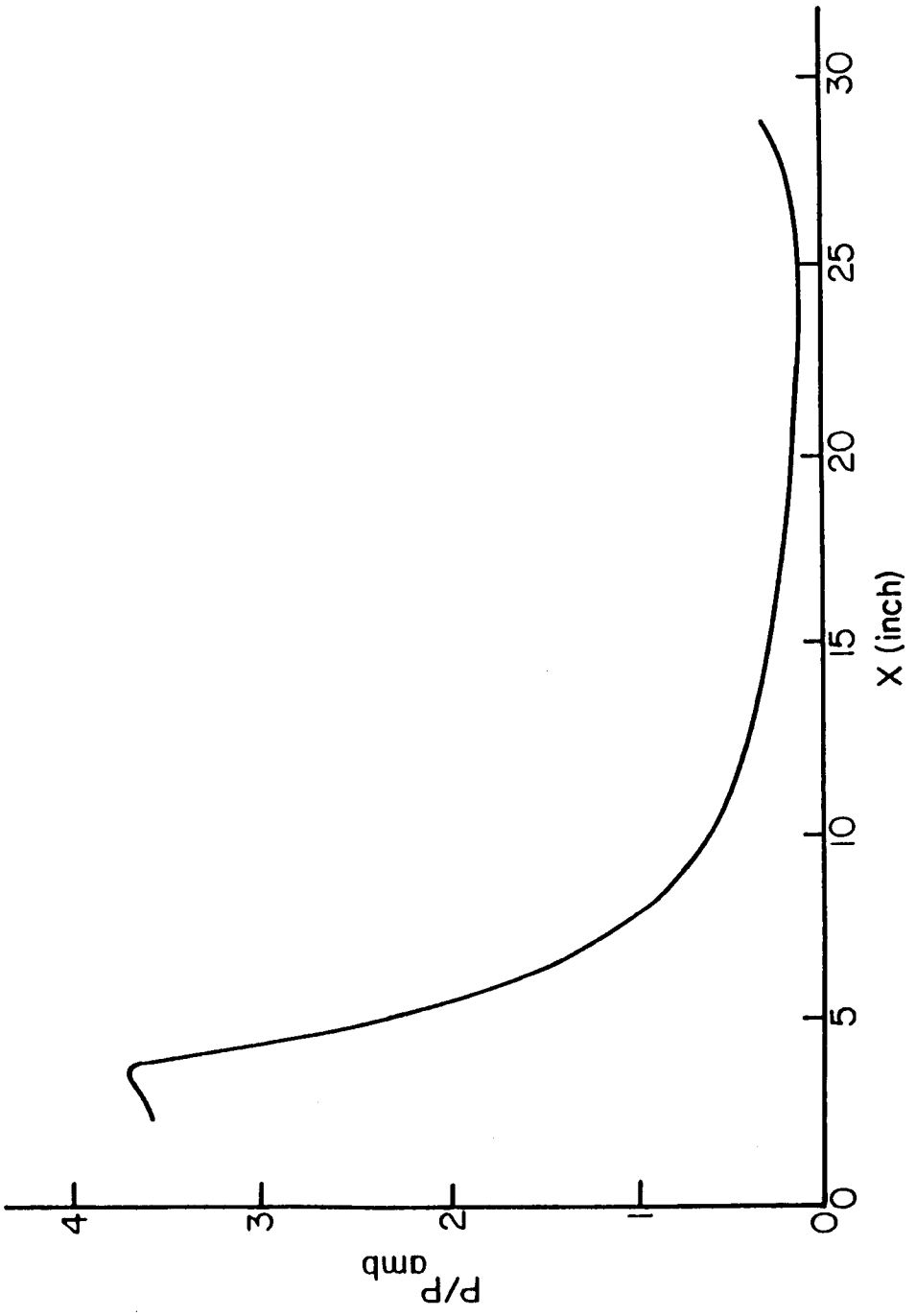

Figure 2.11.5. Case 2: Nozzle pressure ratio = 8. Static pressure distribution along plug wall

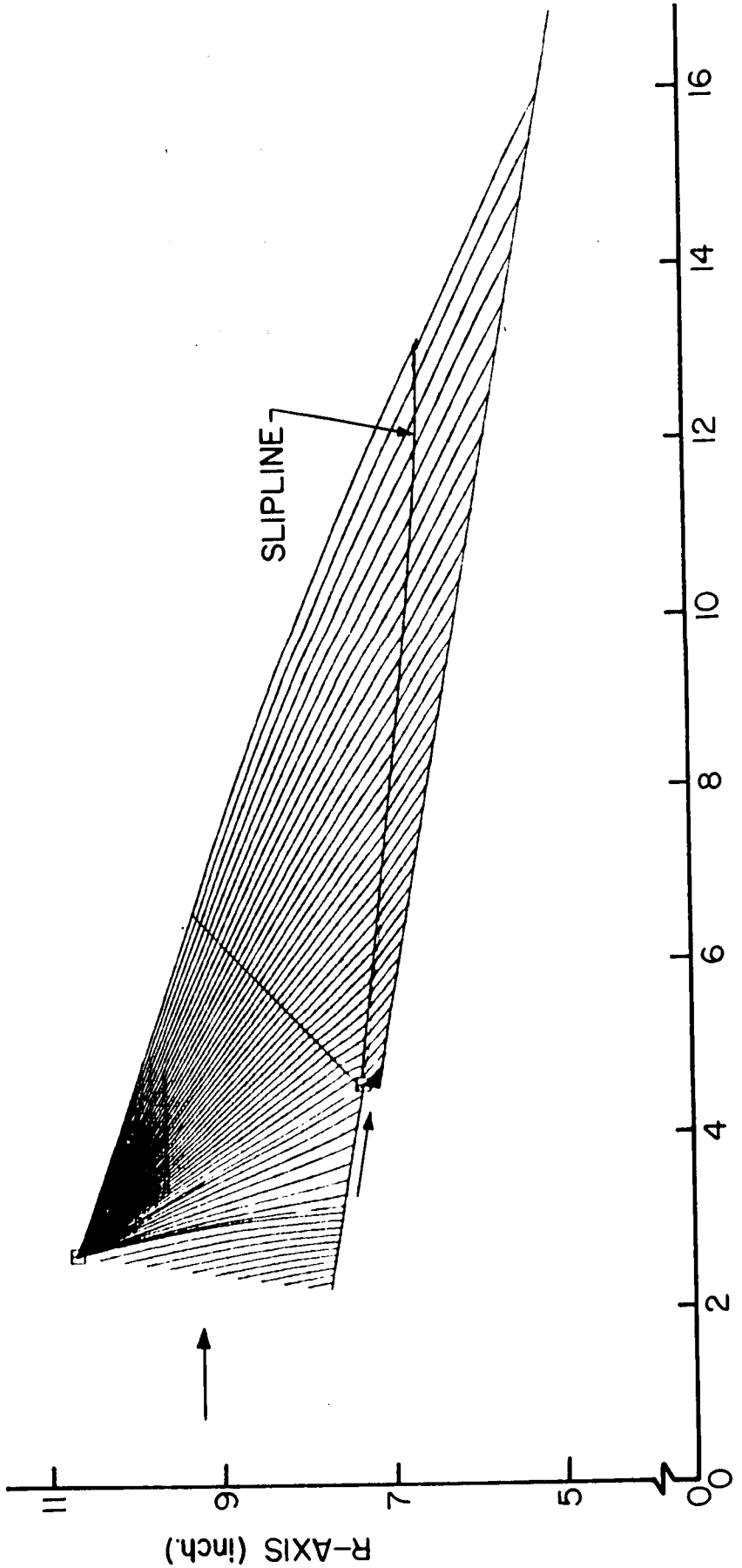

Figure 2.12. Predicted flowfield with primary stream stagnation pressure = 15.13 psia and secondary stream stagnation pressure = 27.0 psia

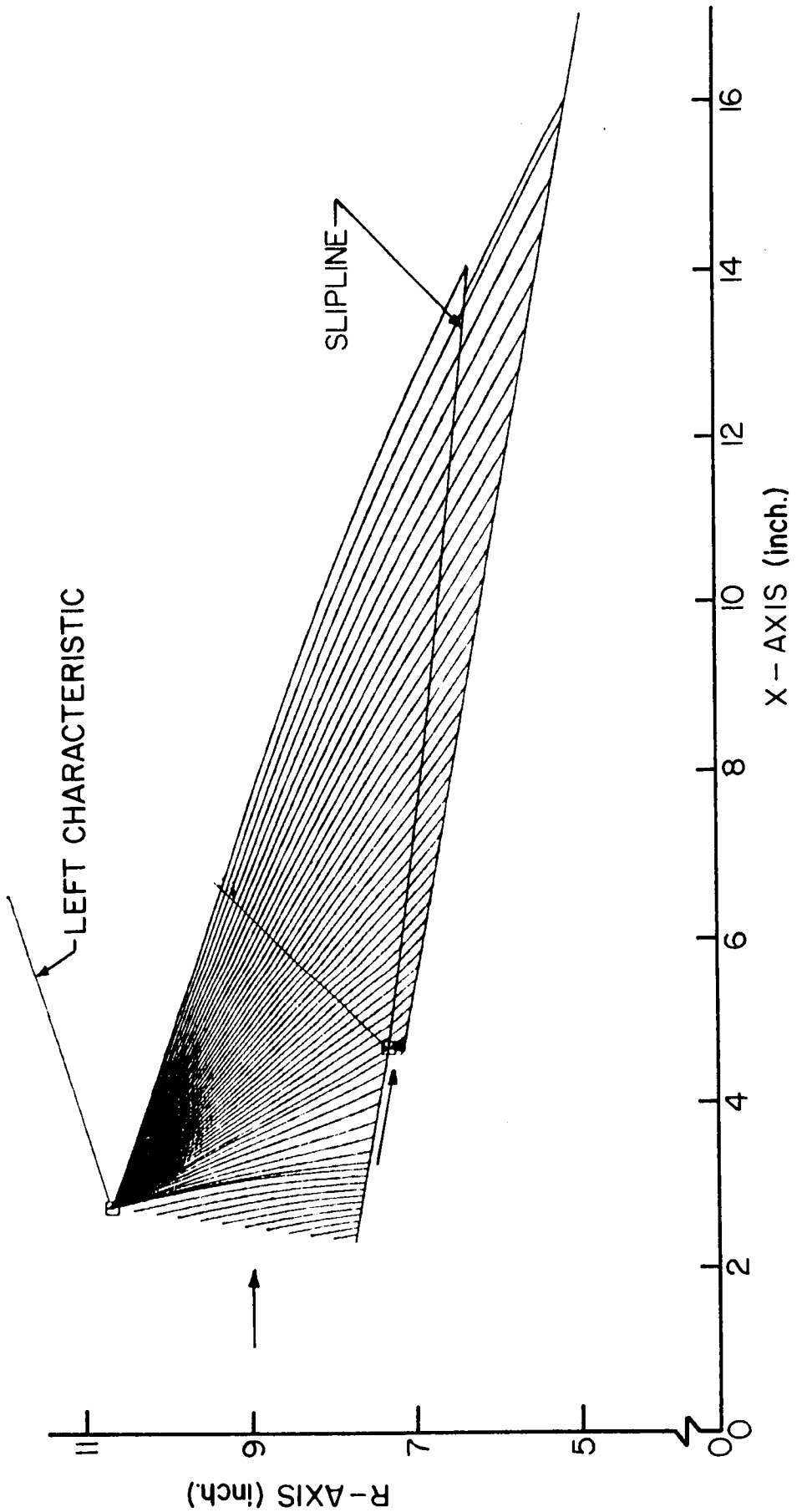

Figure 2.13. Predicted flowfield with primary stream stagnation pressure = 15.13 psia and secondary stream stagnation pressure = 20.0 psia.

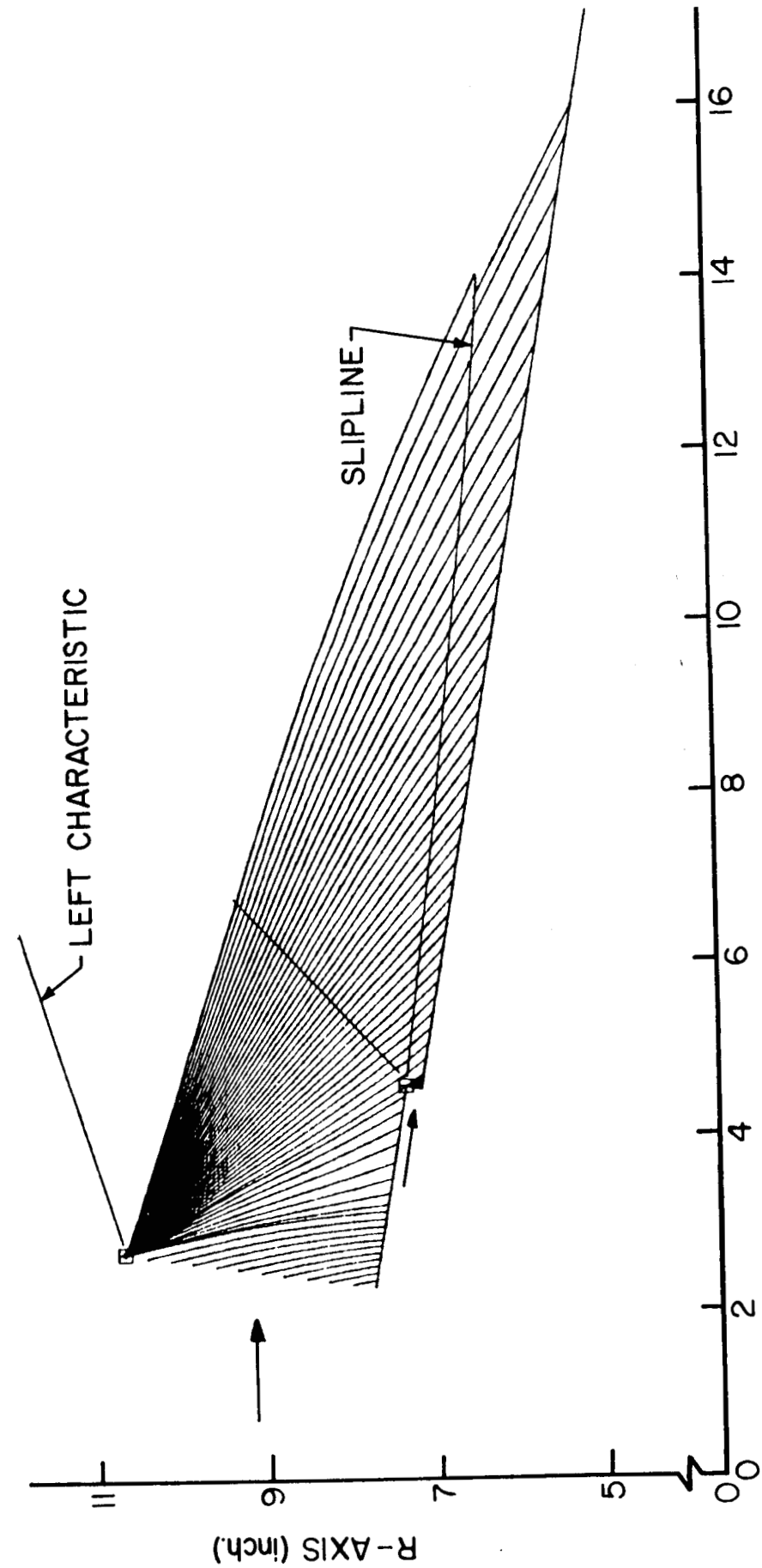

Figure 2.14. Predicted flowfield with primary stream stagnation pressure = 15.13 psia and secondary stream stagnation pressure = 18.0 psia

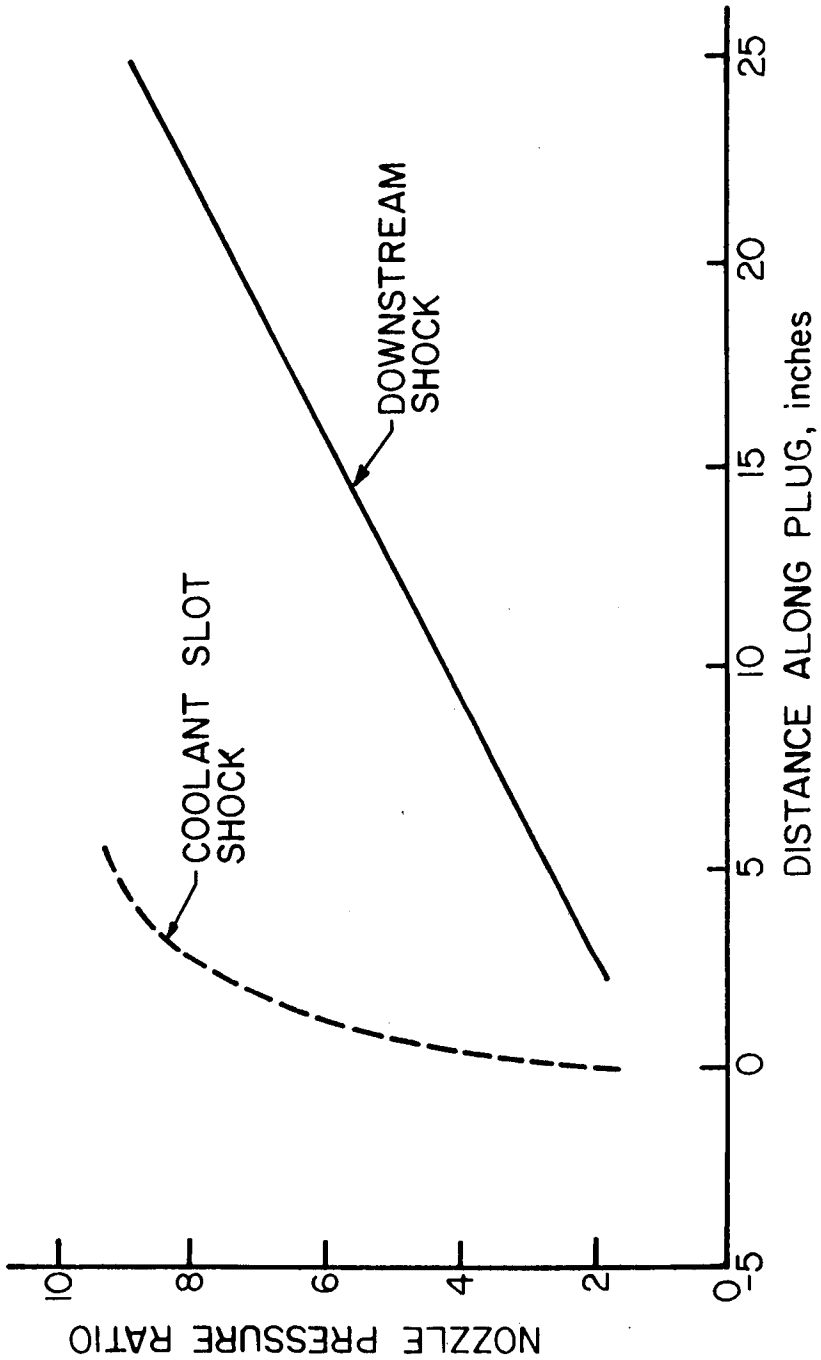

Figure 2.15. Location of coolant slot and downstream flowfield shocks as a function of nozzle pressure ratio

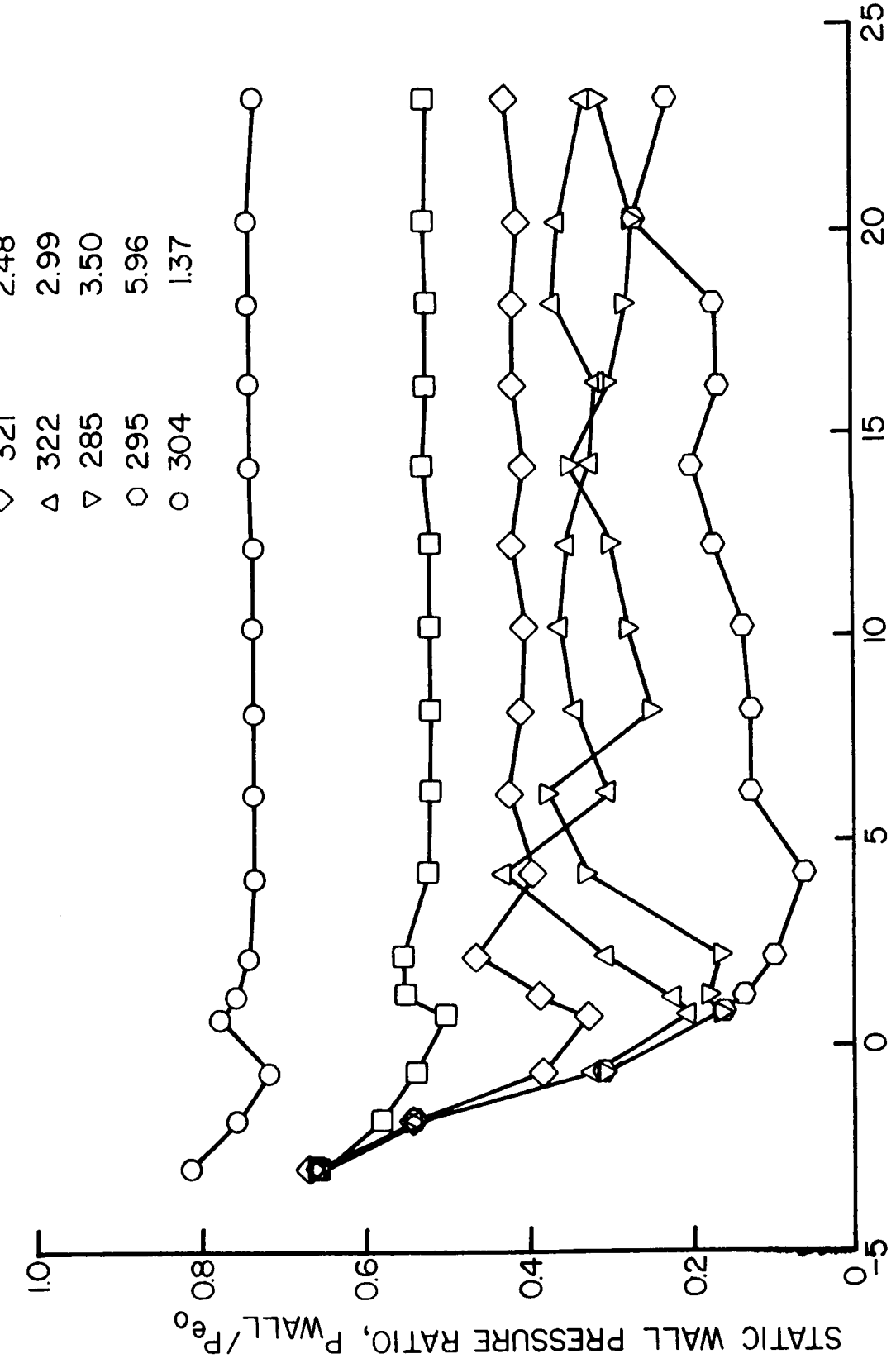

Figure 2.16. NASA Experimental data of static pressure ratio along the wall as a function of nozzle pressure ratio

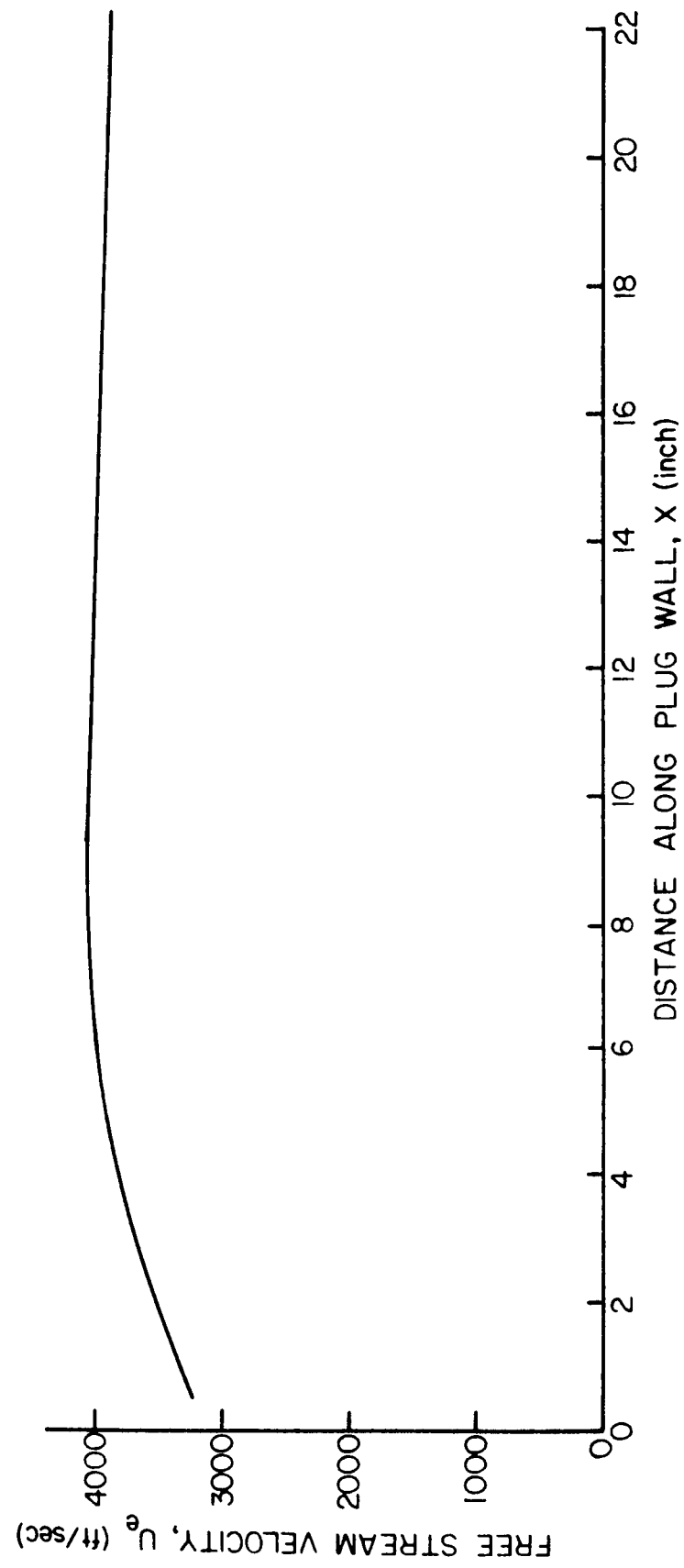

Figure 3.1. Case I of heat transfer studies: External velocity as a function of distance along flow

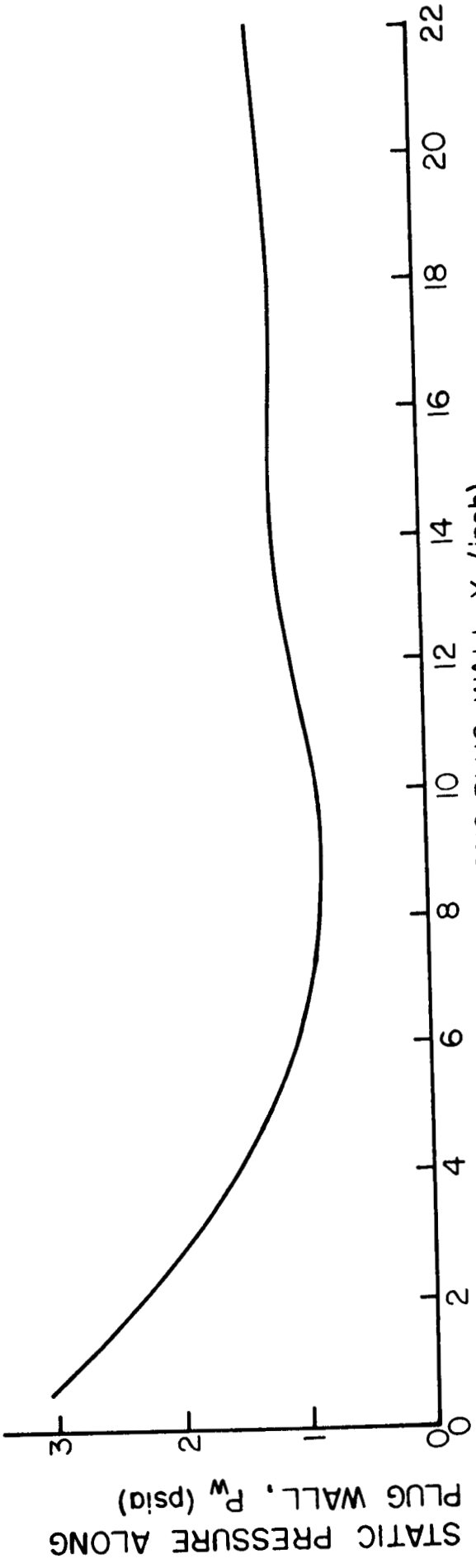

Figure 3.2. Case I of heat transfer studies: Wall static pressure as a function of distance along flow

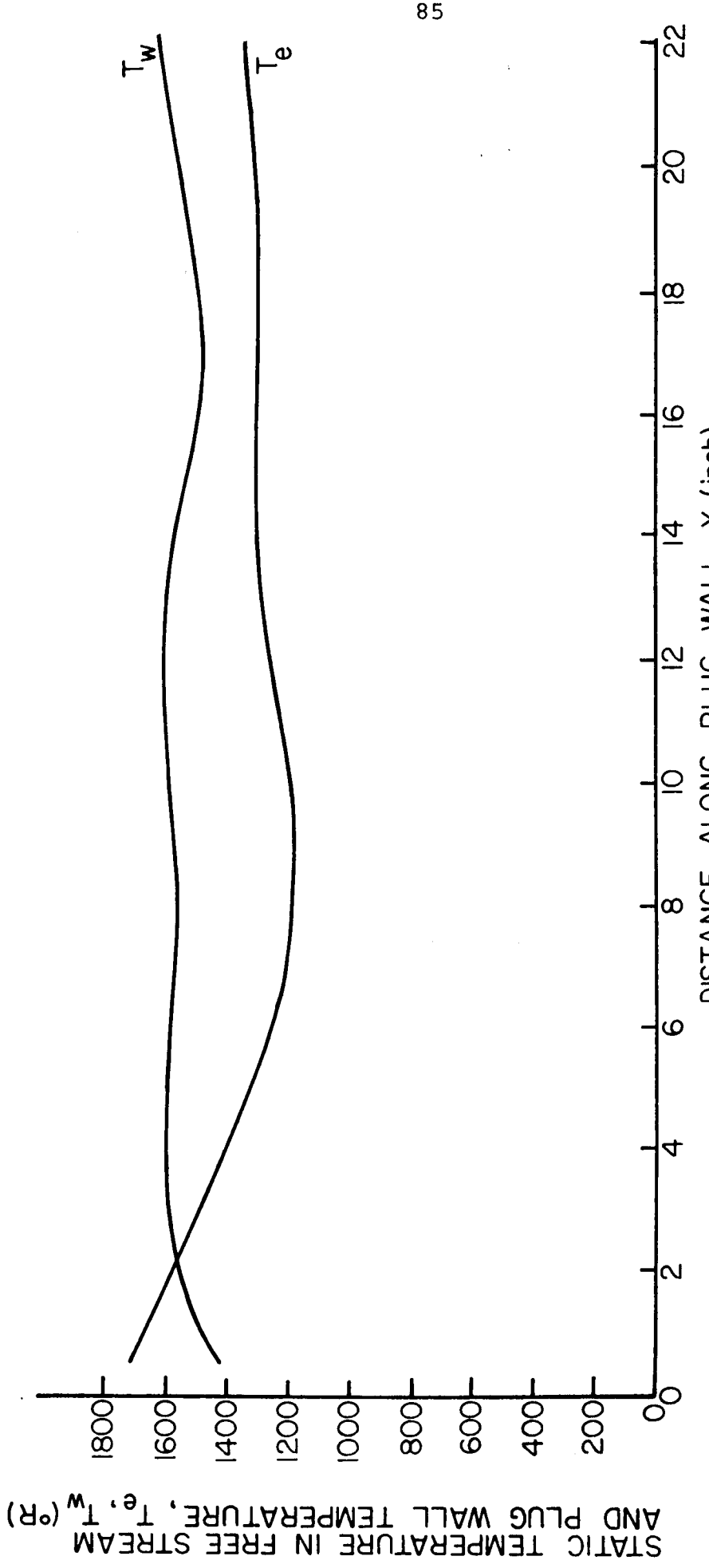

Figure 3.3. Case I of heat transfer studies: Wall and external static temperature as a function of distance along flow

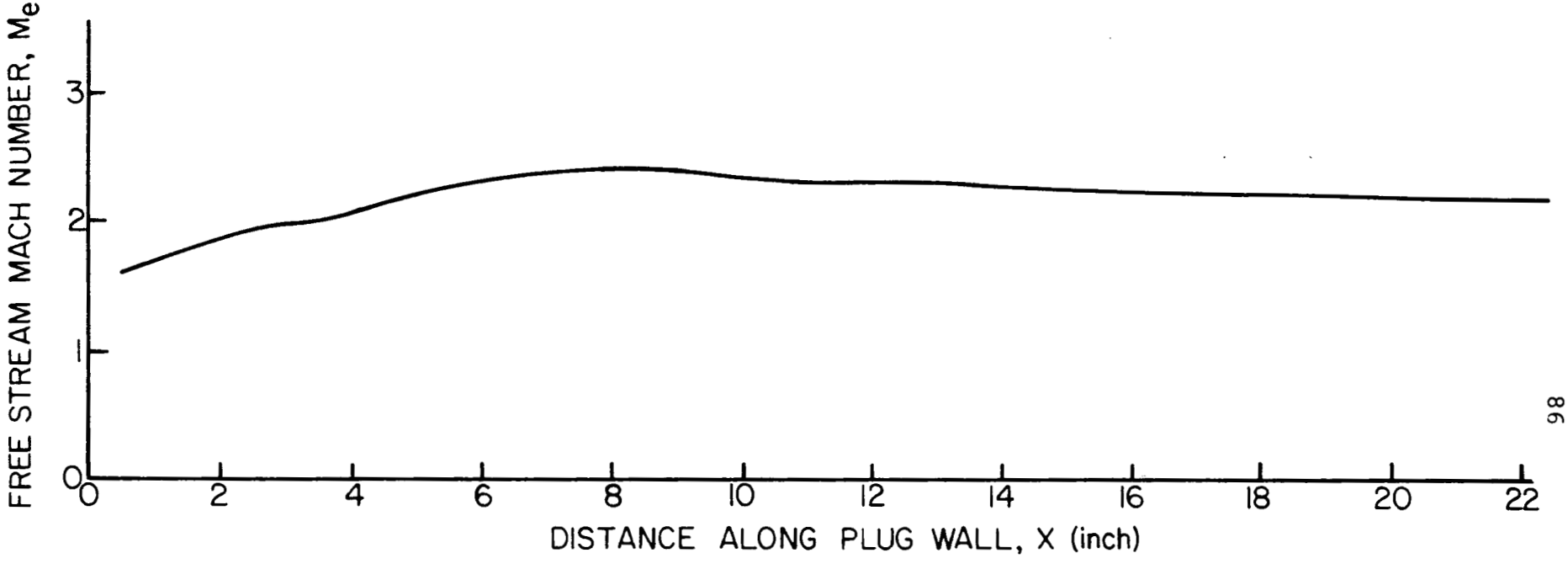

Figure 3.4. Case I of heat transfer studies: External Mach number as a function of distance along flow

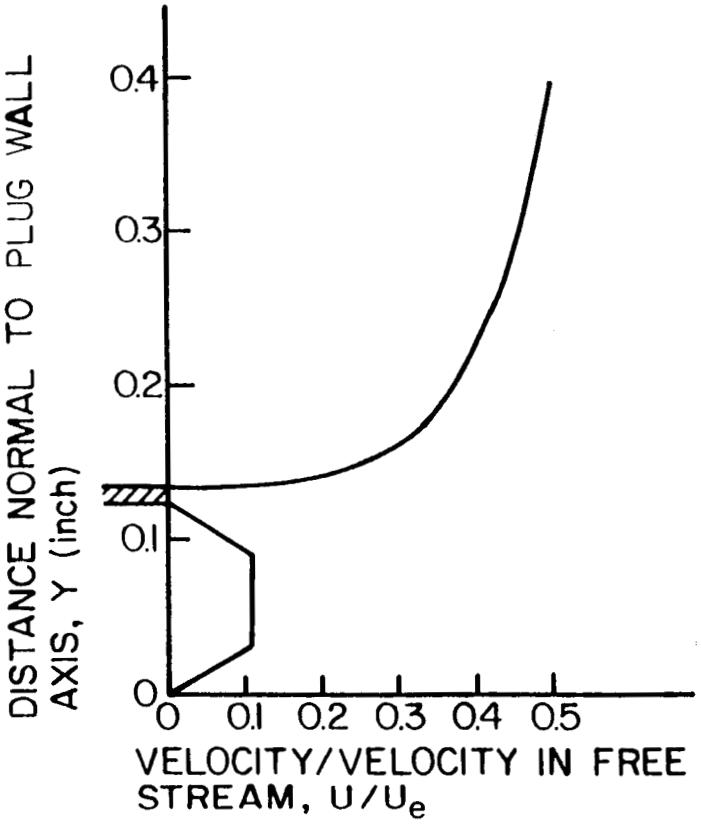

Figure 3.5. Case I of heat transfer studies: Initial velocity profile

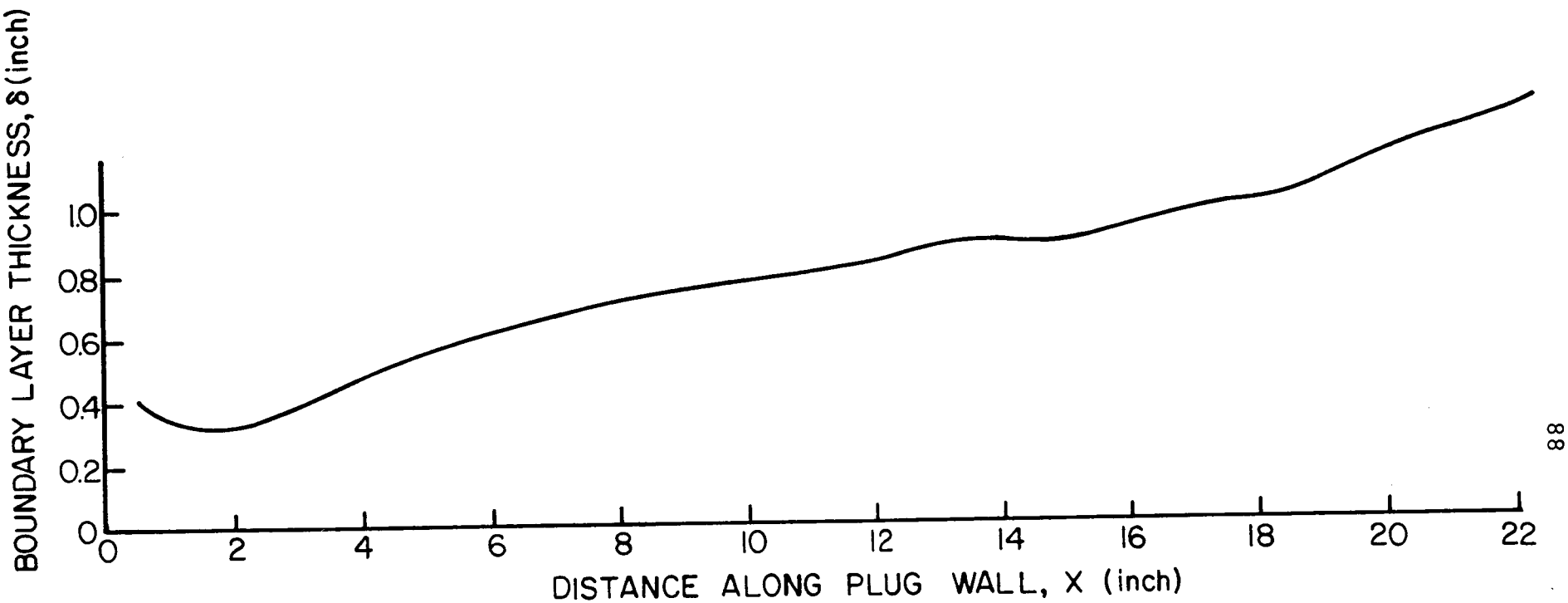

Figure 3.6. Case I of heat transfer studies: Boundary layer thickness as a function of distance along flow

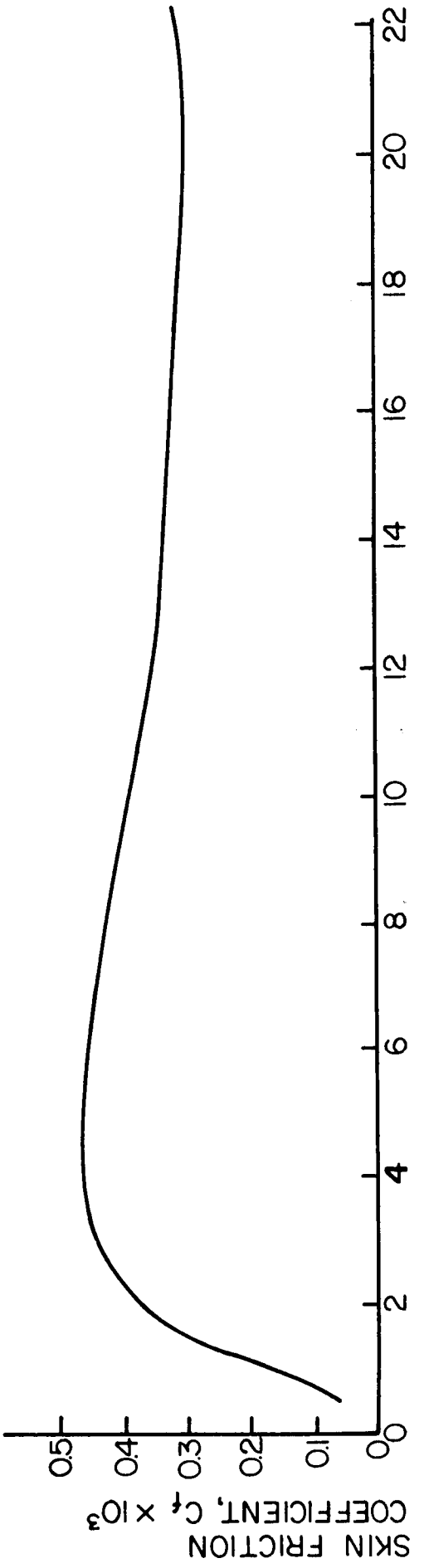

Figure 3.7. Case I of heat transfer studies: Skin friction coefficient as a function of distance along flow

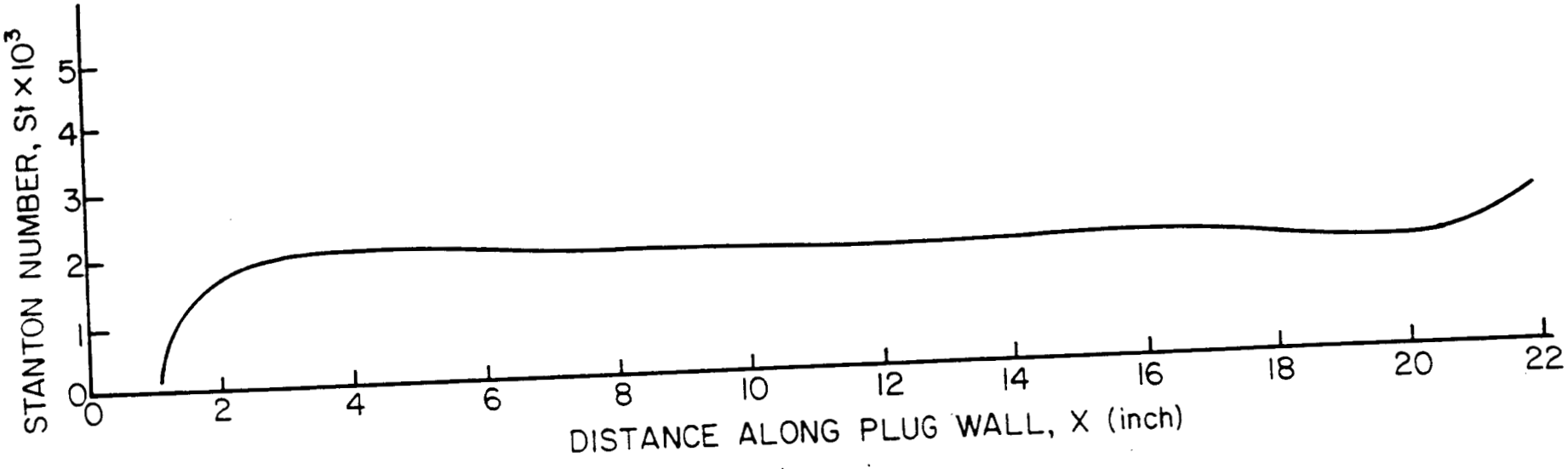

Figure 3.8. Case I of heat transfer studies: Stanton number as a function of distance along flow

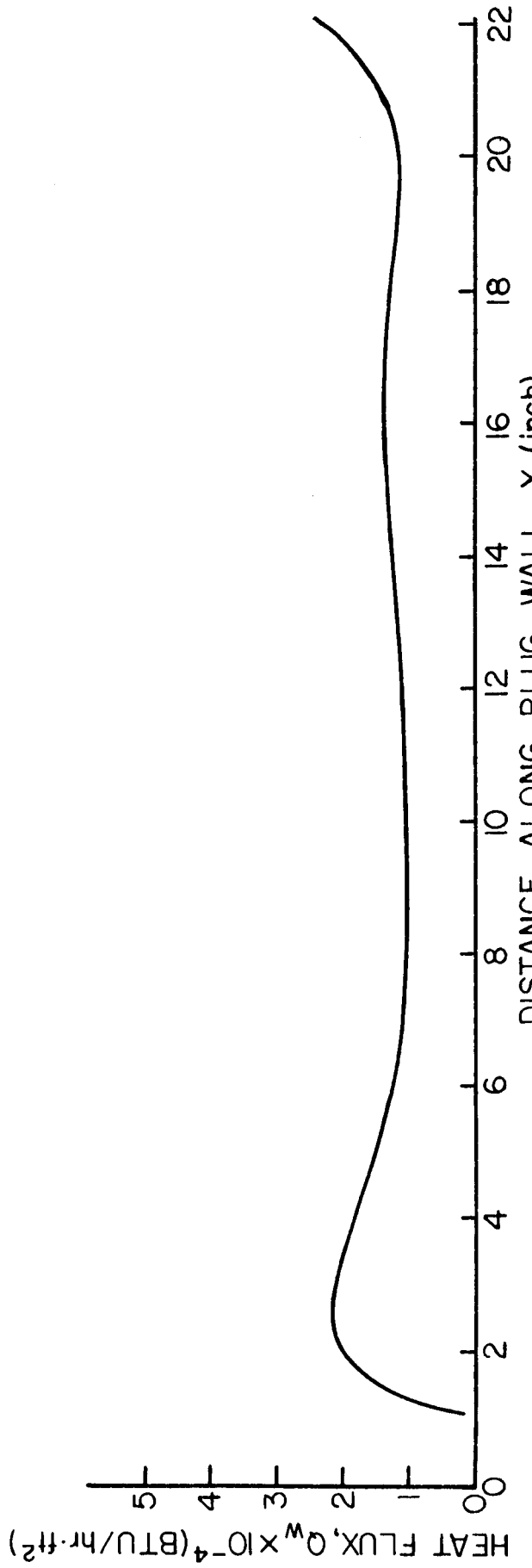

Figure 3.9. Case I of heat transfer studies: Heat flux as a function of distance along flow

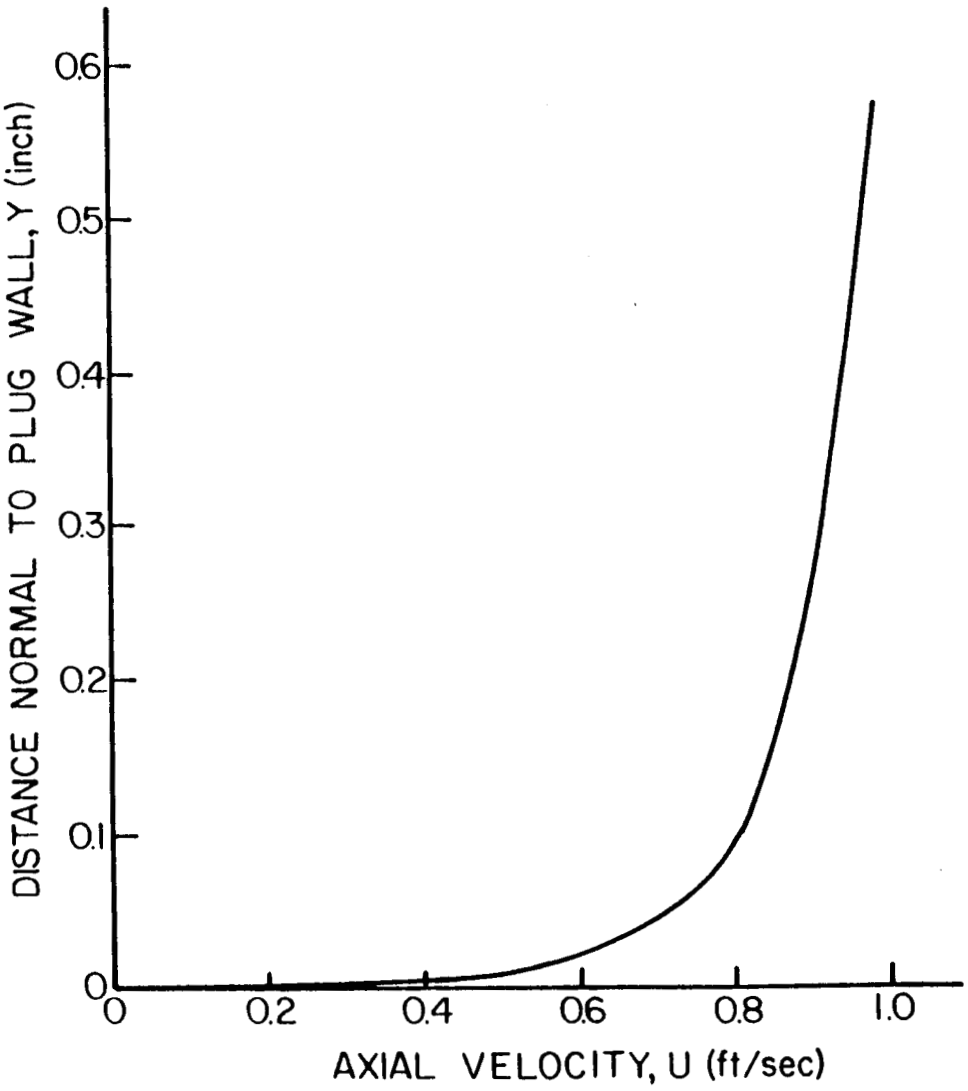

Figure 3.10. Case I of heat transfer studies: Velocity profile at a selected station along flow

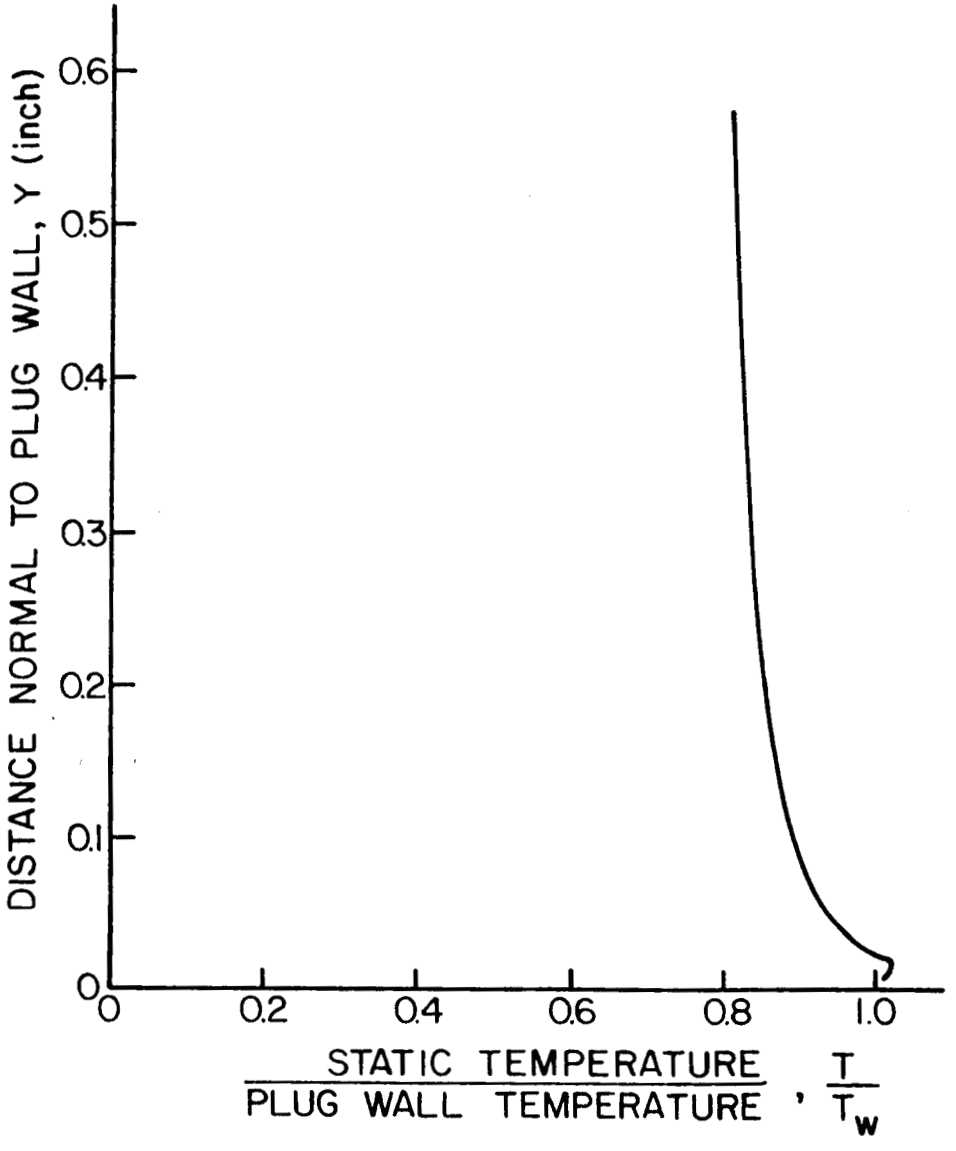

Figure 3.11. Case I of heat transfer studies: Temperature profile at a selected station along the flow

C-2

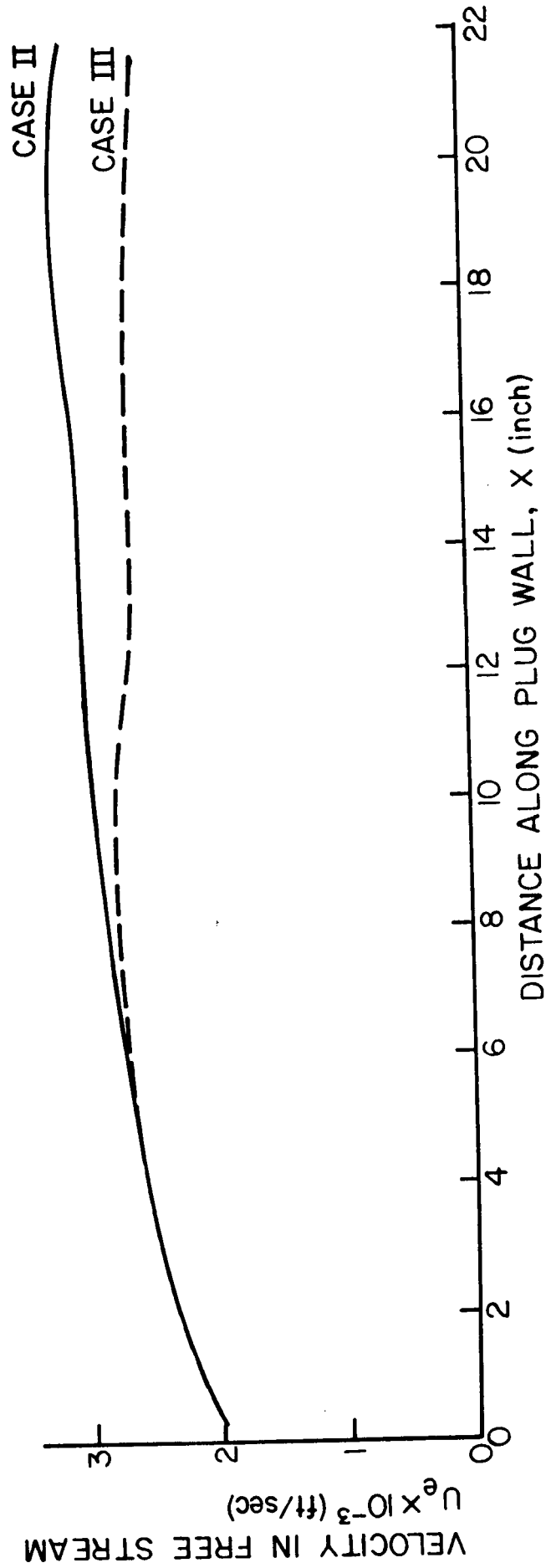

Figure 3.12. Cases II and III of heat transfer studies: External velocity as a function of distance along flow

Figure 3.13. Cases II and III of heat transfer studies: Wall static pressure as a function of distance along flow

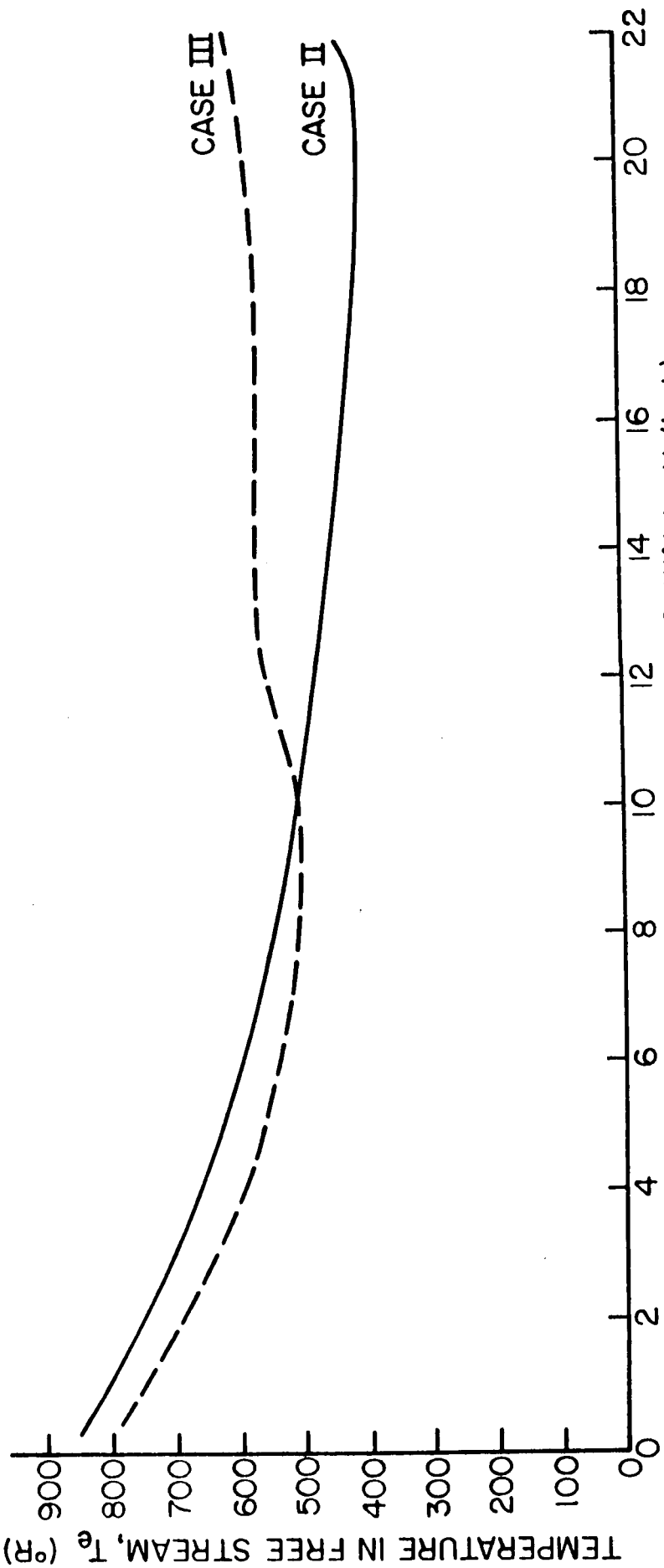

Figure 3.14. Cases II and III of heat transfer studies: External static temperatures as a function of distance along flow

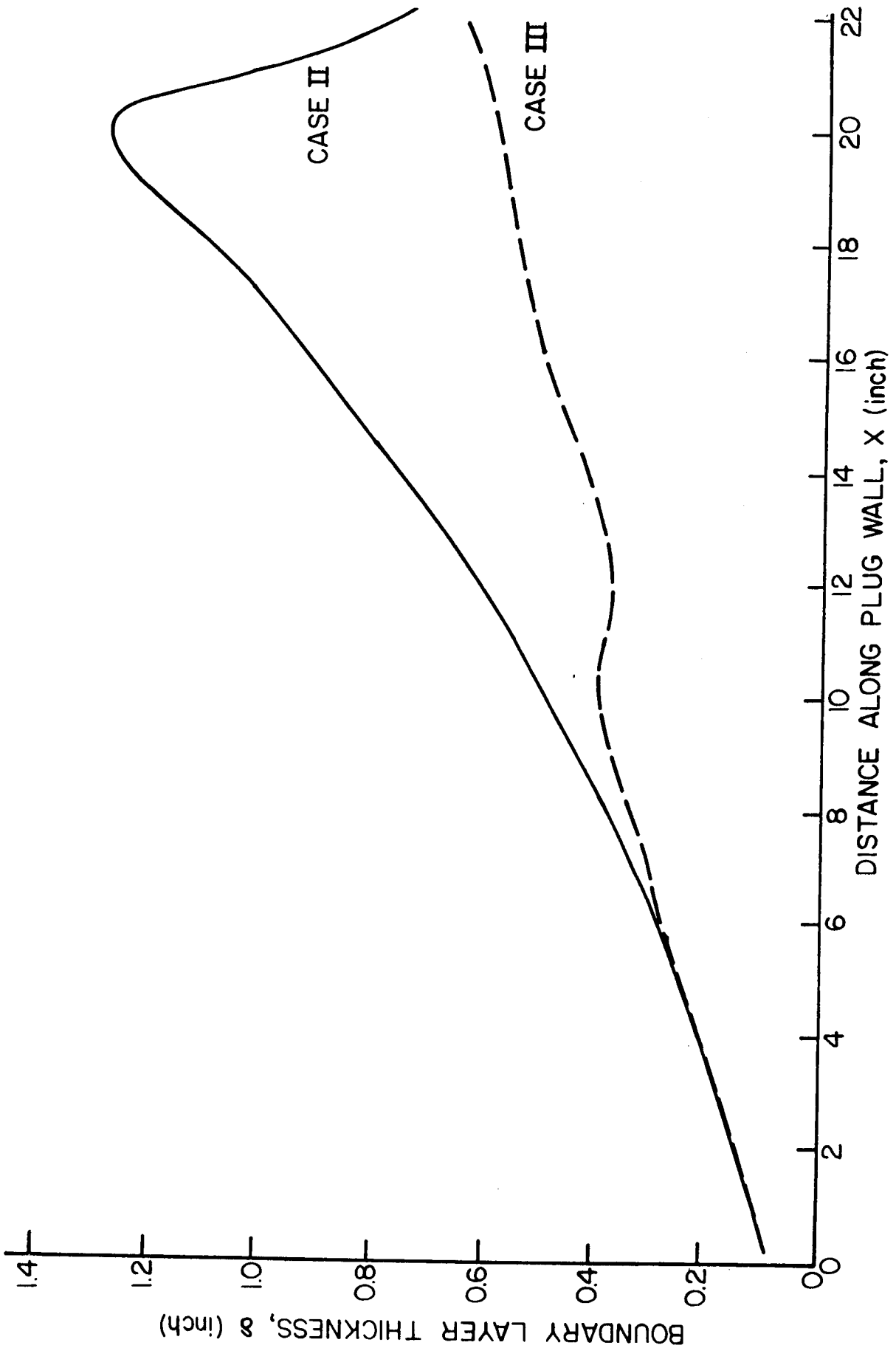

Figure 3.15. Cases II and III of heat transfer studies: Boundary layer thickness as a function of distance along flow

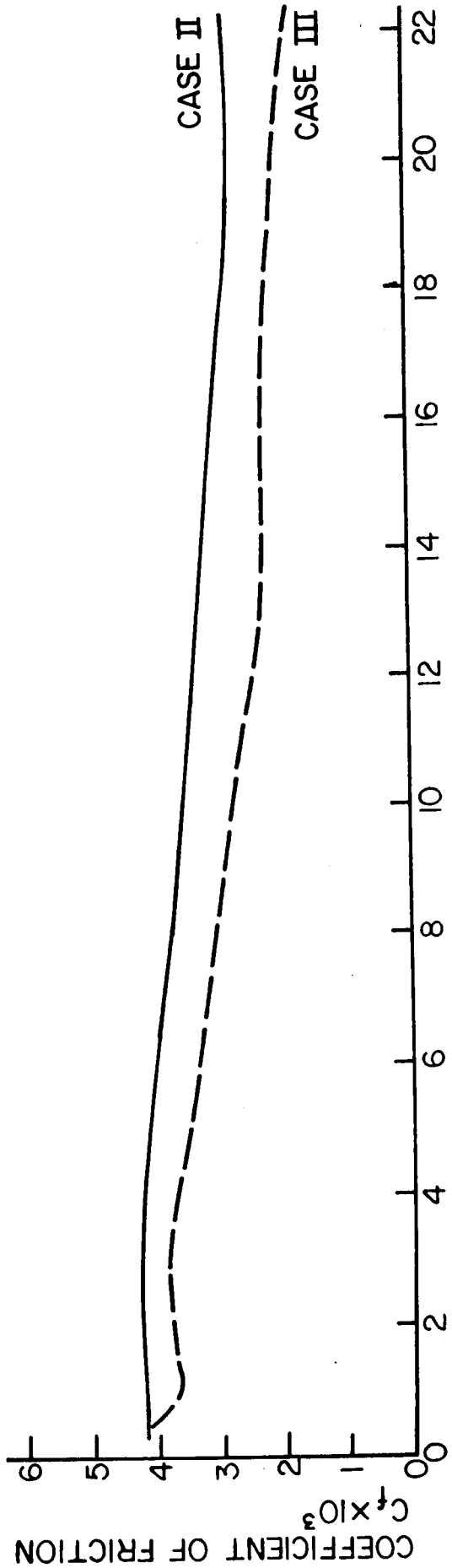

Figure 3.16. Cases II and III of heat transfer studies: Skin friction coefficient as a function of distance along flow

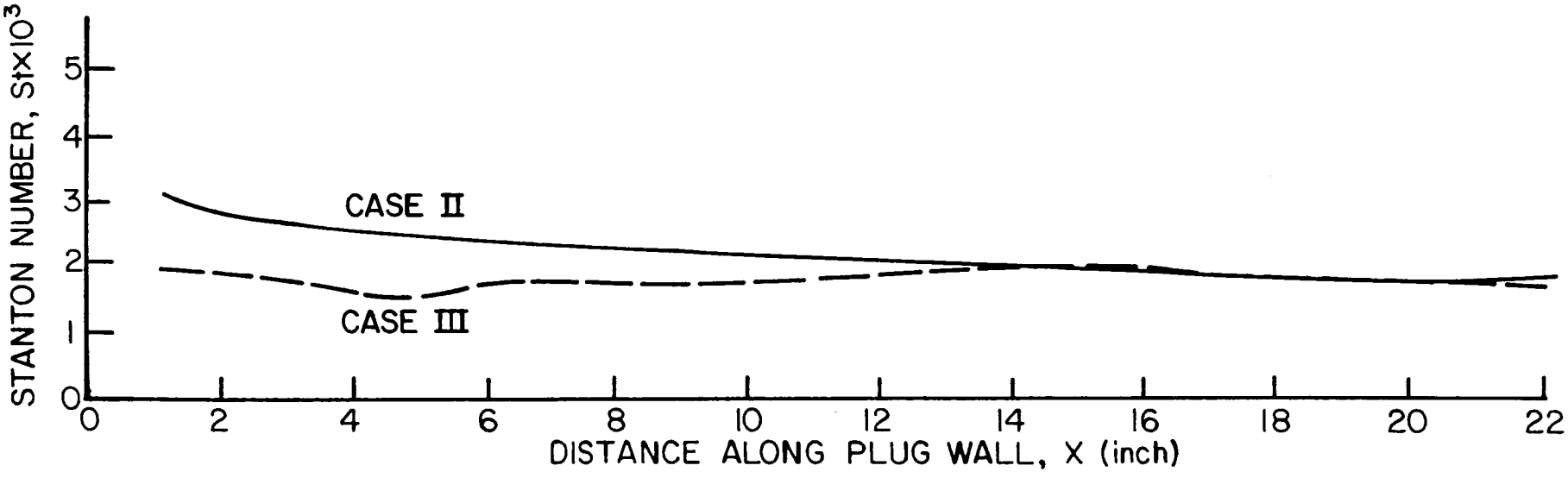

Figure 3.17. Cases II and III of heat transfer studies: Stantion number as a function of distance along flow

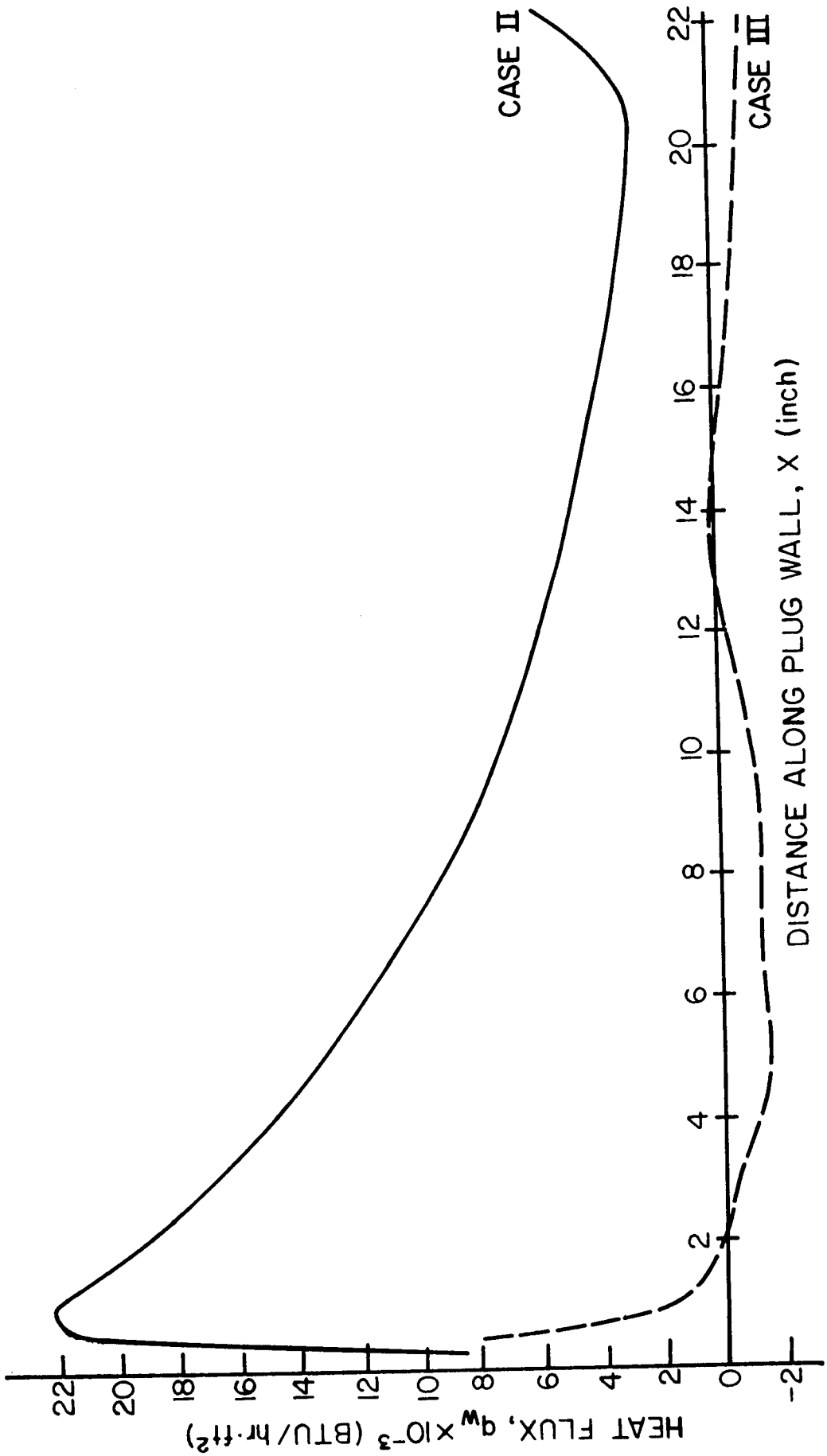

Figure 3.18. Cases II and III of heat transfer studies: Heat flux as a function of distance along the flow

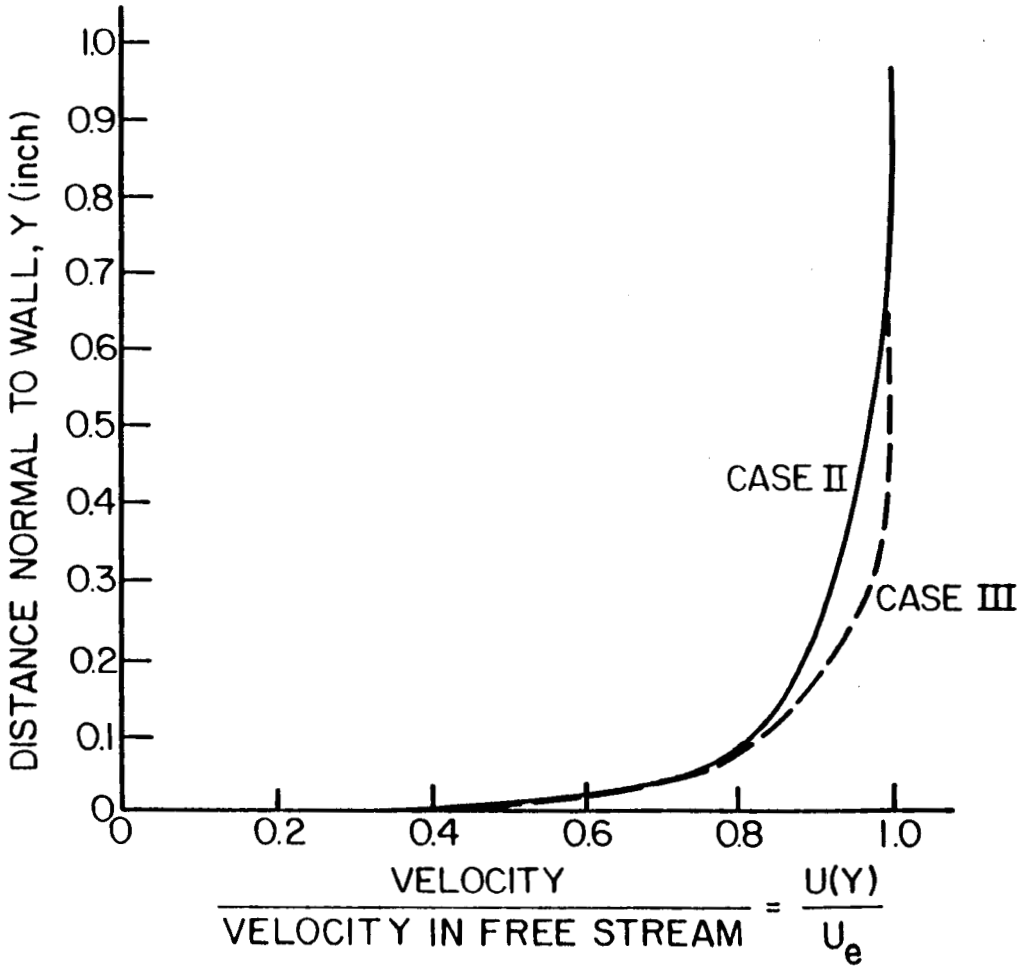

Figure 3.19. Cases II and III of heat transfer studies: Velocity profile at a selected station along the flow

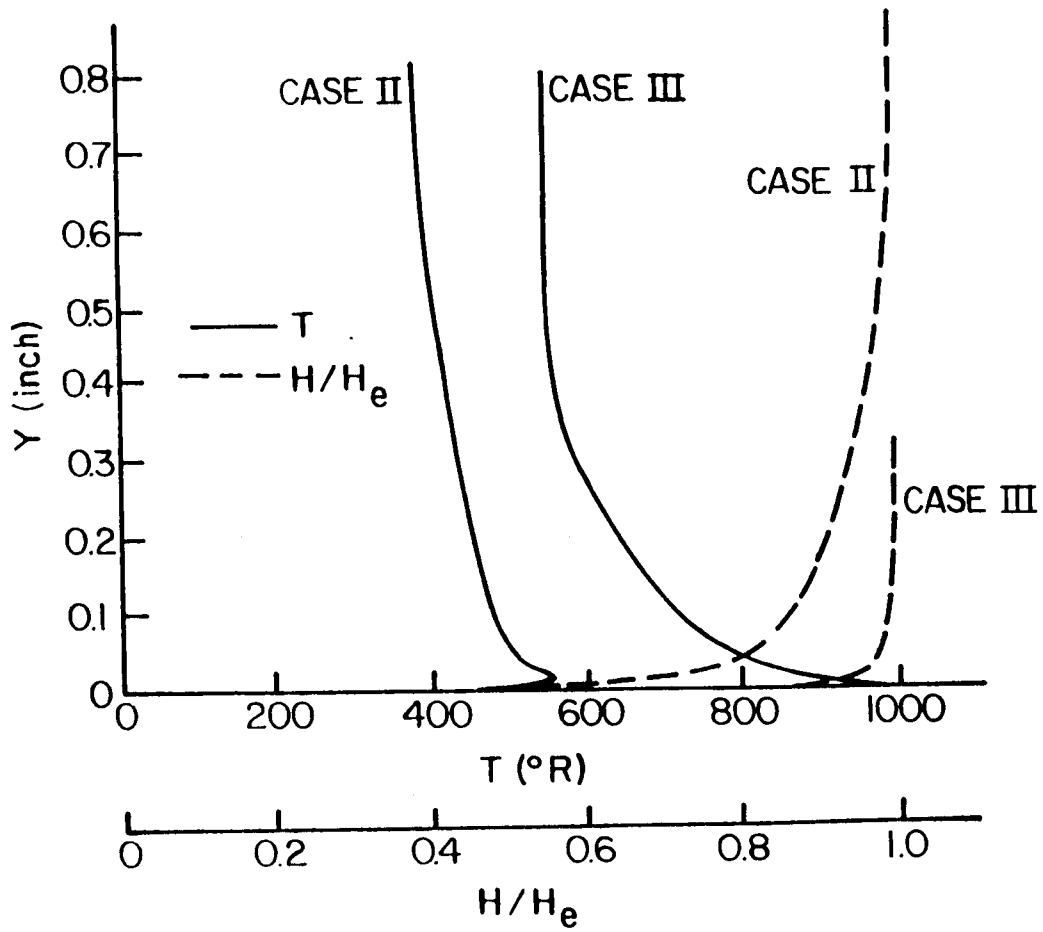

Figure 3.20. Cases II and III of heat transfer studies: Temperature and enthalpy profiles at a selected station along the flow

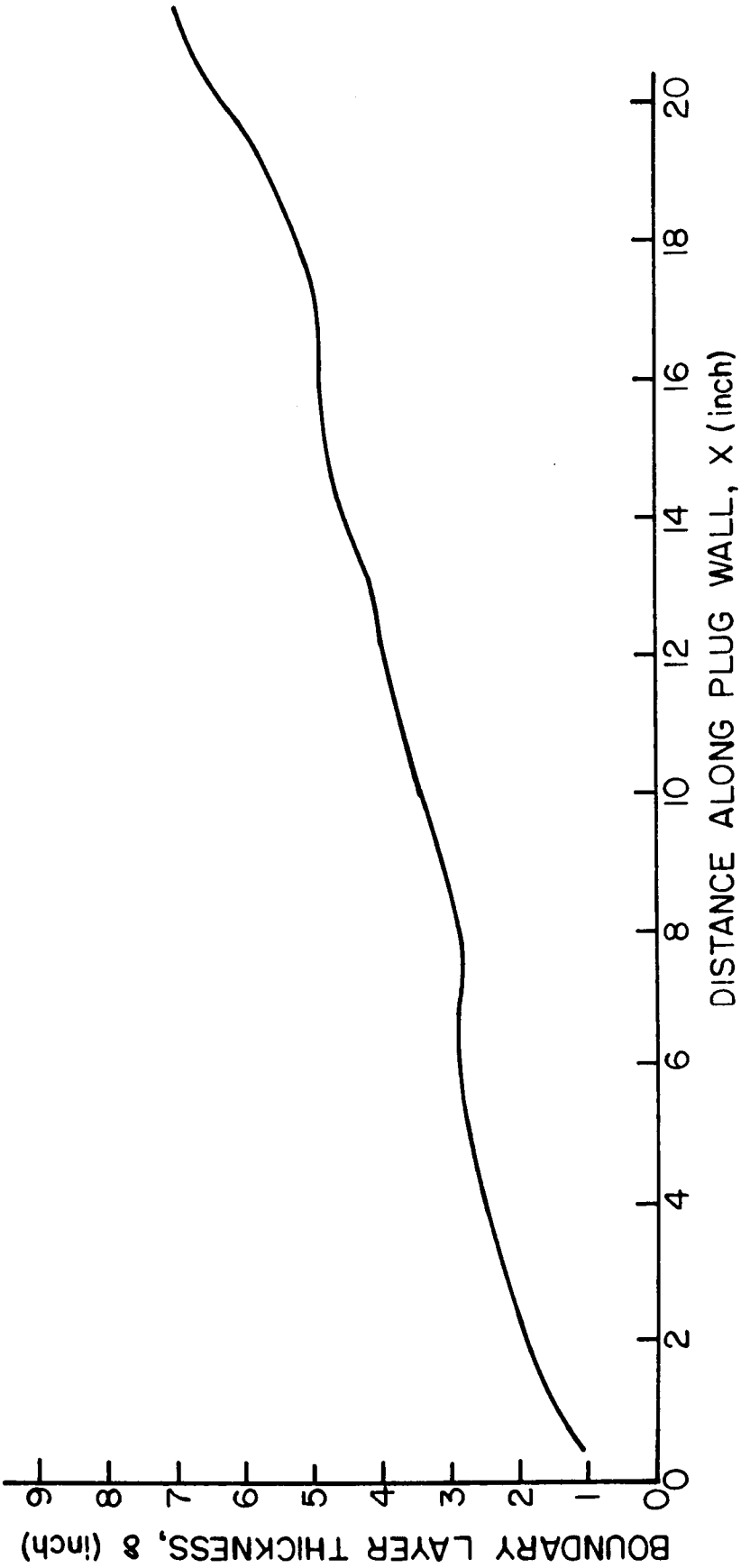

Figure 3.21. Case IV of heat transfer studies: Boundary layer thickness as a function of distance along the flow

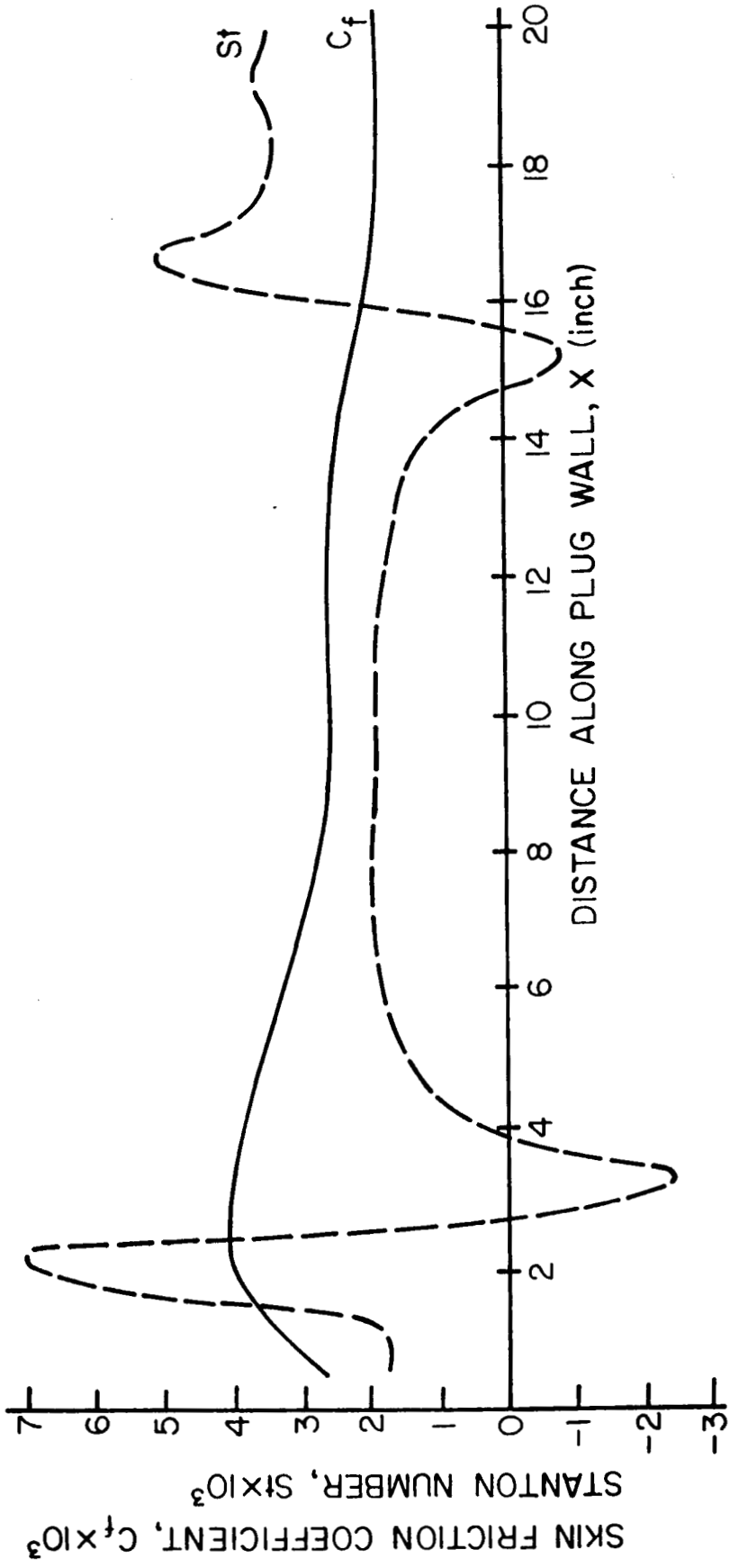

Figure 3.22. Case IV of heat transfer studies: Skin friction coefficient and Stantion number as a function of distance along the flow

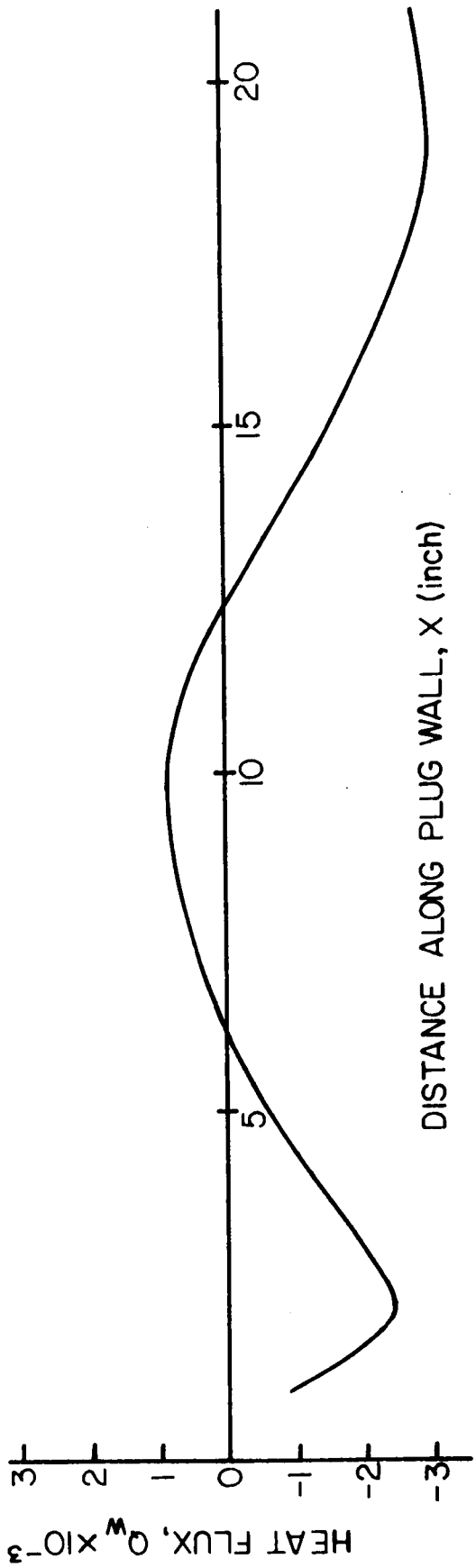

Figure 3.23. Case IV of heat transfer studies: Heat flux as a function of distance along the flow

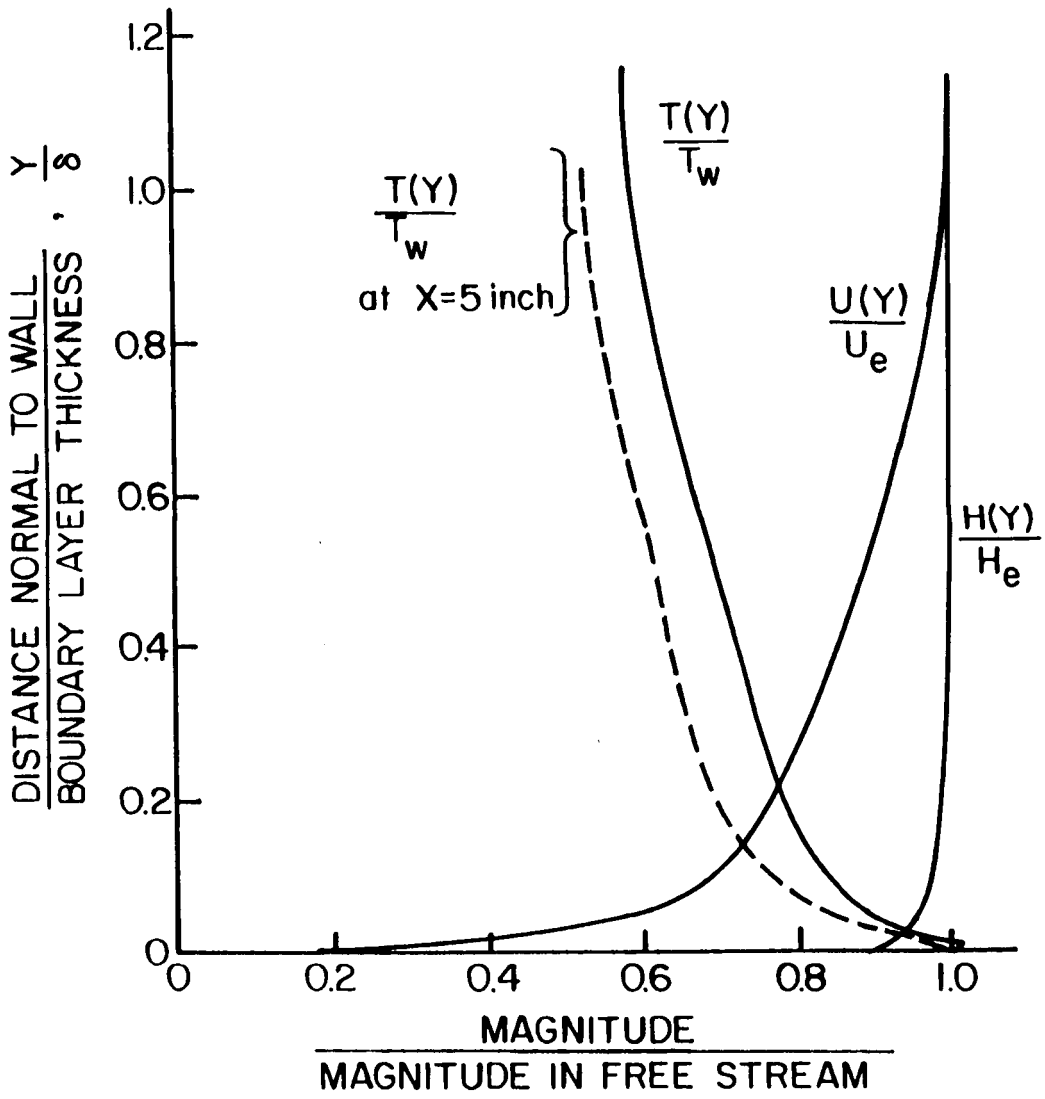

Figure 3.24. Case IV of heat transfer studies: Velocity, temperature, and enthalpy profiles at selected stations along the flow

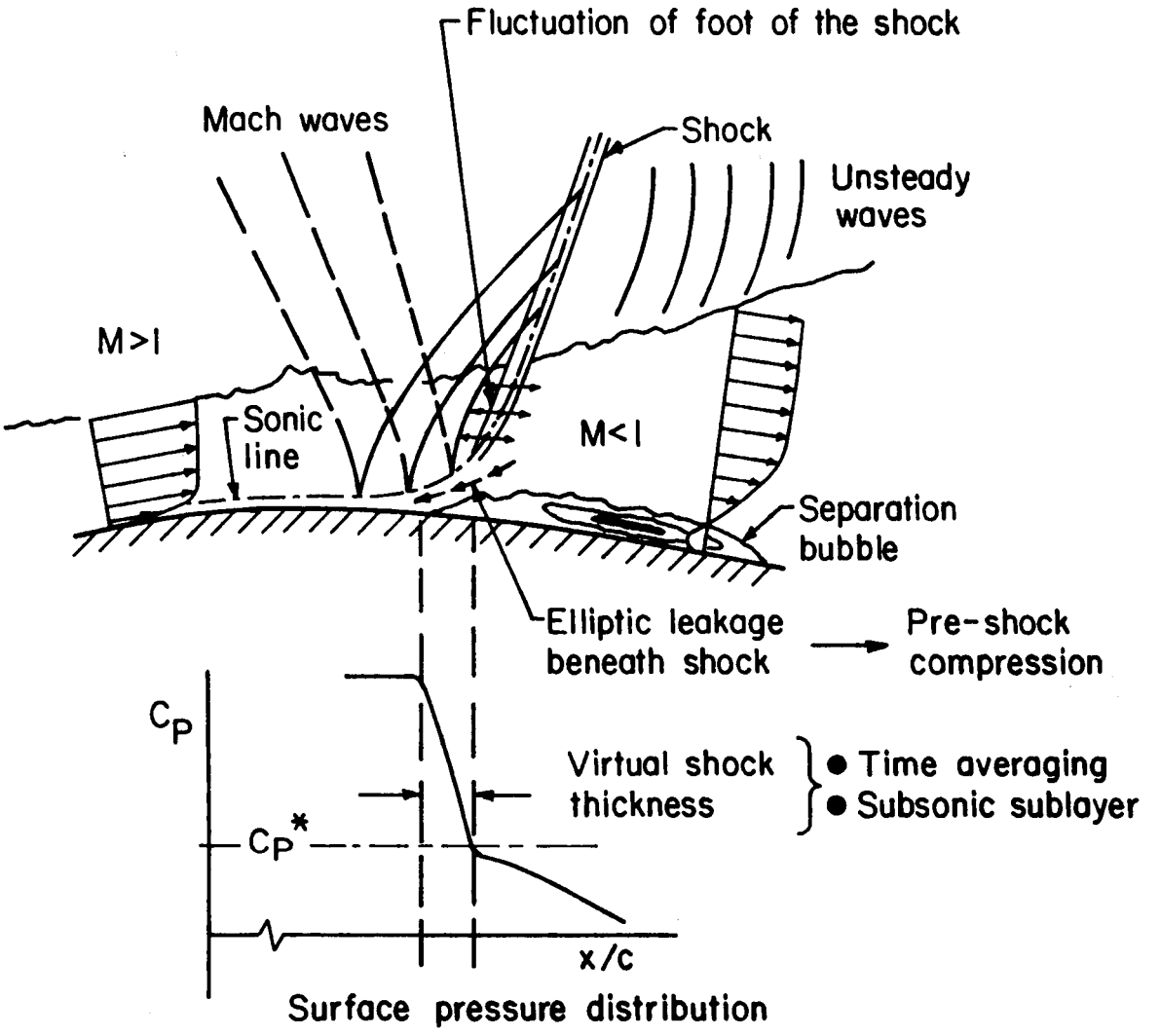

Figure 4.1. Shock-boundary layer interaction flowfield.

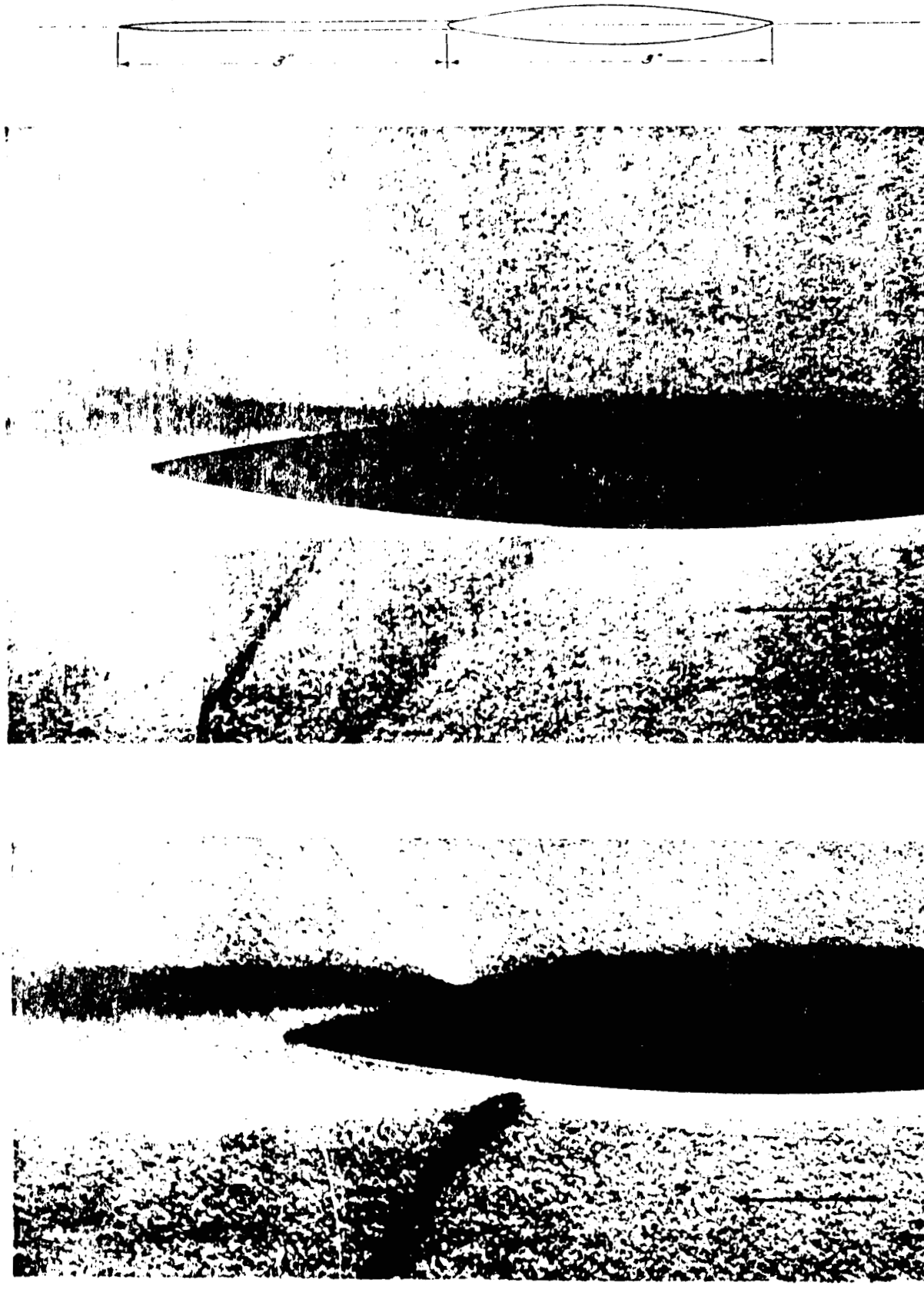

Figure 4.2. **Schematic of shock-boundary layer interaction over the suction surface of an airfoil in laminar flow (Liepman)**

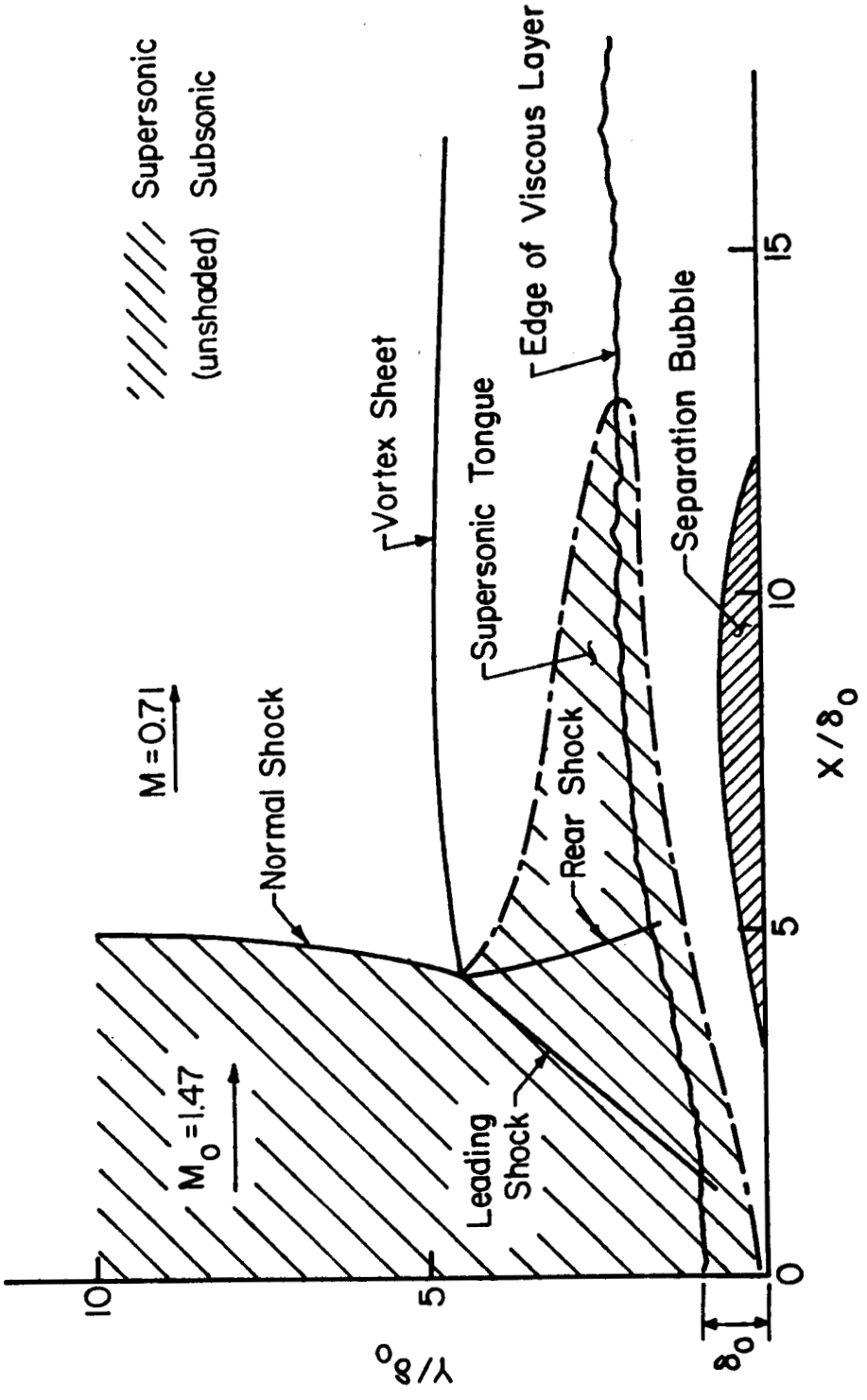

Figure 4.3. Shock-boundary layer interaction with flow separation

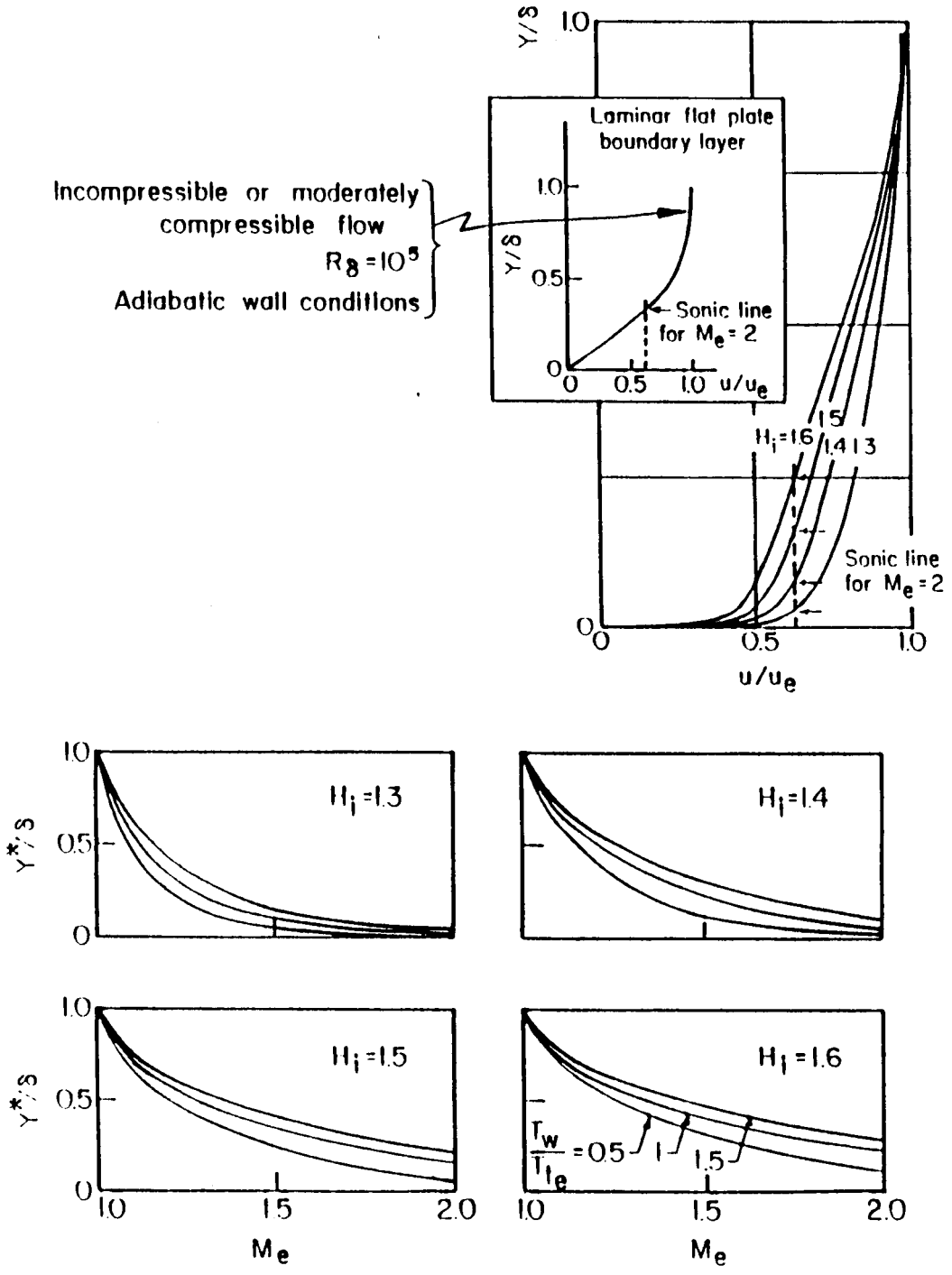

Figure 4.4 Effect of heat transfer on velocity profile. $Y^* = Yu_*/\nu$.

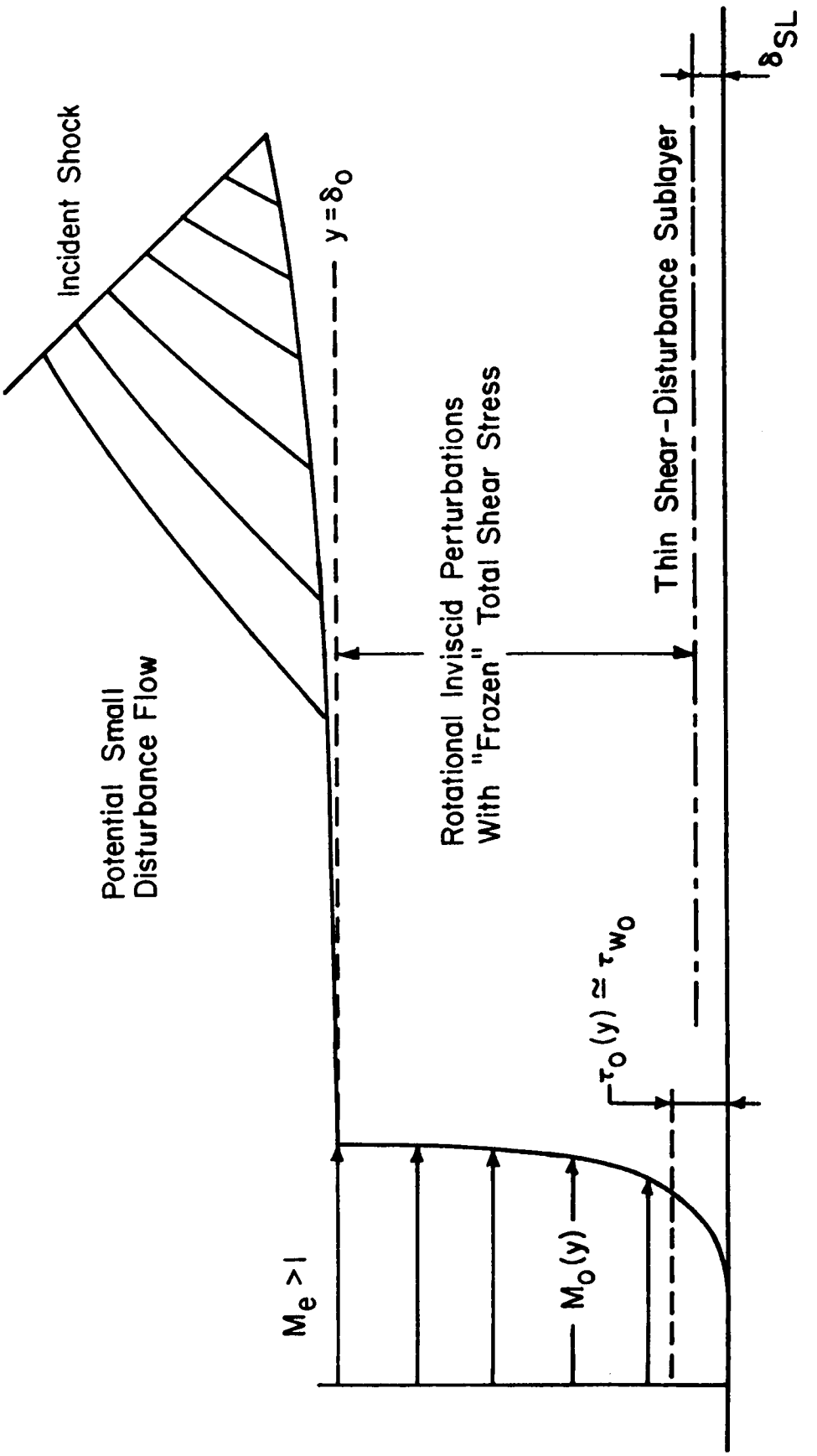

Figure 4.5. Triple-deck scheme

APPENDIX I

INVISCID FLOWFIELD IN PLUG NOZZLE WITH WALL COOLING STREAM

1. Introduction

The plug nozzle flowfield under consideration is shown schematically in Fig. 1.2. It consists of the so-called primary stream and a secondary stream, the latter acting as the coolant stream for the plug surface. The primary stream is expected to be supersonic downstream of the nozzle throat section, the magnitude and distribution of velocity being determined by the geometry of the throat and the boundary wall, and the external ambient conditions. The secondary stream may be subsonic or supersonic depending upon the geometry of the secondary stream duct and the ratio between the primary stream static pressure and the secondary stream stagnation pressure at the exit plane of the secondary stream.

The interaction between the primary and the secondary streams of given pressure and flow Mach number distribution depends upon (a) turbulence and viscosity effects at the walls, (b) mixing that may be turbulent and (c) the finite thickness of the lip of the separator between the two streams giving rise to a "base-flow" region. If all three of the foregoing are neglected in preliminary analysis, the interaction between the two streams becomes determined entirely by pressure and Mach number considerations. It is such a simplified analysis that is discussed in the following.

The plug nozzle flowfield that is discussed here pertains to the supersonic portion, that is the flowfield downstream of the sonic line. It may be observed from Fig. 1.2 that the coolant stream is being admitted into the nozzle slightly downstream of the throat.

Therefore the interaction between the two streams is also discussed only in the supersonic portion of the nozzle.

As noted earlier, the secondary or the coolant stream may be entering the nozzle under subsonic or choked or supersonic condition. When the secondary flow enters at subsonic speed, it can expand further within the nozzle and therefore attain the sonic condition at some location downstream along the wall. On the other hand, when the coolant flow enters in a choked or a supersonic condition, it is possible that after an initial acceleration the flow may undergo various types of changes depending upon the local relation between the magnitudes of static pressures of the coolant and the primary streams. It is clear that the various types of flowfield interactions cited in the foregoing become further affected by the viscous effects at the walls and the diffusion processes in the mixing layer between the two streams; neither of those two processes is included in the current analysis.

The problem analyzed here may therefore be summarized as follows: the primary stream enters the supersonic portion of the nozzle at the throat, the conditions along the sonic surface being fully prescribed; the coolant stream or the secondary stream enters the nozzle downstream of the throat at a specific location, the conditions at the entry plane of the coolant flow being fully prescribed; it is desired to obtain the interactive flowfield in the nozzle in the absence of viscous and heat conduction effects and also the diffusive process between the two streams.

In view of such a formulation, the primary and the secondary (coolant) streams may differ only in molecular weight, stagnation pressure and Mach number.

2. Methodology

The supersonic flowfield is governed by hyperbolic gas dynamic equations. One of the methods that is considered sufficiently accurate and simple to apply for the numerical solution of such equations is the method of characteristics.

A computer program developed at Purdue University, Ref. I.1, utilizes the method of characteristics and is suitable for determining inviscid, nonmixing (meaning non-diffusive), interactive flowfields such as the one under discussion here. That computer program has been the basis for the predictions generated in the current problem.

2.1. Initial Conditions

2.1.1. Coolant Stream

The initial conditions at the exit plane of the coolant (secondary) stream can be generated in a simple fashion, with adequate accuracy, based on one-dimensional flow analysis of the coolant flow in the ducting that feeds the flow. For given plenum or reservoir conditions and given geometry of such ducting, the conditions at the exit plane of the coolant flow can be calculated when the local static pressure of the primary stream is known at the specific location. The latter is obtained from the predictions of the primary stream flow. In case it is desired to account for a nonuniformity in the velocity profile of the coolant stream at the plane of its entry into the nozzle, one can proceed as follows.

(a) The static pressure of the primary stream at the location of interest is obtained from the predictions of the primary stream.

(b) Based on the assumption that the static pressure value applies over the entire cross-section of the coolant stream, the one-dimensional formulation-based value of coolant exit velocity can be obtained.

(c) A nonuniformity factor can be introduced to that value of velocity, in the form of a parameter, to obtain any desired velocity distribution, while paying attention to conversation of mass.

On the other hand, within the framework of other assumptions employed in the current analysis, the assumption of uniform flow in the coolant stream may not prove excessively inaccurate.

2.1.2. Primary Stream

The initial conditions required in the primary stream are those over a surface located in the wholly supersonic region, as close as feasible to the sonic line.

The transonic region can be determined by utilizing one of the existing programs, for example Ref. I.2, developed at Purdue University. The method employed is related to the approach of Ref. I.3, wherein an asymptotic expansion of perturbation velocities in terms of the wall curvature of the throat section has been carried out. The flow passage is assumed to be choked while starting with uniform inlet conditions. Inviscid, steady, non-heat conducting, irrorational flow is assumed.

3. Solution Procedure

The method of characteristics is applied to hyperbolic, gas dynamic equations for an ideal gas in the absence of viscosity and heat conduction effects.

The numerical algorithm involves three characteristics, including the streamline, and the four compatibility equations are solved for velocity, V, flow direction, Θ, pressure, p, and density, ρ, at the solution point where the three characteristics must meet.

A direct marching scheme is employed in the computer program. Figure I.2 provides a sketch of the scheme for an interior point calculation.

The numerical scheme for solving the characteristic and the compatibility equations is based on a modified Euler predictor-corrector method. The corrector step may be applied iteratively or a fixed number of times.

Figures I.2 to I.8 illustrate the procedure for unit processes dealing with (1) direct solid boundary point, (2) pressure boundary point, (3) inverse solid boundary point, 4) flow point at the joining of two streams, (5) shock calculation, (6) slipline calculation, and (7) thrust and mass flow calculation.

REFERENCES

I.1. Thompson, H.D., "Flowfield Analysis of a Dual Flow Plug Nozzle by the Method of Characteristics", Purdue University Report, December 1976.

I.2. Thompson, H.D. and Flack, R.D., "Transonic Flow Computation in Annular and Axisymmetric Two-Dimensional Nozzle", Purdue University Report, December 1973.

I.3. Kliegel, J.R. and Levine, J.N., "Transonic Flow in Small Throat Radius of Curvature Nozzles", AIAA J., Vol. 7, No. 7, July 1969.

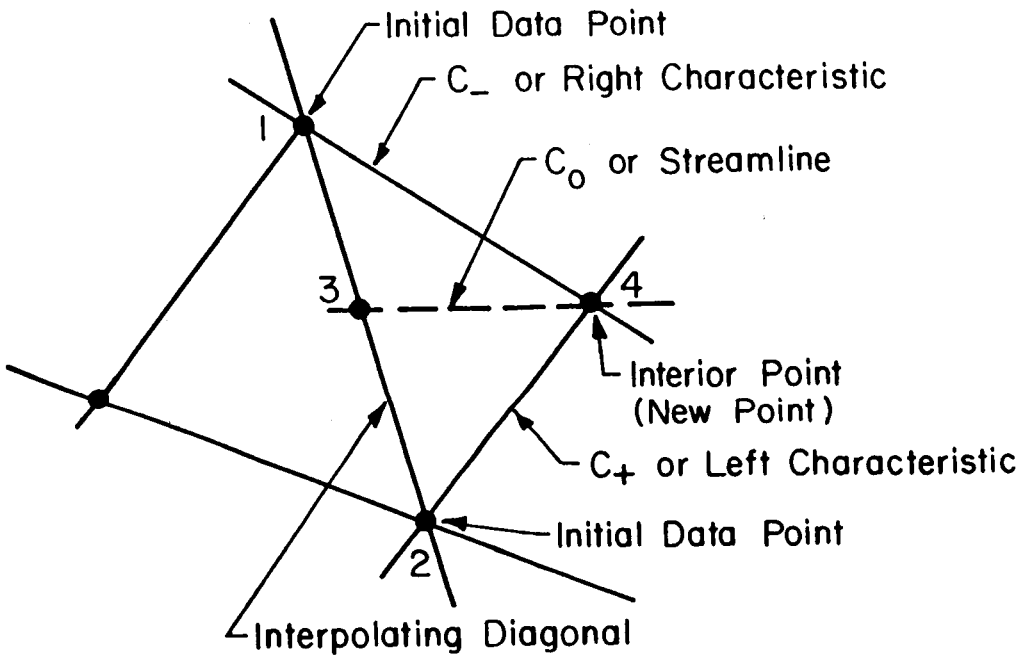

Figure I.1. Schematic for interior point calculation

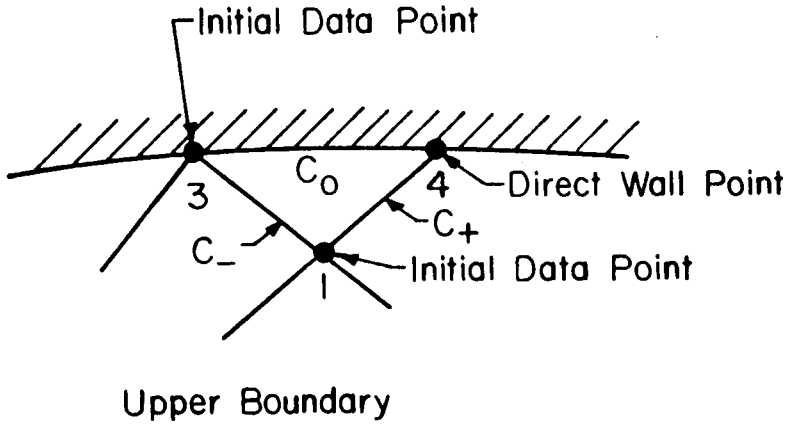

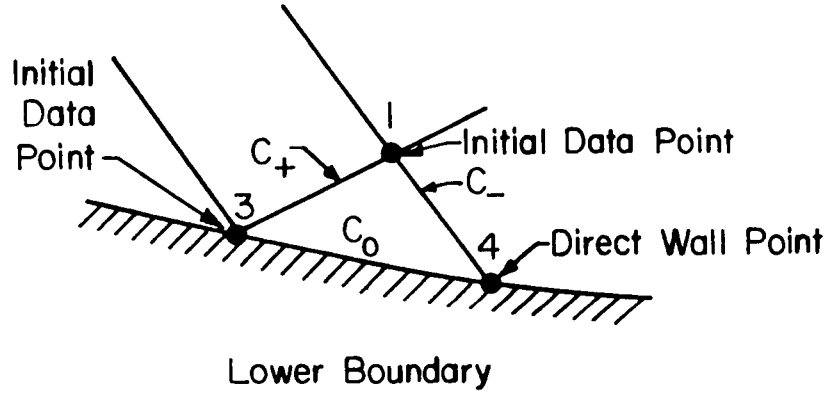

Figure I.2. Scheme for calculation of solid boundary point (direct)

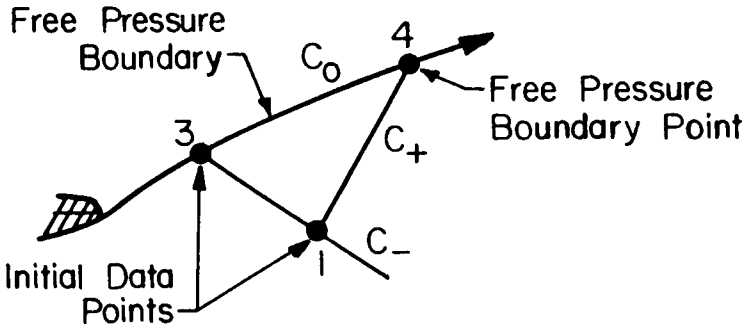

Upper Boundary

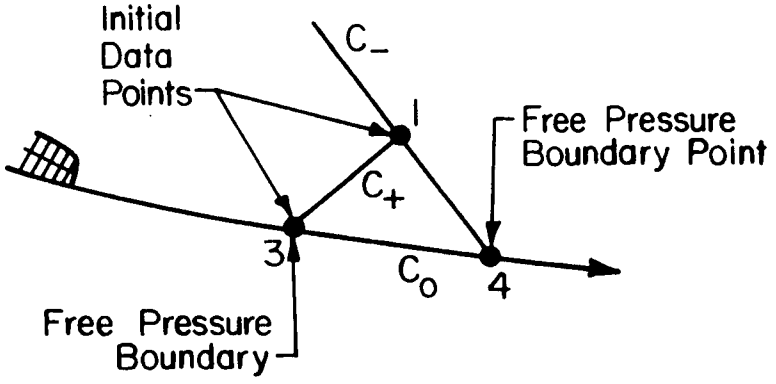

Lower Boundary

Figure I.3. Scheme for calculation of pressure boundary point

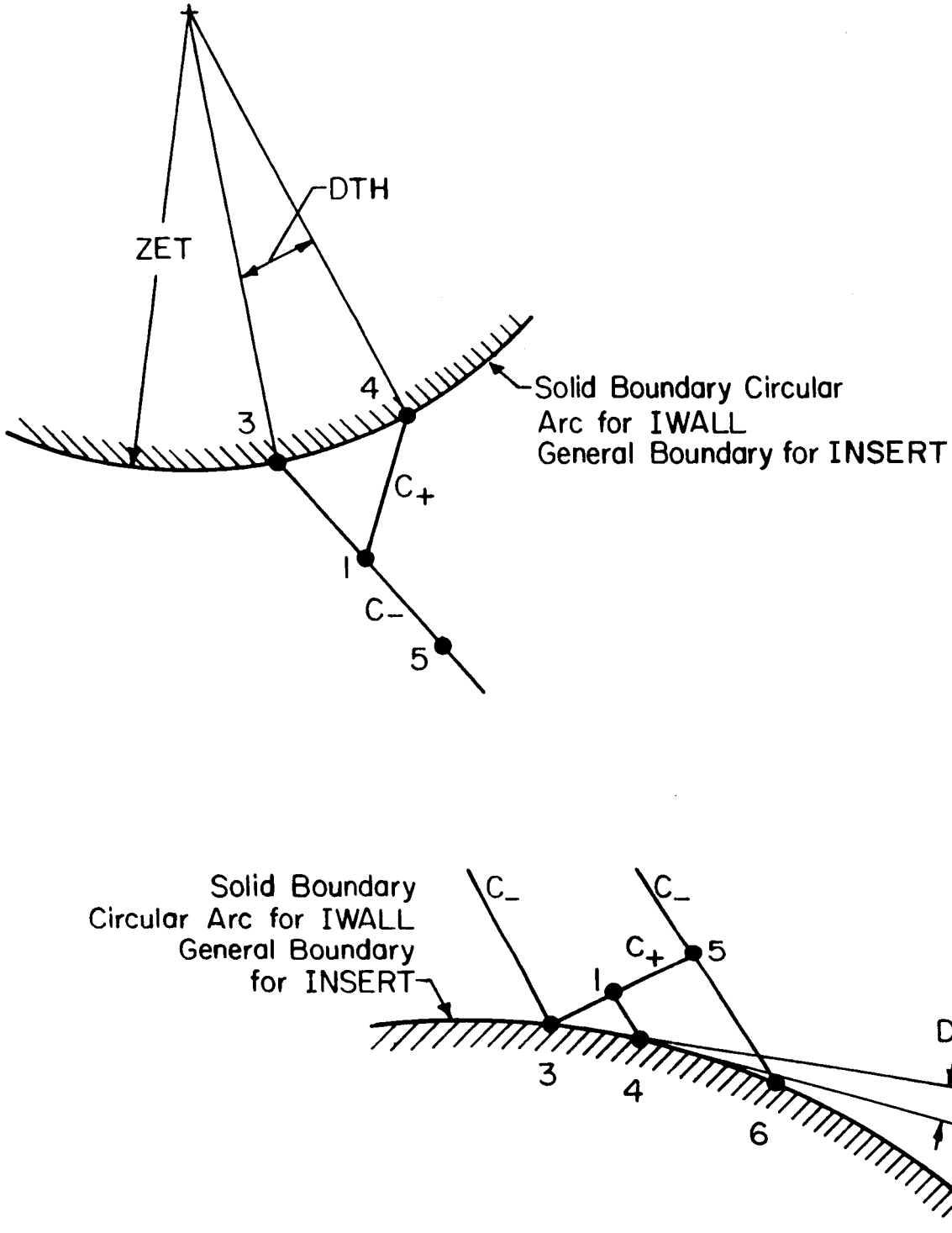

Figure I.4. Calculation of solid boundary point (inverse)

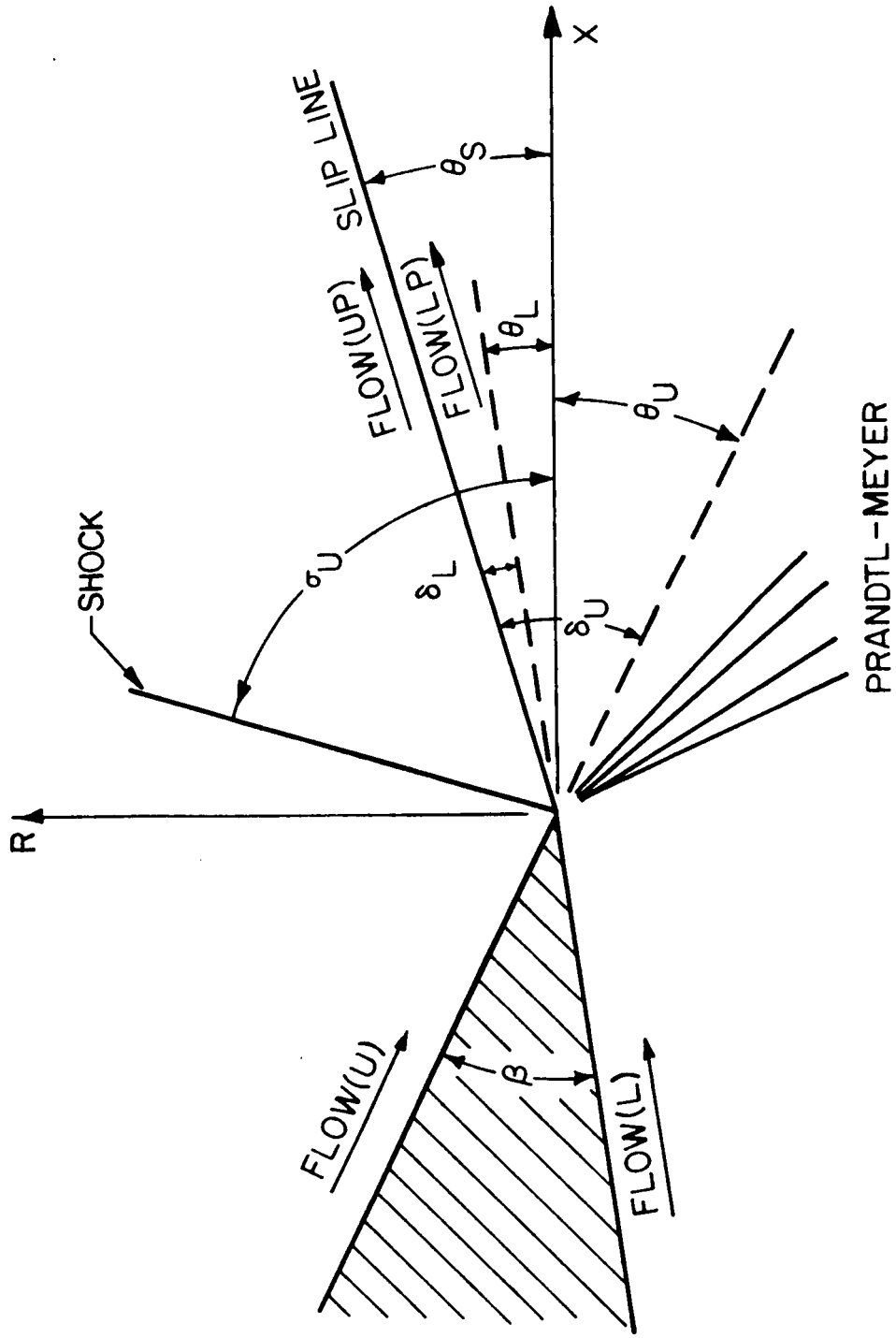

Figure I.5. Procedure for calculation of flow point at joining of two streams

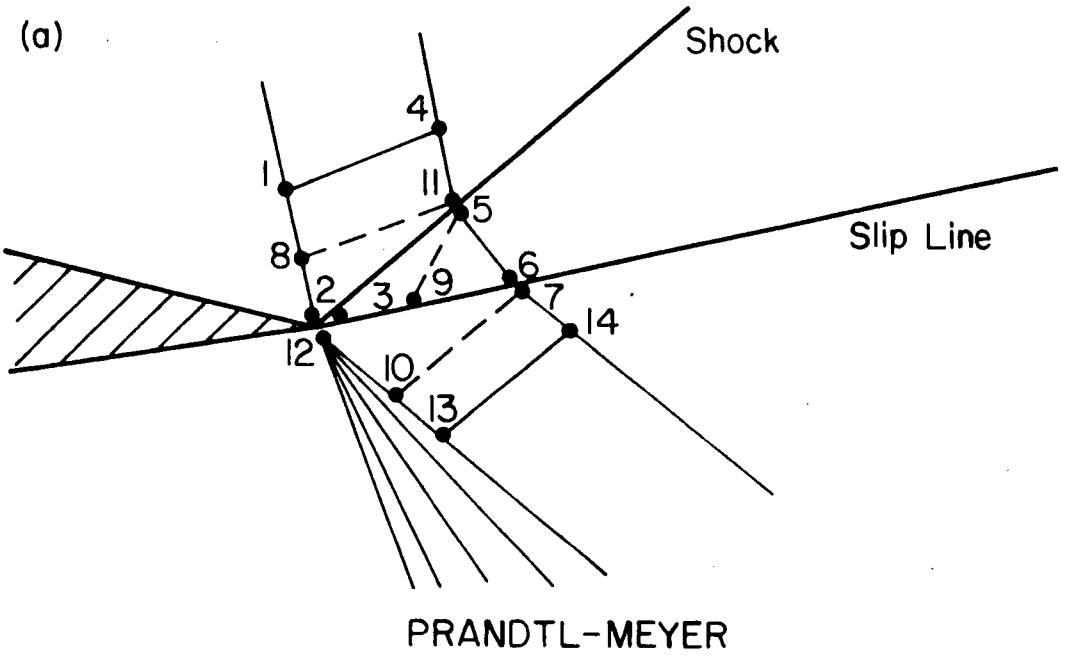

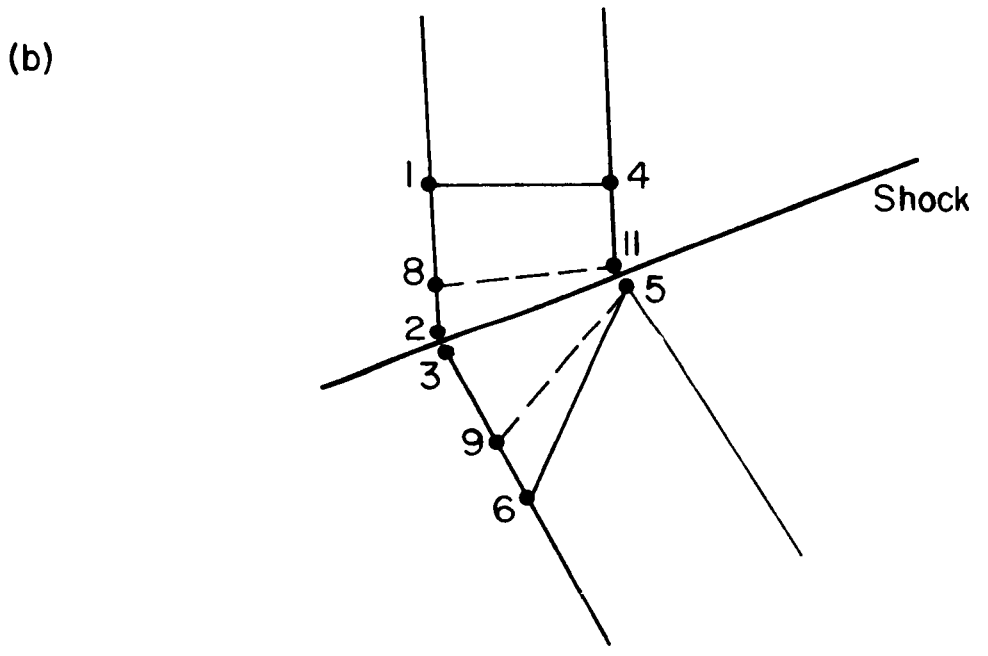

Figure I.6. Calculation of shockwave

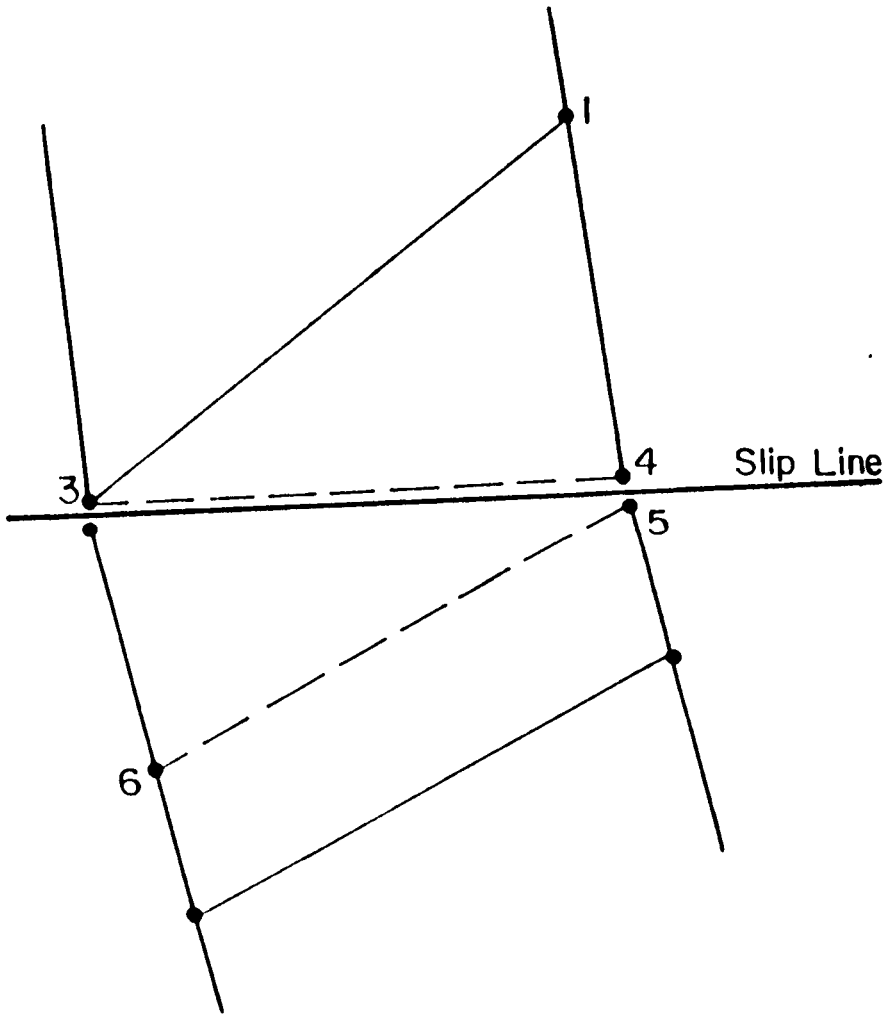

Figure I.7. Procedure for slip line calculation

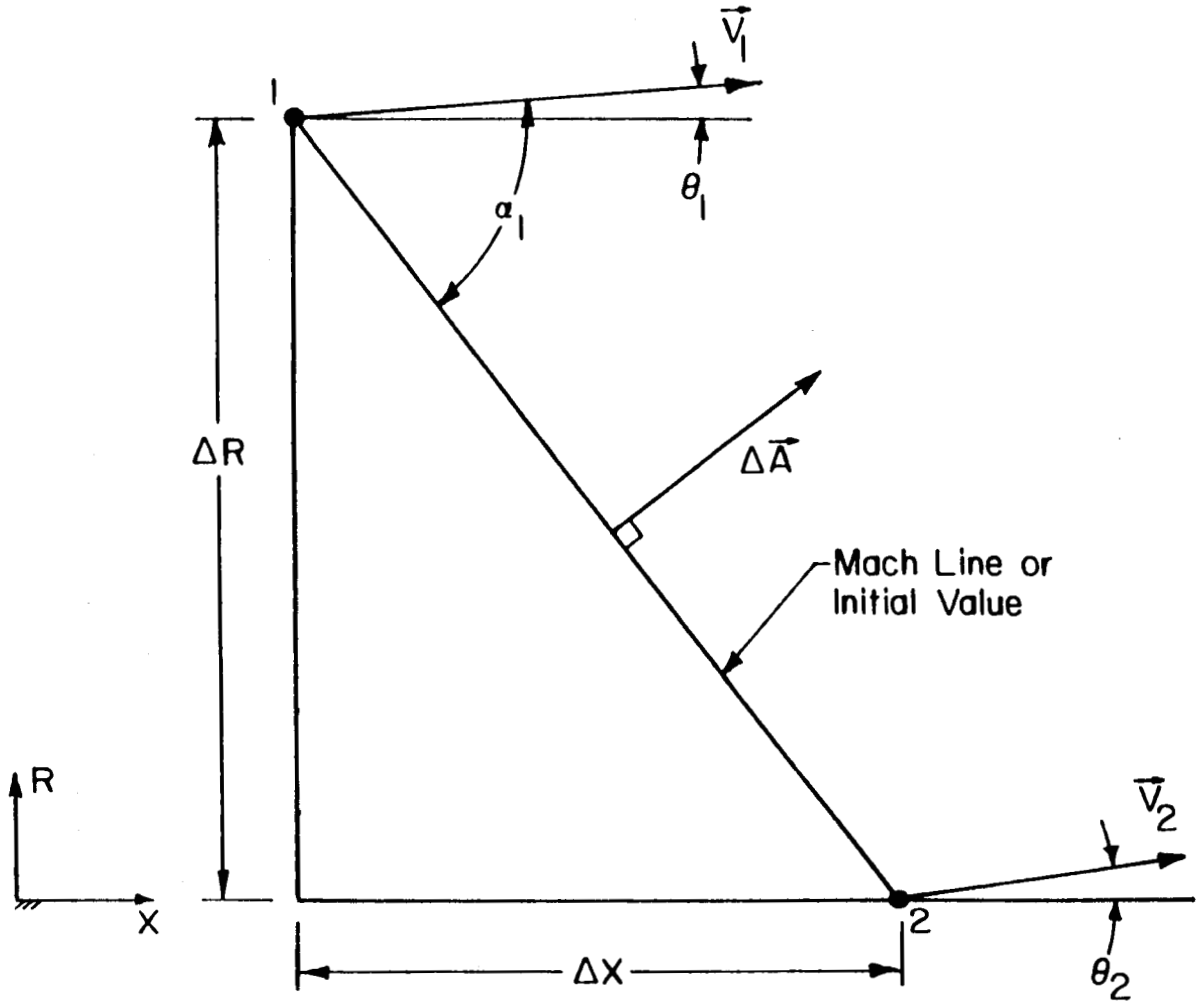

Figure I.8. Establishment of incremental thrust and mass flux

APPENDIX II

TURBULENCE MODELLING FOR COMPRESSIBLE HIGH SPEED FLOWS

1. Introduction

It is generally assumed that Navier-Stokes equations are adequate for analysis of turbulent flows (Ref. II.1). Three approaches to solving those equations for given initial and boundary conditions are: (i) direct simulation based on large scale turbulence dynamics and modelling of small scales (Refs. II.2-3); (ii) simulation based on identification of a large eddy by spectral decomposition and the interaction of the large eddy with all other eddies and the applied strain in the given flowfield (Ref. II.4); and (iii) utilization of time-averaged N-S equations after applying Reynolds decomposition (Ref. II.5). Current experience seems to suggest that approach (i) is most effective, physically and computationally, for comparatively low Reynolds number flows governed by simple boundary conditions. Similarly, approach (ii) has been applied only to some simple flows and involves, at this time, assumptions that are not checked directly from experiments. Approach (iii), generally referred to as conventional modelling, involves a number of unknowns related to various turbulence processes (the so-called closure problem) and they may only be selected based on experience of effectiveness.

Two variations of approach (i) also have been developed (Refs. II.6-7) but they are largely "experimental" schemes. Similarly, the use of probability density functions as the primary variables has been advanced (Ref. II.8), again successfully for simple flows (inert and reactive) but with little experience at this time in the context of complex flows of practical importance.

In the current analysis, therefore, the attempt is to improve conventional modelling in the context of compressible high speed flows.

Morkovin's hypothesis in compressible high speed flows states (Ref. II.9) that the direct effects of density fluctuations on turbulence are small if the root-mean-square density fluctuation is small compared with the mean density. This implies that below a certain value of Mach number, for example about 5 in the case of a boundary layer, turbulence structure is the same as in the corresponding constant-density flow. Although Morkovin's hypothesis does not cover mean density variations in the flow, it has been pointed out (Ref. II.10) that those effects are small at comparatively low Mach numbers and small pressure gradients, consequently, calculations based on structural similarity yield results based on constant density assumptions that are reasonably satisfactory for flows below the afore-mentioned value of Mach number, provided turbulence structure is appropriately scaled. Some advances have occurred in inner layer and outer layer scaling for a boundary layer, both with respect to wall shear stress and heat transfer. References II.11-13 should be consulted for a discussion of such scaling procedures and their usefulness.

In the context of conventional modelling, scaling of turbulence structure (correlations and spectral quantities) implies identification of specific turbulence processes that need to be adjusted for compressibility and high speed effects. The current interest is in application to shock-boundary layer interaction with wall heat transfer and, therefore, several turbulence scales are of interest. We discuss in the following a model for turbulence, applicable to compressible, high speed flow.

In the following the standard tensor notation is utilized with (i,j,k) as free indices and (l,m,n) as dummy variables. Kroneckar delta is designated by δ with appropriate suffices.

1.1. Favre Decomposition

In variable density flows involving density fluctuations, it is found advantageous from several points of view to utilize decomposition and averaging as suggested by Favre (Refs. II.14-15) wherein all of the variables are density-weighed. We adopt Favre-variables in the analysis.

The notation utilized is the same as in Ref. II.11 unless otherwise indicated.

According to Reynolds decomposition, one can write the velocity component in the form

$$u_i(\underline{x}, t) = \bar{u}_i + u_i' \tag{II.1}$$

Assuming that $\bar{u}_i$ varies sufficiently slowly with time and hence the turbulence is stationary, ordinary time-averages may be constructed for any desired quantity of interest.

In variable density flows, according to Favre decomposition, one can write

$$u_i(\underline{x}) = \tilde{u}_i(\underline{x}) + u_i''(\underline{x}, t) \tag{II.2}$$

where the mean value is defined by writing

$$\tilde{u}_i(\underline{x}) = \overline{\rho u_i}/\bar{\rho}\,, \tag{II.3}$$

and $\overline{\rho u_i''} = 0$ by definition. The meaning of density-weighting is clear from Eqn. (II.3). All of the variables of interest except pressure can be similarly density-weighted in the

decomposition.

Density-weighted decomposition introduces considerable complexity in accounting for molecular transport terms. However, there are advantages in modelling turbulent transport. For example, one can consider a term such as $\overline{\rho u_i}\overline{u}_j$ and write the following.

$$\overline{\rho u_i u_j} = \overline{\rho}\,\overline{u_i u_j} + \overline{\rho' u_i' u_j'} + \overline{u_i}\,\overline{\rho' u_j'} + \overline{u}_j\,\overline{\rho' u_j'} \qquad \text{(II.4)}$$

$$+ \overline{\rho' u_i' u_j'}$$

$$= \overline{\rho}\,\tilde{u}_i\tilde{u}_j + \overline{\rho u_i'' u_j''} \qquad \text{(II.5)}$$

From Eqn. (II.5), one can observe that no terms involving density fluctuations appear and the advantage of Favre averaging becomes obvious.

Considering high speed flows with density fluctuations, Morkovin has referred (Ref. II.9) to the third and fourth terms on the right-hand-side of Eqn. (II.4) as mass transfer terms, based on the reasoning that they represent momentum exchange caused by interaction between mean velocity and volume fluctuations, while the last term represents similar momentum exchange due to interactions between fluctuations. They do not appear explicitly in Eqn. (II.5).

2. BASIC EQUATIONS

It is assumed that the gas may be considered a perfect gas with constant specific heats, thermal conductivity, and molecular viscosity.

The equation of state for the gas may be written as follows.

$$p = (\gamma-1)C_v\,\rho T \qquad \text{(II.6)}$$

which becomes on decomposition the following.

$$p = (\gamma-1)\, C_v \rho(\tilde{T} + \Theta'') \quad . \tag{II.7}$$

Although we are mainly interested in steady flows with stationary turbulence, the following equations are written in ($\underline{x}$, t) co-ordinates.

The equation for conservation of mass may be written as follows.

$$\frac{\partial}{\partial t}\,\bar{\rho} + \frac{\partial}{\partial x_k}\,(\bar{\rho}\tilde{u}_k) = 0 \tag{II.8}$$

The equation for momentum balance may be written

$$\frac{\partial}{\partial t}\,(\bar{\rho}\tilde{u}_i) + \frac{\partial}{\partial x_k}\,(\bar{\rho}\,\tilde{u}_i\tilde{u}_k)$$

$$= -\frac{\partial \bar{p}}{\partial x_i} + \frac{\partial}{\partial x_k}\,[\bar{\tau}_{ik} - \frac{2}{3}\,\delta_{ik}\,\bar{\tau} - \overline{\rho u_i'' u_k''}] \tag{II.9}$$

where

$$\bar{\tau}_{ik} \sim \bar{\mu}(\frac{\partial \tilde{u}_i}{\partial x_k} + \frac{\partial \tilde{u}_k}{\partial x_i}) \tag{II.10}$$

and

$$\bar{\tau} \sim \bar{\mu}(\frac{\partial u_i}{\partial x_\ell}) \quad , \tag{II.11}$$

with the quantities in ( ) in Eqns. (II.10-11) representing strains. The signs of approximation in those equations denote neglect of molecular diffusivity.

The equation for energy balance is constructed as follows. We define total energy, E, by writing

$$\rho E = \rho\, C_v\, T + \rho\, \frac{\overline{u_i u_i}}{2} \tag{II.12}$$

$$= \rho(\tilde{E} + E'') \tag{II.13}$$

Here,

$$\bar{\rho}\tilde{E} = \bar{\rho}\, C_V \tilde{T} + \bar{\rho}\frac{\tilde{u}_i \tilde{u}_i}{2} + \bar{\rho}\,\frac{\widetilde{u_i'' u_i''}}{2} \tag{II.14}$$

and

$$\frac{\widetilde{u_i'' u_i''}}{2} = \tilde{k}, \tag{II.15}$$

with $\tilde{k}$ being the so-called turbulent kinetic energy. The equation for total energy balance may then be written as follows.

$$\frac{\partial}{\partial t}(\bar{\rho}\tilde{E}) + \frac{\partial}{\partial x_k}\left[\bar{\rho}\tilde{E}\tilde{u}_k + \bar{\rho}\,\widetilde{u_i'' u_k''}\tilde{u}_i + \bar{\rho}\frac{\widetilde{u_i'' u_i'' u_k''}}{2} + \gamma\, C_v\, \bar{\rho}\;\widetilde{\Theta'' u_k''}\right]$$

$$\simeq \frac{\partial}{\partial x_k}\left[-\bar{P}\tilde{u}_k + \lambda\frac{\partial \tilde{T}}{\partial x_k} + \bar{\tau}_{ik}\tilde{u}_i + \bar{\tau}_{ik}\overline{u_i''} - \frac{2}{3}\left(-\bar{\pi}\tilde{u}_i + \bar{\tau}\,\widetilde{u_i''}\right)\right] \tag{II.16}$$

where the approximation sign again indicates neglect of molecular transport. It may be pointed out that in the foregoing, we have written

$$\overline{\rho E'' u_k''} = \bar{\rho}\;\widetilde{E'' u_k''}$$

$$= \bar{\rho}\, C_v\;\widetilde{\Theta'' u_k''} + \rho\,\widetilde{u_i'' u_k''}\,u_i + \bar{\rho}\;\frac{\widetilde{u_i'' u_i'' u_k''}}{2} \tag{II.17}$$

Also,

$$\bar{\tau}_{ik}\tilde{u}_i = \bar{\mu}\left[\tilde{S}_{ik}\tilde{u}_i + \tilde{S}_{ik}\overline{u_i''} + \tilde{s}_{ik}''\tilde{u}_i + \overline{s_{ik}'' u_i''}\right] \tag{II.18}$$

and

$$\bar{\tau}u_i = \bar{\mu}\left[\tilde{S}\tilde{u}_i + \tilde{S}\overline{\tilde{u}_i''} + \overline{s''}\,u_i + \overline{s''\,u_i''}\right] \tag{II.19}$$

where S and s denote mean and fluctuating values of strains.

The Eqns. (II.7-9) and (II.16) contain various correlations among which there are three "unknown" correlations, namely $\widetilde{\bar{\rho}u_i'' u_k''}$, $\widetilde{\bar{\rho}\,u_i'' u_i'' u_k''}$ and $\widetilde{\bar{\rho}\,u_k''\Theta''}$. They need to be modelled, either directly or through additional transport equations. It is well known

that such transport equations will again involve other unknowns; some modelling becomes unavoidable.

2.1. Reynolds Stresses

In the case of Reynolds stresses, $\overline{\rho}\,\widetilde{u_i'' u_k''}$ for example, one can write, based upon the so-called gradient diffusion approximation, an expression as follows,

$$-\overline{\rho}\,\widetilde{u_i'' u_k''} = \mu_t\left(\frac{\partial \tilde{u}_i}{\partial x_k} + \frac{\partial \tilde{u}_k}{\partial x_i} - \frac{2}{3}\,\delta_{ik}\frac{\partial \tilde{u}_\ell}{\partial x_\ell}\right) - \frac{2}{3}\,\overline{\rho}\,\frac{\widetilde{u_i'' u_i''}}{2} \qquad \text{(II.20)}$$

where μ_t is in the nature of turbulent viscosity. The last term in Eqn. (II.20) involves turbulent kinetic energy which itself is an unknown.

Since gradient diffusion approximation is suspect (as explained in Ref. II.11, for example), one may proceed to set up a describing equation for the Reynolds stresses taking into account production, dissipation, transport and advection processes that together must determine the local value of Reynolds stresses. The equation becomes the following.

$$\frac{\partial}{\partial t}\,(\bar{\rho}\,\widetilde{u_i'' u_j''}) + \frac{\partial}{\partial x_k}\,(\bar{\rho}\,\tilde{u}_k \widetilde{u_i'' u_j''})$$

$$+ \bar{\rho}(\widetilde{u_i'' u_k''}\,\frac{\partial \tilde{u}_j}{\partial x_k} + \widetilde{u_j'' u_k''}\,\frac{\partial \tilde{u}_i}{\partial x_k})$$

$$= -\frac{\partial}{\partial x_k}\,(\bar{\rho}\,\widetilde{u_i'' u_j'' u_k''}) - (\overline{u_i''}\,\frac{\partial \bar{P}}{\partial x_i} + \overline{u_j''}\,\frac{\partial \bar{P}}{\partial x_i}) + \overline{p'(\frac{\partial u_i''}{\partial x_j} + \frac{\partial u_j''}{\partial x_i})}$$

$$- \frac{\partial}{\partial x_k}\,(\delta_{ik}\,\overline{u_j'' p'} + \delta_{jk}\,\overline{u_i'' p'})$$

$$+ \frac{\partial}{\partial x_k}\,[\,(\overline{\mu\, S_{ik} u_j''} + \overline{\mu\, S_{jk} u_i''})$$

$$- \frac{2}{3}(\overline{\mu\, S u_j'' \rho_{ik}} + \mu\,\overline{S u_i'' \delta_{jk}})\,]$$

$$- \overline{\mu\,(S_{ik}\,\frac{\partial u_j''}{\partial x_k} + S_{jk}\,\frac{\partial u_i''}{\partial x_k})}$$

$$+ \overline{\frac{2}{3}\,\mu\, S(\frac{\partial u_i''}{\partial x_j} + \frac{\partial u_j''}{\partial x_i})} \qquad \text{(II.21)}$$

Two observations should be noted concerning Eqn. (II.21): (1) Every term on the right-hand-side and the last term on the left-hand-side require modelling. (2) As described in Ref. II.1, p. 26, we may group the terms as follows.

(a) Generation by interaction of turbulent motion with mean rate-of-strain and mean pressure gradient fields: term 3 on the LHS and term 2 on the RHS.

(b) Generation, destruction or redistribution by pressure fluctuations: term 3 on the RHS.

(c) Transport by velocity fluctuations: term 1 on the RHS.

(d) Transport by pressure fluctuations: term 4 on the RHS.

(e) Destruction or generation and, also, transport by viscous-stress fluctuations: terms 5, 6, and 7 on the RHS.

2.2. Turbulent Flux of Reynolds Stresses

An exact transport equation can be constructed for the transport flux of Reynolds stresses, $\widetilde{\rho u_i'' u_j'' u_k''}$. Such an equation again involves production, dissipation, advection and diffusive terms. Various suggestions have been made, for example Ref. II.16-17, to simplify the equation by neglecting advection and diffusive terms. One approximation, Ref. II.17, consists in writing $\rho u_i'' u_j'' u_k''$ as follows.

$$-\widetilde{\rho u_i'' u_j'' u_k''} = C_s \bar{\rho} \frac{\tilde{k}}{\tilde{\epsilon}} \left[\widetilde{u_i'' u_i''} \frac{\partial}{\partial x_\ell} \widetilde{u_j'' u_k''} + \widetilde{u_j'' u_\ell''} \frac{\partial}{\partial x_k} \widetilde{u_i'' u_k''} + \widetilde{u_k'' u_\ell''} \frac{\partial}{\partial k_i} \widetilde{u_i'' u_j''} \right] \qquad \text{(II.22)}$$

where $\tilde{k} = \widetilde{u_i'' u_i''}/2$ and is the kinetic energy of turbulence, and $\tilde{\epsilon}$ is the turbulent dissipation rate. C_s is a constant.

It is well known, Ref. II.16, that transport equations can be constructed for $\tilde{k}$ and $\tilde{\epsilon}$. They involve other unknown quantities. However, some physical justification can be made for introducing a quantity such as turbulent dissipation rate based on its relation to turbulent length scale. For example the viscous dissipation of energy has been estimated (by G.I. Taylor, 1935) from the large scale dynamics, which do not involve viscosity, by writing $\epsilon \sim u^3/\ell$ where ℓ is a length scale chosen such that the viscous terms are of the same order of magnitude as the inertia terms.

2.2.1. Turbulent Kinetic Energy

An equation for the local balance of turbulent kinetic energy can be written as follows.

$$\frac{\partial}{\partial t}\,\bar{\rho}\tilde{k} + \frac{\partial}{\partial x_k}\,(\bar{\rho}\,\tilde{k}\,\tilde{u}_k) = P_k - \bar{\rho}\,\tilde{\epsilon} + \frac{\partial}{\partial x_k}\,\mu_k\,\frac{\partial \tilde{k}}{\partial x_k} - 2\mu\,(\frac{\partial \sqrt{\tilde{k}}}{\partial x_m})^2 \qquad \text{(II.23)}$$

where P_k represents production of turbulent kinetic energy, given by

$$P_k = \mu_t\,(\frac{\partial \tilde{u}_i}{\partial x_j} + \frac{\partial \tilde{u}_j}{\partial x_i})\;\frac{\partial \tilde{u}_i}{\partial x_j} - \frac{2}{3}\,\bar{\rho}\,\tilde{k}\,\frac{\partial \tilde{u}_i}{\partial x_i} \qquad \text{(II.24)}$$

It may be pointed out that Eq. (II.24) involves eddy viscosity in the first term on the RHS implying gradient diffusion. The production rate represents, in general, the product of mean strain and each of the Reynolds stresses. Similarly, the dissipation rate, $\tilde{\epsilon}$, can be considered as the rate at which turbulence does work against viscous stresses. The remaining terms on the RHS in Eqn. (II.23) represent diffusion.

2.2.2. Turbulent Dissipation

An exact equation for transport of dissipation rate of total kinetic energy, $\tilde{E}$, can be constructed, Ref. II.18, as follows.

$$\frac{\partial}{\partial t}(\bar{\rho}\tilde{\epsilon}) + \frac{\partial}{\partial x_k}(\bar{\rho}\tilde{u}_k\tilde{\epsilon}) + \frac{\partial}{\partial x_k}(\bar{\rho}\widetilde{u_k''\epsilon''})$$

$$= -\bar{\mu}[\widetilde{s_{ij}''u_k''}\frac{\partial}{\partial x_k}\tilde{S}_{ij} - \frac{4}{3}\widetilde{s''u_k''}\frac{\partial}{\partial x_k}\tilde{S}]$$

$$-2\bar{\mu}[\widetilde{s_{ij}''}\frac{\partial u_i''}{\partial x_k}\cdot\frac{\partial\tilde{u}_k}{\partial x_j} + \widetilde{s_{ij}''}\frac{\partial u_k''}{\partial x_k}\frac{\partial\tilde{u}_i}{\partial x_k} - \frac{4}{3}\widetilde{s''}\frac{\partial u_i''}{\partial x_i}\frac{\partial\tilde{u}_k}{\partial n_k}]$$

$$-2\bar{\mu}[\widetilde{s_{ij}''}\frac{\partial u_i''}{\partial x_k}\frac{\partial u_k''}{\partial x_i} - \frac{2}{3}\widetilde{s''}(\frac{\partial u_k''}{\partial x_k})^2]$$

$$-2\frac{\bar{\mu}}{\bar{\rho}}(\overline{s_{ij}''\frac{\partial^2 p'}{\partial x_i\partial x_j}} - \frac{2}{3}\overline{s''\frac{\partial^2 p'}{\partial x_i\partial x_i}}) + 2\frac{\bar{\mu}}{\bar{\rho}}(\overline{s_{ij}''\frac{\partial^2\tau_{ik}}{\partial x_j\partial x_k}} - \frac{2}{3}\overline{s''\frac{\partial\tau_{ik}}{\partial x_i\partial x_k}})$$

$$-\frac{4}{3}\frac{\bar{\mu}}{\bar{\rho}}(\frac{\overline{s_{ij}''\partial^2\tau}}{\partial x_i\partial x_j} - \frac{2}{3}\overline{s''\frac{\partial^2\tau}{\partial x_i\partial x_i}})$$

$$-2\frac{\bar{\mu}}{\bar{\rho}}(\overline{s_{ij}''}\frac{\partial^2\bar{P}}{\partial x_i\partial x_j} - \frac{2}{3}\overline{s''}\frac{\partial^2\bar{P}}{\partial x_i\partial x_i})$$

$$+2\frac{\bar{\mu}}{\bar{\rho}}[(\frac{\overline{s_{ij}''}}{\rho}\frac{\partial P}{\partial x_i} - \frac{2}{3}\frac{\overline{s''}}{\rho}\frac{\partial P}{\partial x_i})(\frac{\partial P}{\partial x_i} - \frac{\partial\tau_{ik}}{\partial x_k} + \frac{2}{3}\frac{\partial\tau}{\partial x_i})] \qquad \text{(II.25)}$$

$$\widetilde{S_{ij}} = \frac{\partial\widetilde{u_i}}{\partial x_j} + \frac{\partial\widetilde{u_j}}{\partial x_i}\ ;\ \tilde{S} = \frac{\partial u_k}{\partial x_k}$$

$$\widetilde{s_{ij}} = \frac{\partial\widetilde{u_i''}}{\partial x_j} + \frac{\partial\widetilde{u_j''}}{\partial x_i}\ ;\ s = \frac{\partial u_k''}{\partial x_k}$$

$$\tau_{ij} = \mu(\frac{\partial u_i}{\partial x_j} + \frac{\partial u_j}{\partial x_i})\ ;\ \tau = \mu\frac{\partial u_k}{\partial x_i}$$

The last three terms on the RHS of Eqn. (II.25) require modelling.

2.3. Flux of Temperature Fluctuations

It may be recalled that Eqn. (II.16) involves the turbulent flux term $\bar{\rho}\ u_k''\Theta''$. An exact equation for the transport of that term can be constructed in the same manner as

Eqn. (II.21). Such an equation represents the balance between advection, production, dissipation and diffusion, including the effects of pressure fluctuations. Again, a number of terms require modelling.

3. MODELLING

The modelling of turbulent governing equations is classified, Ref. II.1, into the so-called (a) zero equation models, (b) one equation models, (c) two equation models and (d) second order closure models. The latter is currently considered the most general and engineering-wise practical model. It involves the Reynolds stress equation, such as Eqn. (II.21), a corresponding equation for the turbulent flux of temperature fluctuations, such as that referred to in Section 2.3 of this Appendix, and a scale equation, generally written in terms of turbulence kinetic energy dissipation rate, for example Eqn. (II.25). Each of those three equations requires modelling for various terms.

3.1. Equation II.21

In Eqn. (II.21), several terms are modelled as follows.

First, the turbulent flux of Reynolds stress is modelled as in Eqn. (II.22). It is often suggested that the pressure fluctuation-induced diffusion term, $(\overline{u_i'' p'} \delta_{jk} + \overline{u_j'' p'} \delta_{ik})$, be included with the tripple-correlation term. Then one writes the following.

$$-\bar{\rho}\,\widetilde{u_i'' u_j'' u_k''} + \rho_{ik}\,\overline{u_j'' p'} + \rho_{jk}\,\overline{u_i'' p'} \simeq C_s' \bar{\rho}\,\frac{\tilde{k}}{\tilde{\epsilon}}\,\widetilde{u_k'' u_\ell''}\,\frac{\partial}{\partial x_\ell}\,\widetilde{u_i'' u_j''} \qquad \text{(II.26)}$$

where C_s' is a constant.

3.1.1. Pressure-Strain Correlation

As pointed out in Ref. II.1, the pressure fluctuation-strain fluctuation correlation term is considered in constant density flows as representing the redistribution of Reynolds stresses and hence contributing to a reduction of anisotropy. In the case of compressible flows, $\partial u_i''/\partial x_i \neq 0$, and therefore $\overline{(p' \partial u_i''/\partial x_i)}$ is not equal to zero. Therefore, in addition to redistribution, the pressure fluctuation actually contributes to production and destruction.

Next, in the case of an incompressible flow, the pressure fluctuation is obtained formally through the integration of the Poisson equation. When the equation is considered in Favre-decomposed variables, a new term appears as follows in integration.

$$+ \frac{1}{4\pi} \int_{Vol} \overline{\left[\frac{\partial^2}{\partial x_m \partial x_\ell} \rho\, u_m'' u_\ell''\right]_B \cdot \left(\frac{\partial u_i''}{\partial x_i} + \frac{\partial u_j''}{\partial x_i}\right)} \cdot \frac{d\,Vol(B)}{r} \quad .$$

and that term is not equal to zero.

Finally, the integration of Poisson equation requires taking into account the variable properties.

The foregoing difficulties make the use of the incompressible flow approximation for pressure fluctuation-strain fluctuation in the compressible case considerably doubtful in validity. However, no attempt has been made here to improve the modelling compared to that of Refs. II.15 and 19 for incompressible flow. According to those references, one may write for a wall boundary layer the following expression.

$$\overline{p'\left(\frac{\partial u_i''}{\partial x_j} + \frac{\partial u_j''}{\partial x_i}\right)}$$

= redistribution in the free stream + that due the wall

$$= \{-\frac{C_2+8}{11}\left(P_{ij} - \frac{2}{3}\delta_{ij}P\right) - \frac{8C_2-2}{11}\left(\mathcal{D}_{ij} - \frac{2}{3}\delta_{ij}\mathcal{D}\right)$$

$$- \frac{30\,C_2-2}{55}\bar{\rho}\tilde{k}\tilde{S}_{ij} - C_1\,\bar{\rho}\frac{\tilde{\epsilon}}{k}\left(\widetilde{u_i''u_j''} - \frac{2}{3}\delta_{ij}\tilde{k}\right)\}$$

$$+ \{\frac{\tilde{k}^{3/2}}{\epsilon x_w}[C_3\,\bar{\rho}\,\frac{\tilde{\epsilon}}{\tilde{k}}\left(\widetilde{u_i''u_j''} - \frac{2}{3}\delta_{ij}\tilde{k}\right)$$

$$+ C_4\left(P_{ij} - \mathcal{D}_{ij}\right) + C_5\,\bar{\rho}\tilde{k}\left(\frac{\partial\tilde{u_i}}{\partial x_j} - \frac{\partial\tilde{u_i}}{\partial x_i} - \frac{2}{3}\delta_{ij}\frac{\partial\tilde{u_\ell}}{\partial x_\ell}\right)\}] \qquad \text{(II.27)}$$

$$P = \mathcal{D} = -\bar{\rho}\,\widetilde{u_j''u_k''}\frac{\partial\tilde{u_x}}{\partial x_j}$$

$$P_{ij} = -\bar{\rho}\left(\widetilde{u_i''u_k''}\frac{\partial\tilde{u_j}}{\partial x_k} + \widetilde{u_j''u_k''}\frac{\partial\tilde{u_i}}{\partial x_k}\right)$$

$$\mathcal{D}_{ij} = -\bar{\rho}\left(\widetilde{u_i''u_k''}\frac{\partial\tilde{u_k}}{\partial x_i} + \widetilde{u_j''u_k''}\frac{\partial\tilde{u_k}}{\partial x_i}\right)$$

and C_1, C_2, C_3, C_4 and C_5 are constants.

3.1.2. Mean Pressure Gradient Term

The mean pressure gradient $\partial\bar{p}/\partial x_i$ couples with the velocity fluctuation $\overline{u_i''}$ Based on Ref. II.20, one can write

$$\overline{u_i''} = \frac{1}{(n-1)C_p T} \widetilde{u_k \, u_i'' u_k''} \qquad \text{(II.28)}$$

3.1.3. Viscous-Diffusion Term

The term under consideration is the following.

$$-\left(\widetilde{u_j'' \mu S_{ik}} + \delta_{ik} \overline{u_j'' p'} + \delta_{jk} \overline{u_i'' p'}\right) + \frac{2}{3}\left(\overline{u_j'' \mu S \delta_{ik}} + \overline{u_i'' \mu S \delta_{jk}}\right)$$

Assuming that (a) the correlation between viscosity fluctuations and other quantities is small, (b) the correlations between $\overline{u_j''}$ and $\partial \tilde{u}_i/\partial x_k$, etc., are small, (c) μ = constant and (d) $\partial u_\ell''/\partial x_\ell = 0$, one can write the term under consideration in the form,

$$\frac{\partial}{\partial x_k}\left[\bar{\mu} \frac{\partial}{\partial x_k} \widetilde{u_i'' u_j''}\right] .$$

3.1.4. Viscous Non-Diffusive Term

Based on Refs. II.19 and II.20, the viscous non-diffusive term is approximated by setting it equal to

$$\bar{\rho} \frac{\tilde{\epsilon}}{\tilde{k}} \left[\widetilde{u_i'' u_j''} f_s + (1-f_s) \frac{2}{3} \delta_{ij} \tilde{k}\right]$$

where $f_s = 1/[1 + R_t/10]$

and $R_t = \tilde{k}^2/\nu\tilde{\epsilon}$.

3.1.5. Modelled Reynolds Stress Equation

Introducing the foregoing approximations, Eqn. (II.21) may be written in the following form

$$\frac{\partial}{\partial t}\,(\overline{\rho}\,\widetilde{u_i'' u_j''}) + \frac{\partial}{\partial x_k}\,(\overline{\rho}\,\widetilde{u_i'' u_j'' u_k})$$

$$= P_{ij} - \frac{C_2+8}{11}\,(P_{ij} - \frac{2}{3}\,\delta_{ij}P)$$

$$- \frac{8C_2-2}{11}\,(\mathcal{D}_{ij} - \frac{2}{3}\,\mathcal{D}) - \frac{30C_2-2}{55}\,\overline{\rho}\,\tilde{k}\left(\frac{\partial u_i}{\partial x_j}\right) + \left(\frac{\partial \widetilde{u_i}}{\partial x_j} + \frac{\partial \widetilde{u_j}}{\partial x_i}\right)$$

$$- C_1\,\overline{\rho}\,\frac{\epsilon}{\tilde{k}}\,(\widetilde{u_i'' u_j''} - \frac{2}{3}\,\delta_{ij}\tilde{k})$$

$$+ \{C_3\,\overline{\rho}\,\frac{\tilde{\epsilon}}{\tilde{k}}(\widetilde{u_i'' u_j''} - \frac{2}{3}\,\delta_{ij}\tilde{k}) + C_4(P_{ij} - \mathcal{D}_{ij})$$

$$+ C_5\,\overline{\rho}\,\tilde{k}\,(\frac{\partial \widetilde{u_i}}{\partial x_j} + \frac{\partial \widetilde{u_j}}{\partial x_i} - \frac{2}{3}\,\delta_{ij}\,\frac{\partial \widetilde{u_\ell}}{\partial x_\ell})\}\,\frac{\tilde{k}^{3/2}}{\tilde{\epsilon}\,x_n}$$

$$+ \frac{\partial}{\partial x_k}\,\{C_2'\,\overline{\rho}\,\frac{\tilde{k}}{\tilde{\epsilon}}\,\widetilde{u_k'' u_\ell''}\,\frac{\partial}{\partial x_\ell}\,\widetilde{u_i'' u_j''} + \mu\,\frac{\partial}{\partial x_k}\,\widetilde{u_i'' u_j''}\}$$

$$- \overline{\rho}\,\frac{\tilde{\epsilon}}{\tilde{k}}\,[\widetilde{u_i'' u_j''}\,f_2 + (1 - f_2)\,\frac{2}{3}\,\delta_{ij}\tilde{k}]$$

$$- (\overline{u_i''}\,\frac{\partial \overline{p}}{\partial x_j} + \overline{u_j''}\,\frac{\partial \overline{p}}{\partial x_i}) \qquad \text{(II.29)}$$

where $\overline{u_i''} = \dfrac{\widetilde{u_k u_i'' u_k''}}{(n-1)C_P\,\tilde{T}}$.

3.2. Modelling for Eqn. (II.16)

The turbulent flux of temperature fluctuations is modelled by writing

$$\widetilde{\Theta'' u_k''} = - C_6\,\frac{\tilde{k}}{\tilde{\epsilon}}\,\widetilde{u_k'' u_\ell''}\,\frac{\partial \tilde{T}}{\partial x_\ell} \qquad \text{(II.30)}$$

where C_6 is a constant.

The work done on shear stresses is approximated by neglecting $\overline{s_{ik}''}\,\tilde{u}_i$, $\overline{s_{ik}''\,u_i''}$ and $\tilde{S}_{ik}u_i''$.

Equation (II.16) may then be written as follows.

$$\frac{\partial}{\partial t}(\bar{\rho}\tilde{E}) + \frac{\partial}{\partial x_k}[\bar{\rho}\tilde{E}u_k - \gamma C_v \bar{\rho} C_e \frac{\tilde{k}}{\tilde{\epsilon}} \widetilde{u_k'' u_\ell''} \frac{\partial T}{\partial x_\ell}]$$

$$= \frac{\partial}{\partial x_k}[-\bar{P} u_k - (\bar{\rho} \widetilde{u_i'' u_k''} - \mu \frac{\partial \tilde{u}_k}{\partial x_i}) \tilde{u}_i - \frac{2}{3} \bar{\mu} \frac{\partial \tilde{u}_\ell}{\partial x_\ell} u_k$$

$$+ \mu \frac{\partial}{\partial x_k} (\frac{\widetilde{u_i u_i}}{2} + \frac{\widetilde{u_i'' u_i''}}{2})$$

$$+ C_6 \bar{\rho} \frac{\tilde{k}}{\tilde{\epsilon}} (\widetilde{u_k'' u_\ell''} \frac{\partial}{\partial x_\ell} \widetilde{u_i'' u_i''} + 2 \widetilde{u_i'' u_\ell''} \frac{\partial}{\partial x_\ell} \widetilde{u_i'' u_i''})$$

$$+ \delta_{\ell k} \lambda \frac{\partial T}{\partial x_\ell} + (\frac{\partial \tilde{u}_i}{\partial x_k} + \frac{\partial \tilde{u}_k}{\partial x_i} - \frac{2}{3} \delta_{ik} \frac{\partial \tilde{u}_\ell}{\partial x_\ell}) \cdot \frac{\widetilde{u_k}}{(n-1)C_p \tilde{T}} \widetilde{u_i'' u_k''}] . \qquad \text{(II.31)}$$

3.3. Modelling for Eq. (II.25)

The model suggested in Ref. II.16 is as follows.

$$\frac{D}{Dt}(\bar{\rho}\tilde{E}) = C_{\epsilon 1} \frac{\tilde{\epsilon}}{\tilde{k}} P - C_{\epsilon 2} \bar{\rho} \frac{\tilde{\epsilon}^2}{k}$$

$$- C_\epsilon \frac{\partial}{\partial x_k} \left\{ \bar{\rho} \frac{\tilde{k}}{\tilde{\epsilon}} \widetilde{u_k'' u_\ell''} \frac{\partial \tilde{\epsilon}}{\partial x_k} \right\} . \qquad \text{(II.32)}$$

It is important to note here that, according to Ref. II.18, the inclusion of production term requires further consideration.

In a boundary layer region, it is necessary to include two other effects: (1) the decay rate is modified near the wall; and (ii) the viscous diffusion term does not vanish at the wall. Taking those into account, Eqn. (II.32) may finally be written as follows.

$$\frac{D}{Dt}(\bar{\rho}\tilde{\epsilon}) = -C_{\epsilon 1}\,\bar{\rho}\,\frac{\tilde{\epsilon}}{\tilde{k}}\,\widetilde{u_i'' u_k''}\,\frac{\partial u_i}{\partial x_k}$$

$$- C_{\epsilon 2}\, f_\epsilon\, \bar{\rho}\,\frac{\tilde{\epsilon}}{\tilde{k}}\left[\tilde{\epsilon} - 2\nu\left(\frac{\partial\sqrt{\tilde{k}}}{\partial x_n}\right)^2\right]$$

$$+ \frac{\partial}{\partial x_k}\left[\left(\bar{\mu} + C_\epsilon\,\bar{\rho}\,\frac{\tilde{k}}{\tilde{\epsilon}}\,\widetilde{u_k'' u_\ell''}\right)\frac{\partial\tilde{\epsilon}}{\partial x_\ell}\right]$$

$$+ C_{\epsilon 3}\,\bar{\mu}\,\frac{\tilde{k}}{\tilde{\epsilon}}\,\widetilde{u_j'' u_k''}\left(\frac{\partial^2 \tilde{u}_i}{\partial x_j \partial x_\ell}\right)\left(\frac{\partial^2 \tilde{u}_i}{\partial x_k \partial x_\ell}\right)$$

$$- C_{\epsilon 4}\,\frac{\tilde{\epsilon}}{\tilde{k}}\,u_i''\,\frac{\partial\bar{P}}{\partial x_i} \qquad \text{(II.33)}$$

where $f_\epsilon = 1.0 - 0.222\,\exp\left[-\left(\frac{R_t}{6}\right)^2\right]$

and, $R_t = \frac{\tilde{k}^2}{\nu\epsilon}$. $C_{\epsilon 1} - C_{\epsilon 4}$ are constants.

We thus have Eqns. II.29, II.31 and II.33 for Reynolds stress, total energy and turbulent dissipation.

REFERENCES

II.1. Bradshaw, P. (Ed.), "Turbulence", *Springer-Verlag*, New York, 1978.

II.2. Mansoor, N.N., Ferziger, J.H., and Reynolds, W.C., "Large Eddy Simulation of the Turbulent Mixing Layer", Report TF11, Stanford University, 1978.

II.3. Schumann, U., Grotzbach, G., and Kleiser, L., "Direct Numerical Simulation of Turbulence", in *Prediction Methods for Turbulent Flows*, Hemisphere, New York, 1980.

II.4. Hong, S.K. and Murthy, S.N.B., "Structure of Turbulence in Curved Wall-Boundary Layers", AIAA Paper No. 83-0457, Jan. 1983.

II.5. Launder, B.E., Reece, G.J., and Rodi, W., *J. Fluid Mech.*, Vol. 68, 1975.

II.6. Kwak, D. and Reynolds, W., Report TF5, Stanford University, 1975.

II.7. Orzag, S.A. and Israeli, M., *Ann. Rev. Fluid Mech.*, Vol. 6, 1974.

II.8. Pope, S., "PDF Methods for Turbulent Reactive Flows", Prog. Energy Combust. Sci., Vol. 11, 1985.

II.9. Morkovin, M.V., "Effects of Compressibility on Turbulent Flows", in *The Mechanics of Turbulence*, Gordon and Breach, New York, 1961.

II.10. Bradshaw, P., "Compressible Turbulent Shear Layers", *Ann. Revs. Fluid Mech.*, Vol. 9, 1977.

II.11. Maise, G. and McDonald, H., "Mixing Length and Eddy Viscosity in a Compressible Boundary-Layer", AIAA Paper No. 67-199, 1967.

II.12. Bradshaw, P., "A Skin Friction Law for Compressible Turbulent Boundary Layers", Imperial College Report 76-2, 1976.

II.13. Cary, A.M. and Bertram, M.H., "Engineering Prediction of Turbulent-Skin Friction and Heat Transfer", NASA Tech. Note D-7507, 1974.

II.14. Murthy, S.N.B., "On Turbulent Energy Transfer", The Bull. Res. Israel, Vol. 11c, No. 2, 1962.

II.15. Favre, A., "Equations Statistiques des Fluides Turbulentz Compressibles", Vth CANCAM, New Brunswick, 1975.

II.16. Hanjalic, K. and Launder, B.E., "A Reynolds Stress Model of Turbulence", J. Fluid Mech., Vol. 52, No. 4, 1973.

II.17. Daly, B.J. and Harlow, F.H., "Transport Equations in Turbulence", Vol. 13, No. 11, 1970.

II.18. Ha Minh H., Kollman, W., and Vandromme, D.D., "Reynolds Stress Model for Compressible Flows", NASA Ames Report NASA-NCC2-186, 1983.

II.19. Lumley, J.L., "Prediction Methods for Turbulent Flows", Lecture Sereis VKI, No. 765, 1975.

II.20. Hanjalic, K. and Launder, B.E., "Contribution Towards a Reynolds Stress Closure", J. Fluid Mech., Vol. 52, No. 4, 1973.

APPENDIX III

NEAR WALL REGION APPROXIMATIONS

Four major considerations in the wall region are: (1) anisotropic dissipation; (2) redistribution of stresses due to pressure-strain; (3) diffusion; and (4) influence of normal stresses. They are strongly related to the low-Reynolds-number character of the flow in the vicinity of the wall.

The asymptotic values of the dissipation tensor components, namely ϵ_{11}, ϵ_{22}, ϵ_{33}, ϵ_{12}, depend on the instantaneous velocity.

In the case of incompressible flow, based on the expansion of instantaneous velocity with respect to y, the direction normal to the wall, Launder and Reynolds (Reference III.1) have deduced that

$$\epsilon_{11} = \frac{\overline{u'^2}}{k}\,\bar{\epsilon},$$

$$\epsilon_{22} = 4\,\frac{\overline{v'^2}}{k}\,\bar{\epsilon},$$

$$\epsilon_{33} = \frac{\overline{w'^2}}{k}\,\bar{\epsilon}, \text{ and}$$

$$\epsilon_{12} = 2\,\frac{\overline{u'v'}}{k}\,\bar{\epsilon}.$$

It is possible to introduce anisotropy near the wall by decreasing $\overline{v'^2}$ and $\overline{u'v'}$ according to the foregoing.

Several considerations then arise as follows (Reference III.2):

(i) The approximation is not tensorially exact, the sum of the components not yielding the dissipation rate. Physically the kinetic energy is probably being allowed to decrease too fast through $\overline{v'^2}$. Correlations can be introduced but, as of now, on an ad hoc basis.

(ii) The dissipation rate can be expanded in different ways and becomes different.

(iii) Compressibility effects may be quite significant.

Regarding the latter, it must be noted that fluctuations in the Stokes convective derivative depend directly upon density fluctuations. Thus, for an ideal gas, under the assumption of a polytropic process near the wall with a fixed exponent n,

$$\frac{D}{Dt} \sim - \frac{1}{n-1} \left(\frac{1}{T} \frac{\partial T}{\partial t} \right)_w$$

where $( )_w$ indicates vicinity of the wall. However, for an expansion process with a positive total derivative n is less than γ, γ being the ratio of specific heats.

Next, considering pressure-strain no rational schemes exists for modifying $\phi_{ij,1}$ and $\phi_{ij,2}$, although they seem necessary. Physically there arise two considerations: introduction of anisotropy and correct magnitude of turbulent kinetic energy near the wall.

Regarding turbulent kinetic energy, it follows that

$$\bar{k} = \bar{E} - \bar{\epsilon} - \frac{1}{2}\tilde{U}_i \tilde{U}_i,$$

where the three terms on the right hand side represent, respectively, the total energy, the specific mean internal energy and the specific mean kinetic energy. All of the components are time-averaged and Favre density-weighted.

In regions where an inviscid flow approximation is valid, the energy budget remains as stated. But in regions of high shear and low mean velocities, as near the wall, the turbulent kinetic energy becomes comparable to the mean motion kinetic energy.

Considering pressure, an effective pressure can then be defined as follows.

$$p^* = \bar{p} + \frac{2}{3}\bar{\rho}\tilde{k}$$

It should be noted carefully that the effective pressure cannot be isotropic since the Reynolds stress tensor is anisotropic. Thus, considering the i-momentum equation.

$$p_i^* = \bar{p} + \bar{\rho}\,\overline{u_i''^2}$$

Now, relating the pressure to the temperature, through the utilization of the assumption of a perfect gas law, two temperatures may be defined as follows.

$$\bar{p} = \bar{\rho}\, R\, \tilde{T}, \text{ and}$$

$$p^* = \bar{\rho}\, R\, T^*$$

$$\text{with } T^* = \tilde{T} + \frac{2}{3}\frac{\tilde{k}}{R}.$$

It may be observed that the quantities of interest in the coupling between temperature and pressure are such quantities as (a) pressure gradient and (b) gradient

of $\left(\frac{2}{3}\tilde{k}\,\overline{\rho}\right)$. In high shear regions, (b) can be much larger than (a). On the other hand, in a process such as a shockwave, the pressure gradient is obviously the more dominant. Thus, the manner of including pressure-strain depends upon the particular problem when considering the wall region.

Finally, in general, diffusion reduces dissipation near the wall. Hence changes are required in the dissipation rate equation. However, they may be introduced only in an ad hoc manner at present.

REFERENCES

III.1. Launder, B.E. and Reynolds, W.C., "Asymptotic Near-Wall Stress Dissipation Rates in a Turbulent Flow", *Phys. Fluids*, Vol. 26, 1983.

III.2. Rosallo, R.S., NASA TM 81315, 1981.

APPENDIX IV

NASA LEWIS RESEARCH CENTER TEST DATA

During the tests, among various parameters, the following have been varied.

1. Nozzle throat area, A_8, in^2.
2. Nominal hot gas temperature, T_{7cc}, R.
3. Nominal nozzle pressure ratio, P_{T7}/P_o.
4. Upstream stagnation pressure, P_{T7}, $lbf./in^2$.
5. Hot gas flow rate, W_{G7}, lbm./sec..
6. Nominal plug coolant flow rate, W_{csp}, lbm./sec.
7. Coolant stagnation pressure, P_{csp}, $lbf./in^2$.
8. Coolant stagnation temperature, T_{csp} R.

In addition to pressure and temperature data acquired at the walls, the stagnation pressure distribution and the stagnation temperature distribution in the vicinity of the wall has been measured by means of traversing probes.

A part of the data, referred to as NASA DATA, is reproduced in Table IV.I and IV.II, and in Figures IV.1-IV.14. The data given in the tables and in the figures should be considered as supplementary. Furthermore, there does not exist a complete correspondence between the cases identified in the tables and those in the figures.

TABLE IV.I

NASA DATA: SELECTED TEST DATA, PART A

Test No.	A_8	T_{7cc}	P_{T7}/P_o	W_{csp}	Figure No.
A-1	115	1750.	1.4	.05	IV.2
A-2	"	"	2.5	.1	"
A-3	"	"	3.0	"	"
A-4	"	"	4.0	"	"
A-5	"	"	5.0	"	"
A-6	"	"	8.0	"	IV.2,3
C-1	175	2500.	1.6	.4	IV.1
C-2	"	"	2.0	.25	"
C-3	"	"	3.0	.2	"
C-4	"	"	4.5	"	"
C-5	"	"	8.0	"	IV.1,IV.4
F-1	115	1750.	5.0	-0-	IV.4
F-2	"	1180.	2.0	"	IV.4
F-3	175	1180.	2.0	"	"
F-4	"	"	4.5	"	"
F-5	"	"	8.0	"	IV.1

NOTE: Figures referred to in the table provide data pertaining to tests that are either very close to or of the same conditions as the tests indicated by Test No.

TABLE IV.II

NASA DATA: SELECTED TEST DATA, PART B

Test No.	A_8	P_{T8}/P_o	P_{T8}	T_7	W_{G7}	W_{cs}	P_{csp}	T_{csp}	Figure No.
192	175	5.92	12.75	2,502	21.34	.1497	3.93	,1480	IV.5,6
193	"	5.97	12.83	2,524	21.32	.104	347	1,601	"
194	"	5.99	12.86	2,529	21.31	.051	2.90	1,749	"
195	"	5.92	12.80	2,515	21.29	.201	4.83	1,343	IV.5,6
196	"	4.53	12.79	2,517	21.39	.202	4.77	1,338	IV.7,8
197	"	4.50	12.71	2,507	21.34	.329	6.46	1,173	"
198	"	4.59	12.85	2,515	21.33	.107	3.50	1,580	"
199	"	2.92	12.81	2,521	21.20	.142	4.05	1,507	IV.5,6
200	"	2.91	12.76	2,504	21.22	.200	4.84	1,357	IV.9,10
201	"	2.90	12.71	2,509	21.28	.296	6.23	1,210	"
211	"	2.98	7.38	2,484	12.31	.107	2.68	1,490	"
213	"	5.91	24.54	2,541	41.88	.393	8.39	1,256	IV.5,6
214	"	4.49	24.42	2,583	41.26	.393	8.48	1,276	IV.7,8
300	115	9.94	15.05	1,743	20.97	.102	2.93	1,364	IV.11,12
302	"	9.82	14.89	1,720	20.94	.412	7.35	973	"
303	"	9.84	14.60	1,687	20.90	1.043	15.11	749	"
398	175	3.09	24.84	2,552	41.98	.396	8.50	1,288	IV.9,10
429	"	2.96	15.07	3,386	22.16	.949	16.99	1,038	IV.13,14
430	"	4.45	15.20	3,429	22.14	.605	11.73	1,273	"
431	"	7.78	15.13	3,416	22.14	.415	8.68	1,447	"

NOTE: Figures referred to in the table provide data pertaining to tests that are either very close to or of the same conditions as the tests indicated by Test No.

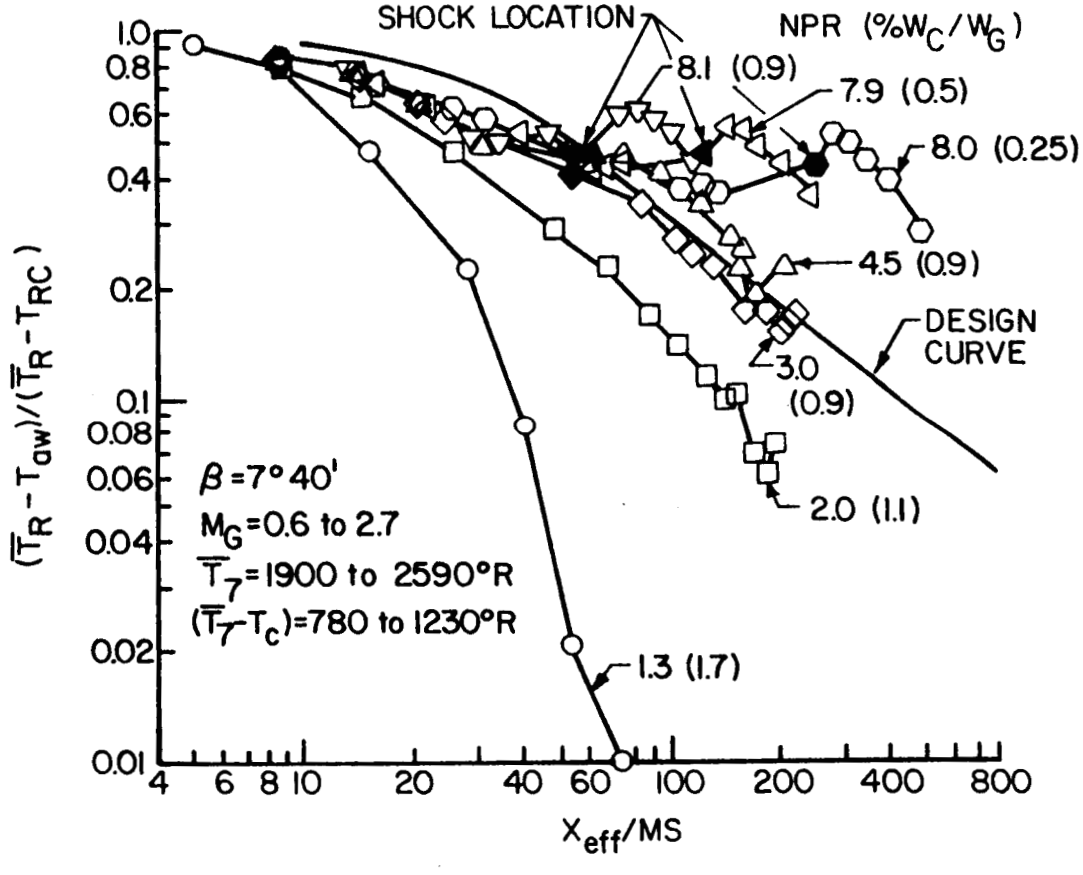

Figure IV.1. Effect of nozzle pressure ratio and coolant flow rate on film cooling effectiveness. NASA Test Data (Continued)

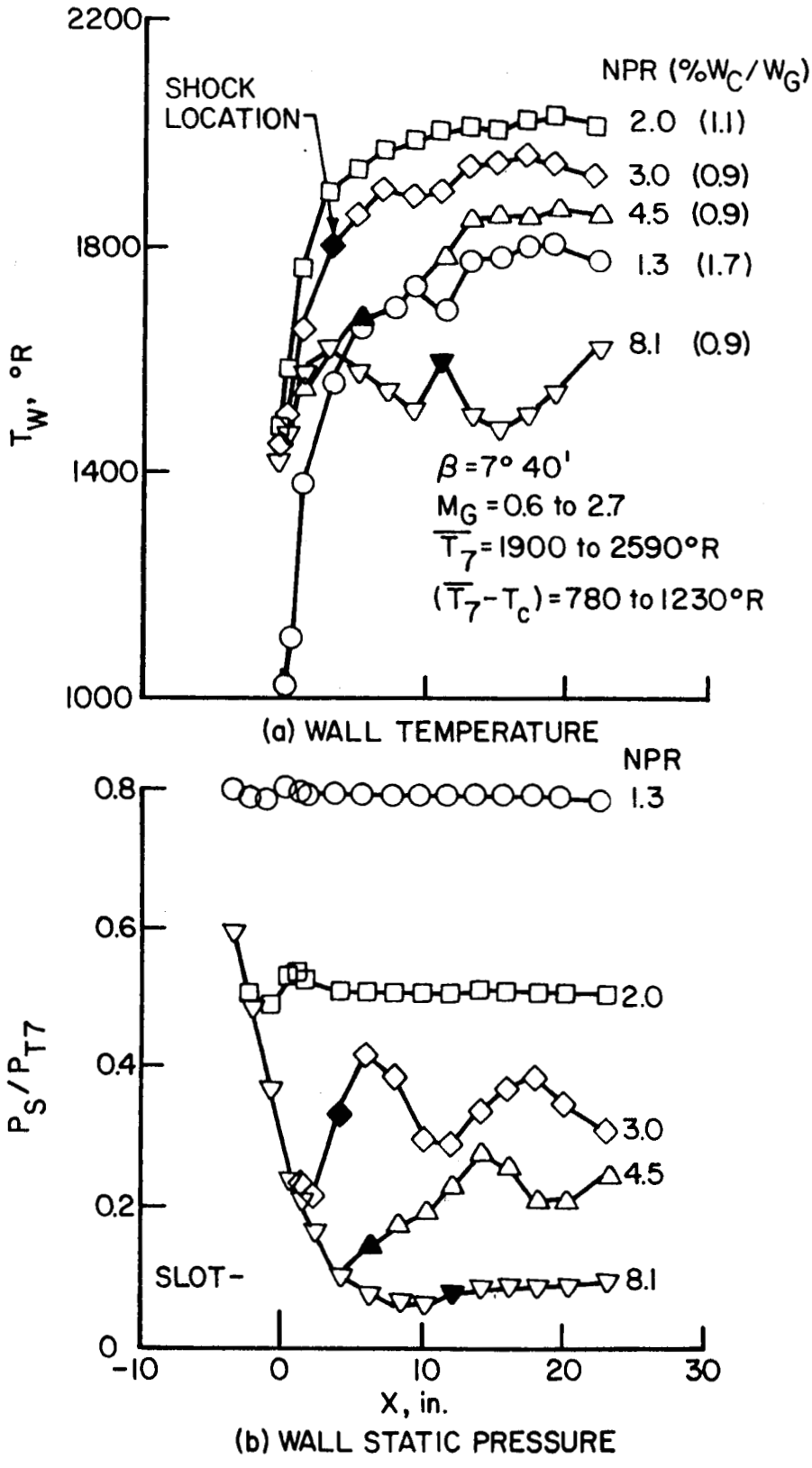

Figure IV.1. Effect of nozzle pressure ratio and coolant flow rate on film cooling effectiveness. NASA Test Data (Concluded)

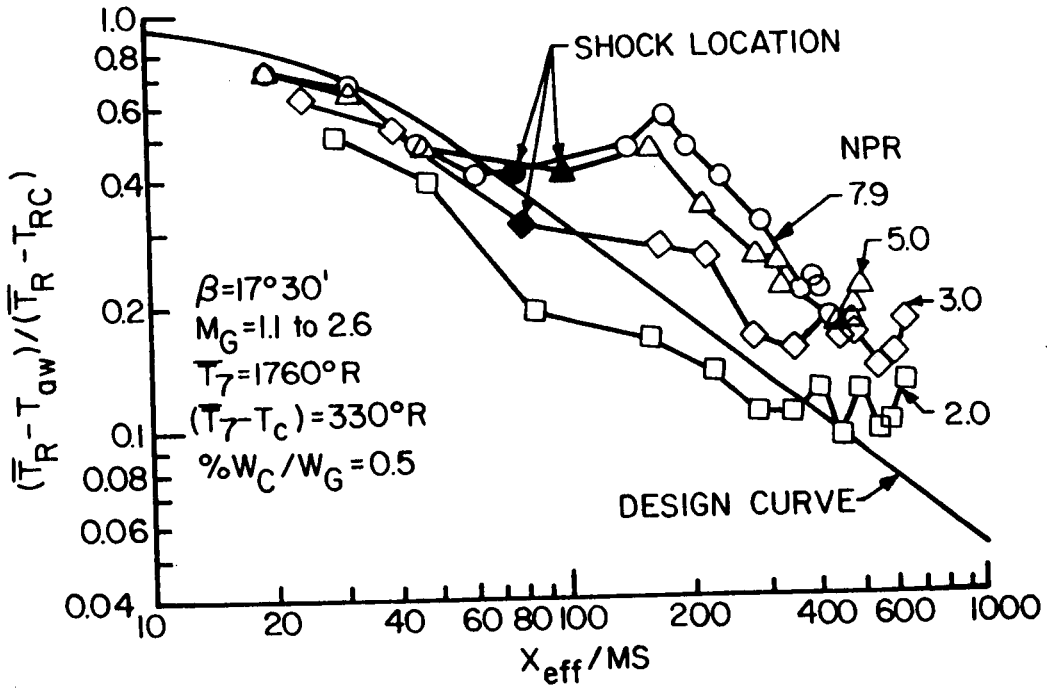

Figure IV.2. Effect of nozzle pressure ratio and coolant flow rate on film cooling effectiveness. NASA Test Data

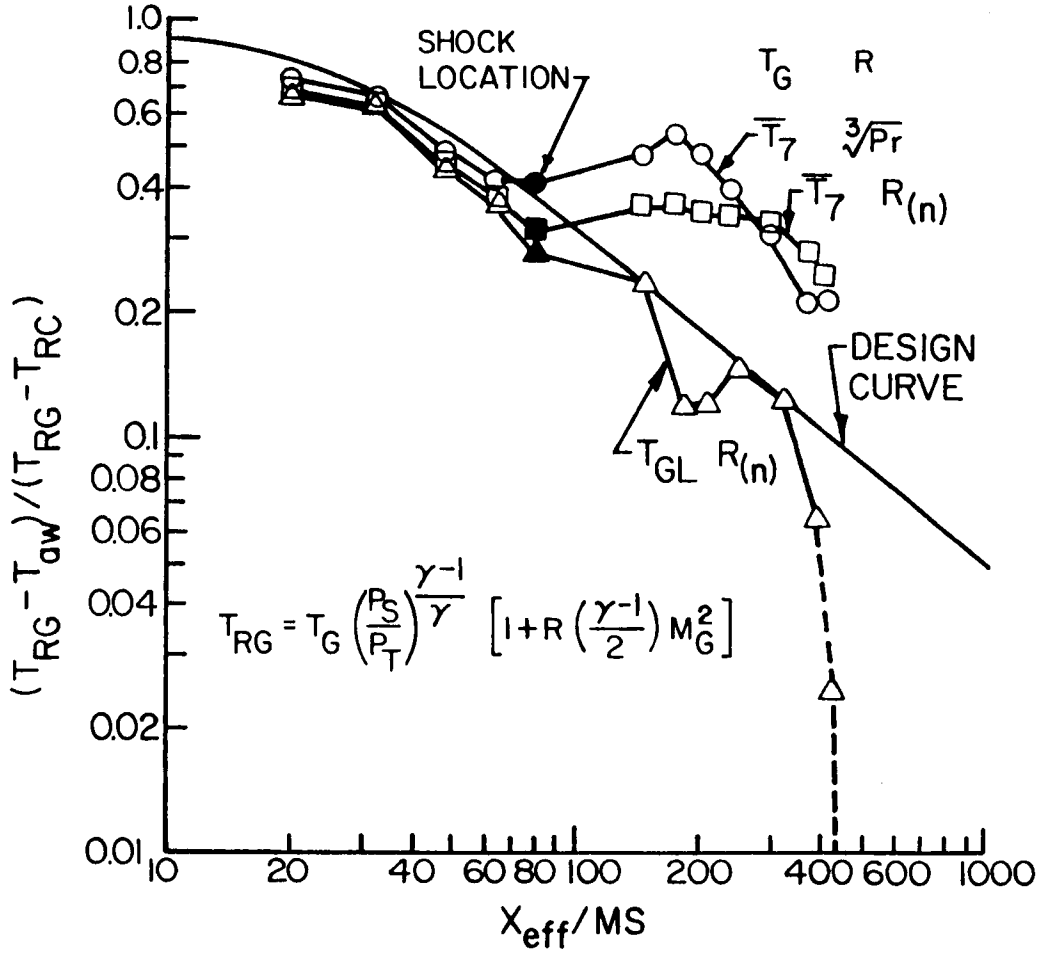

Figure IV.3. Development of local film cooling effectiveness. NASA Test Data

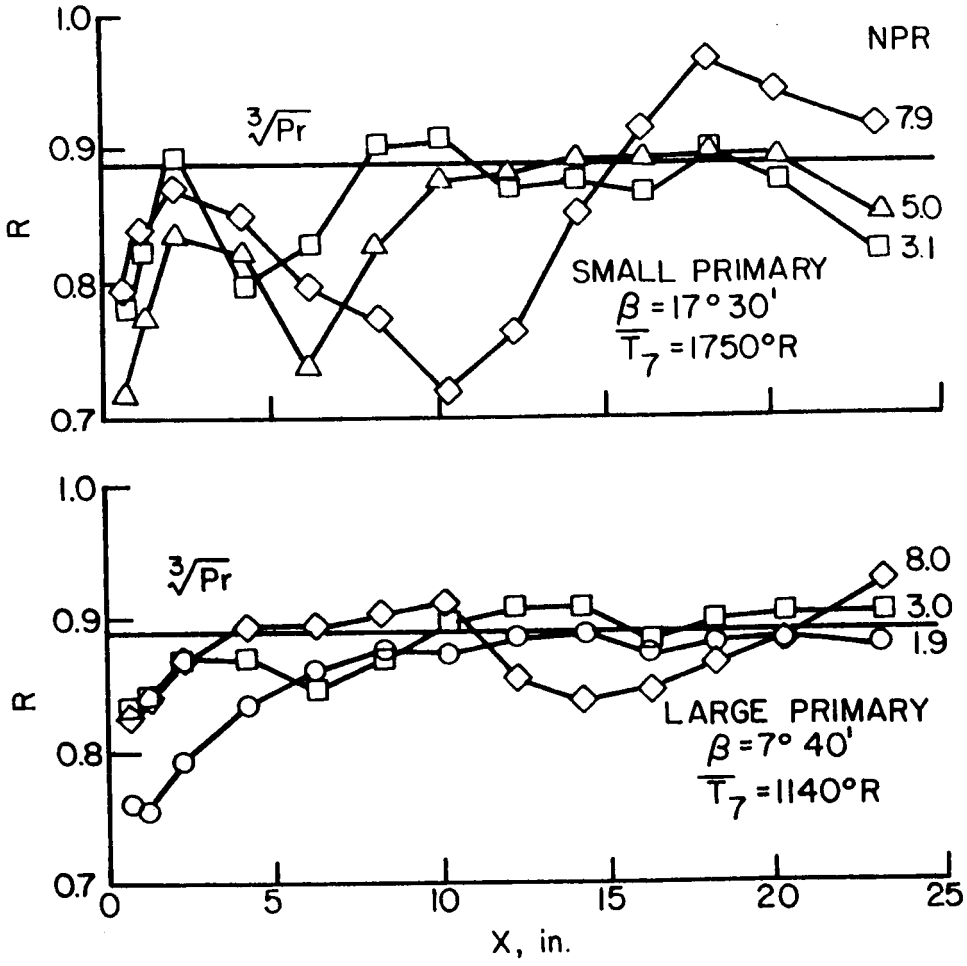

Figure IV.4. Effect of nozzle pressure and configuration on local recovery factor along plug wall with no coolant flow. NASA Test Data (Continued)

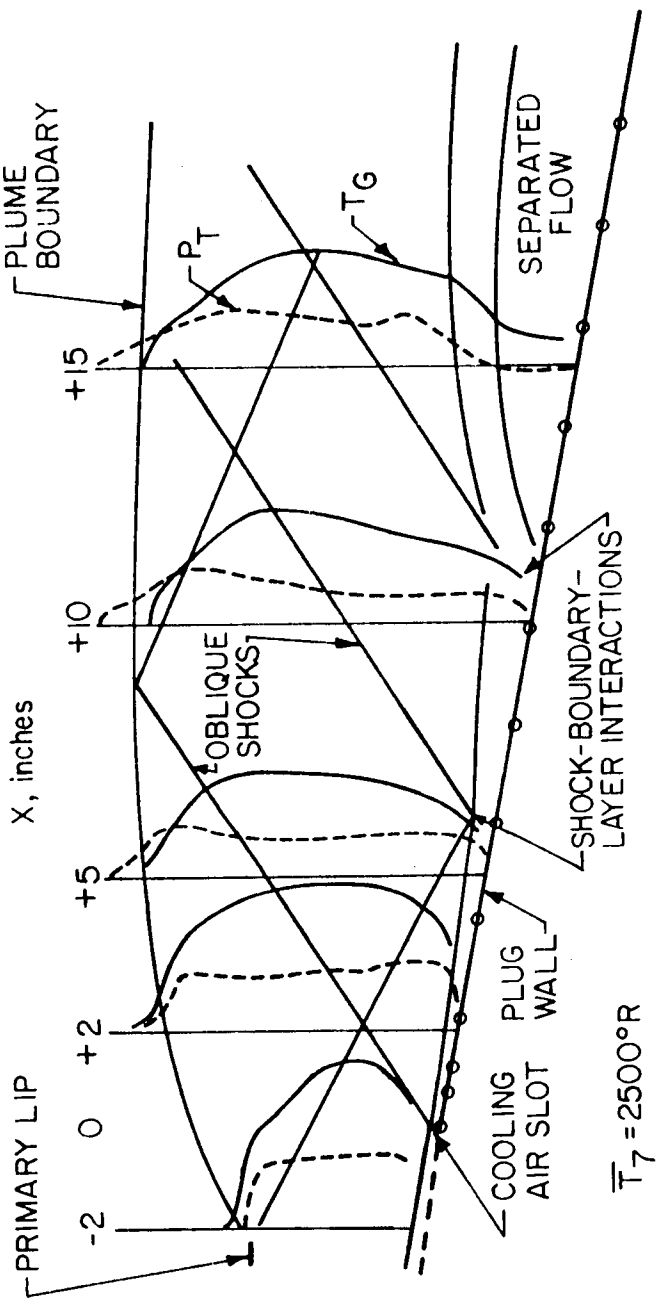

Figure IV.4. Effect of nozzle pressure ratio and configuration on local recovery factor along plug wall with no coolant flow. NASA Test Data (Concluded)

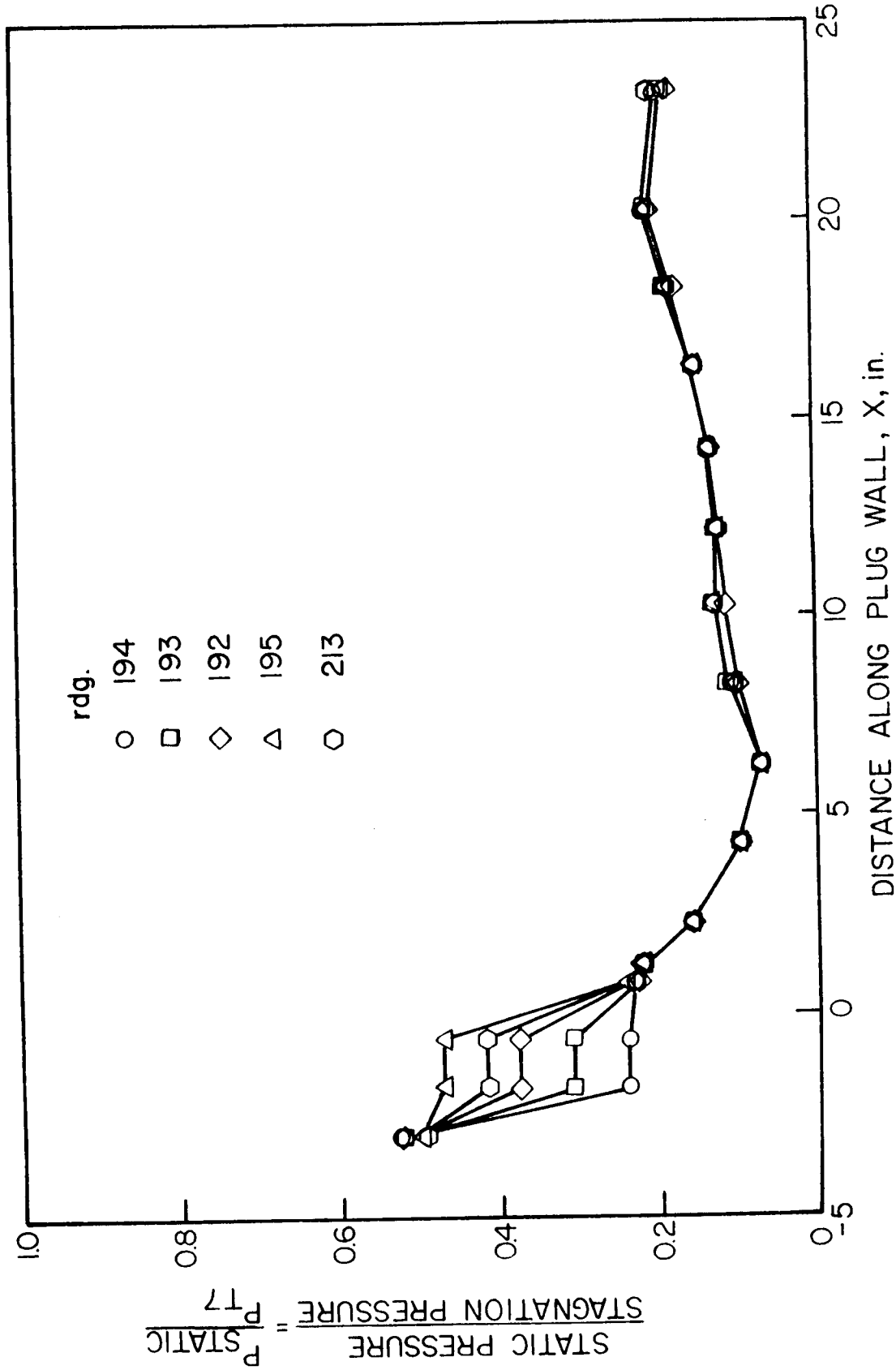

Figure IV.5. Distribution of static pressure along plug wall. NASA Test Data

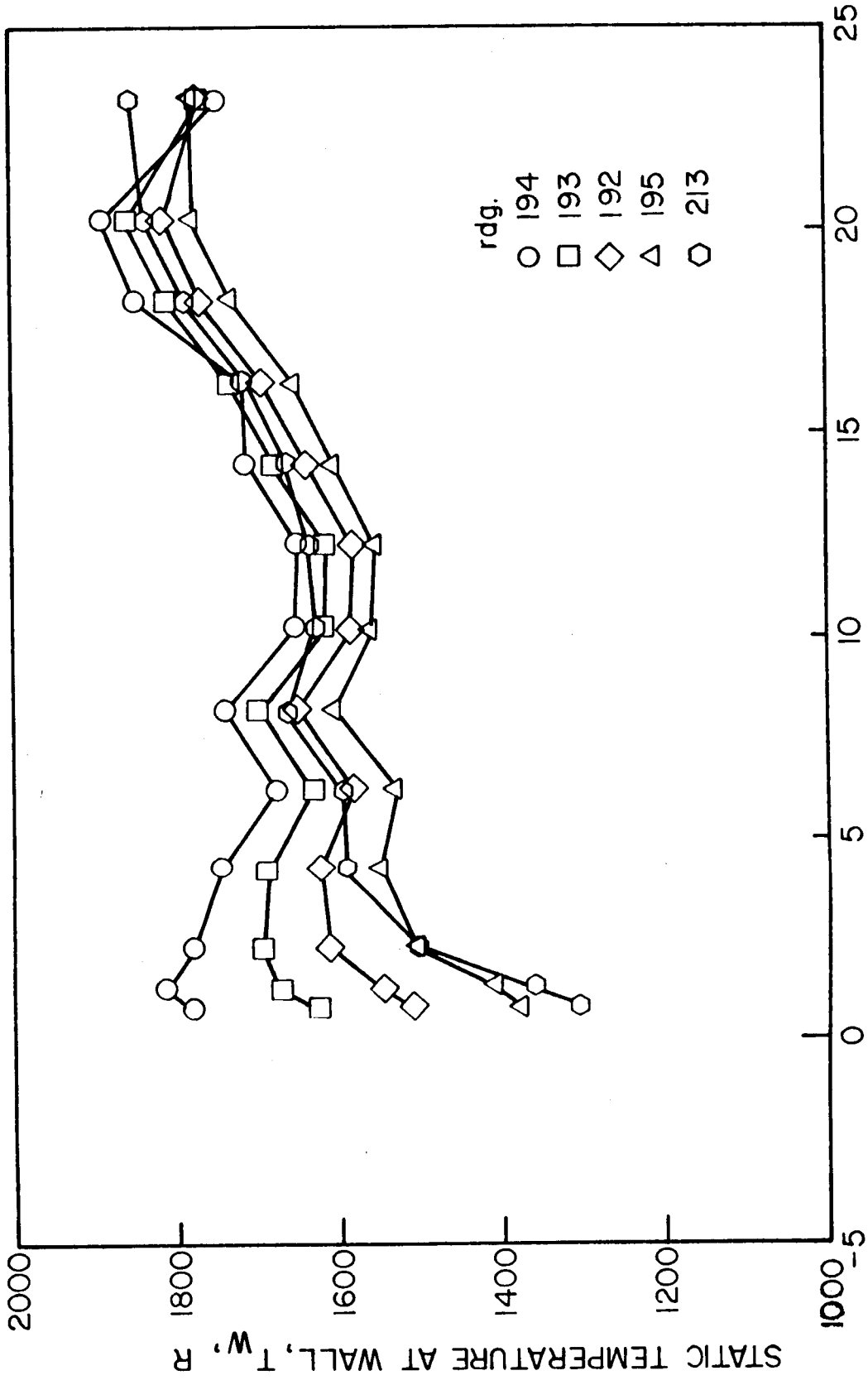

Figure IV.6. Distribution of static temperature along plug wall. NASA Test Data

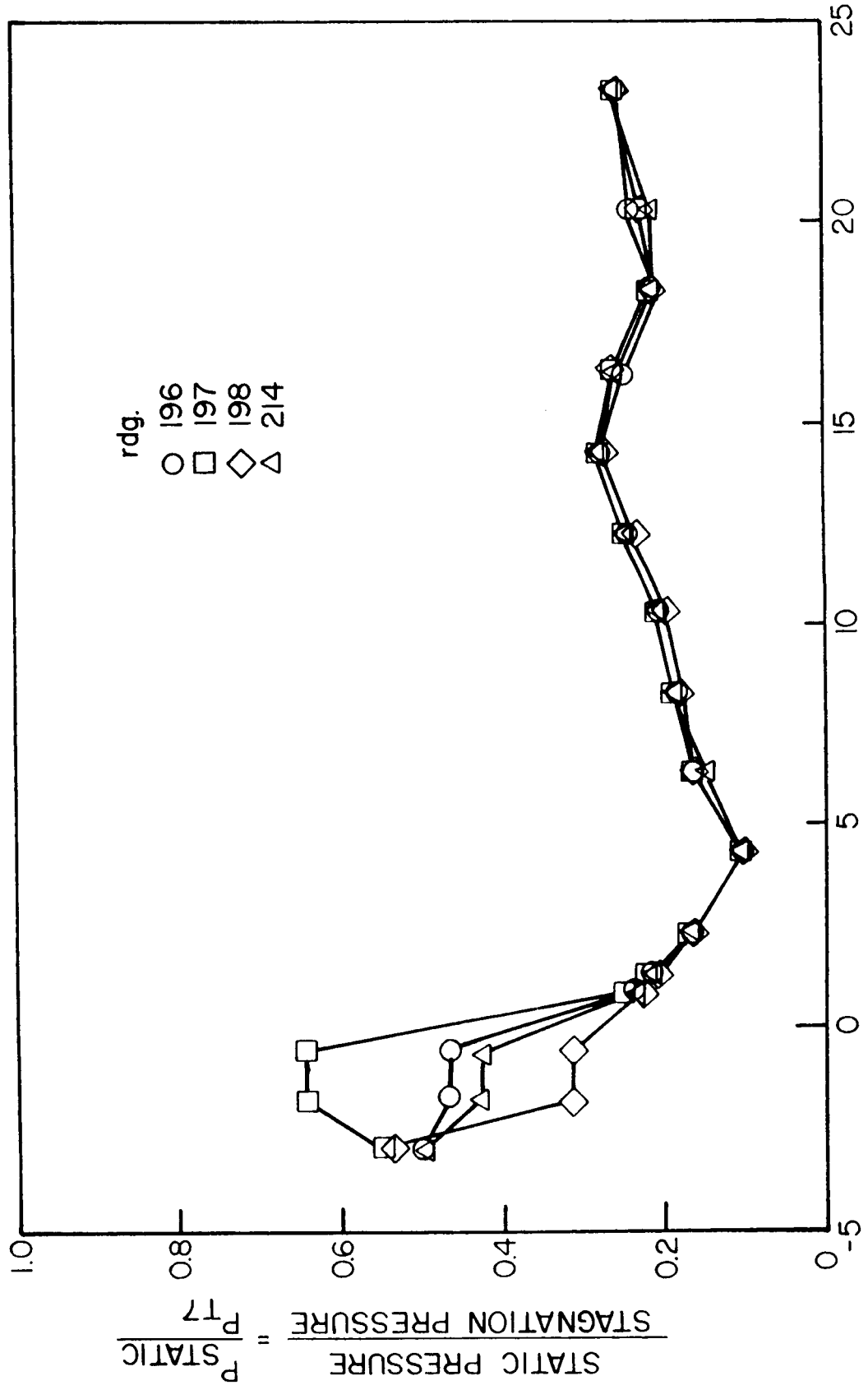

Figure IV.7. Distribution of static pressure along plug wall. NASA Test Data

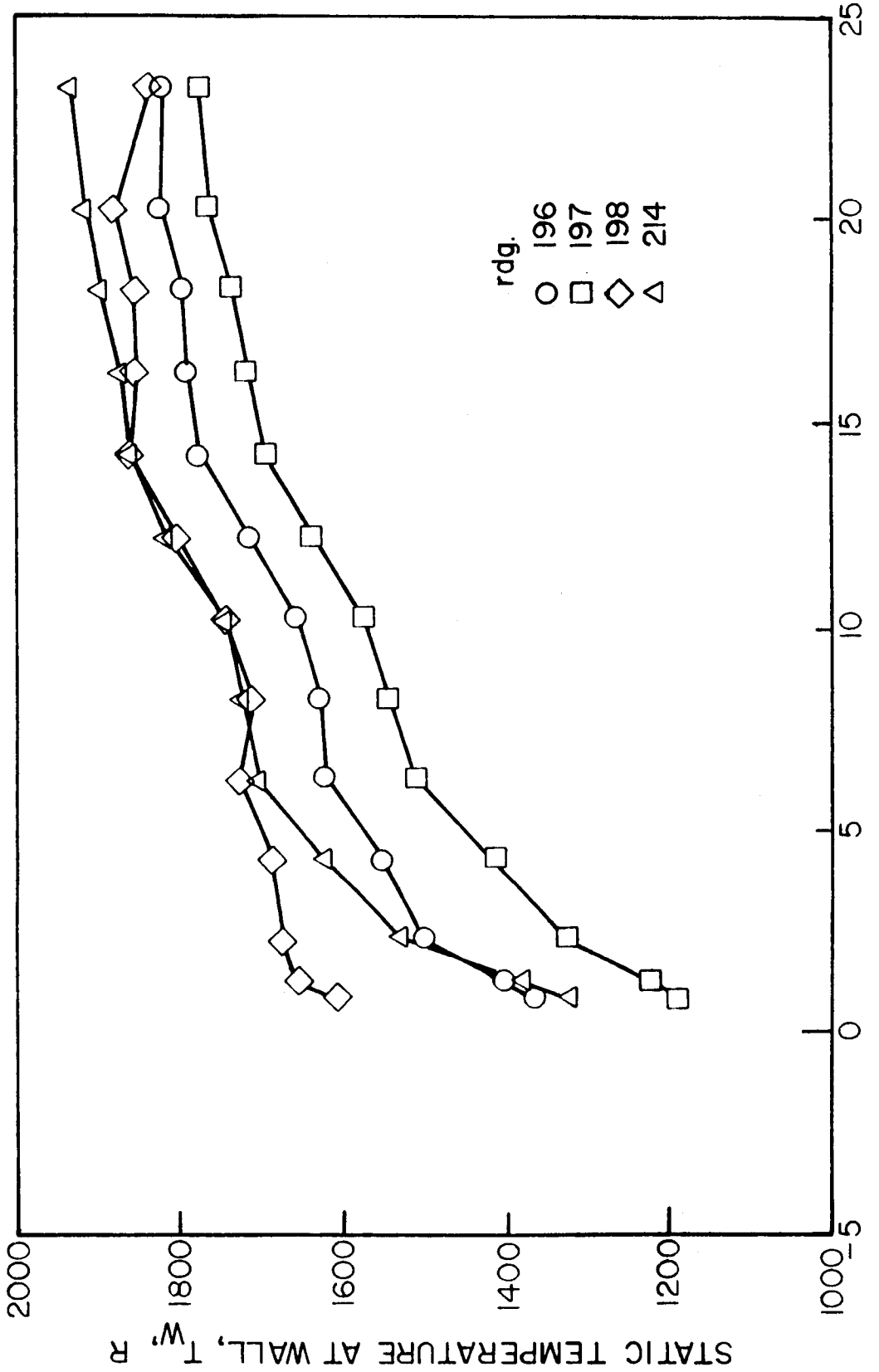

Figure IV.8. Distribution of static temperature along plug wall. NASA Test Data

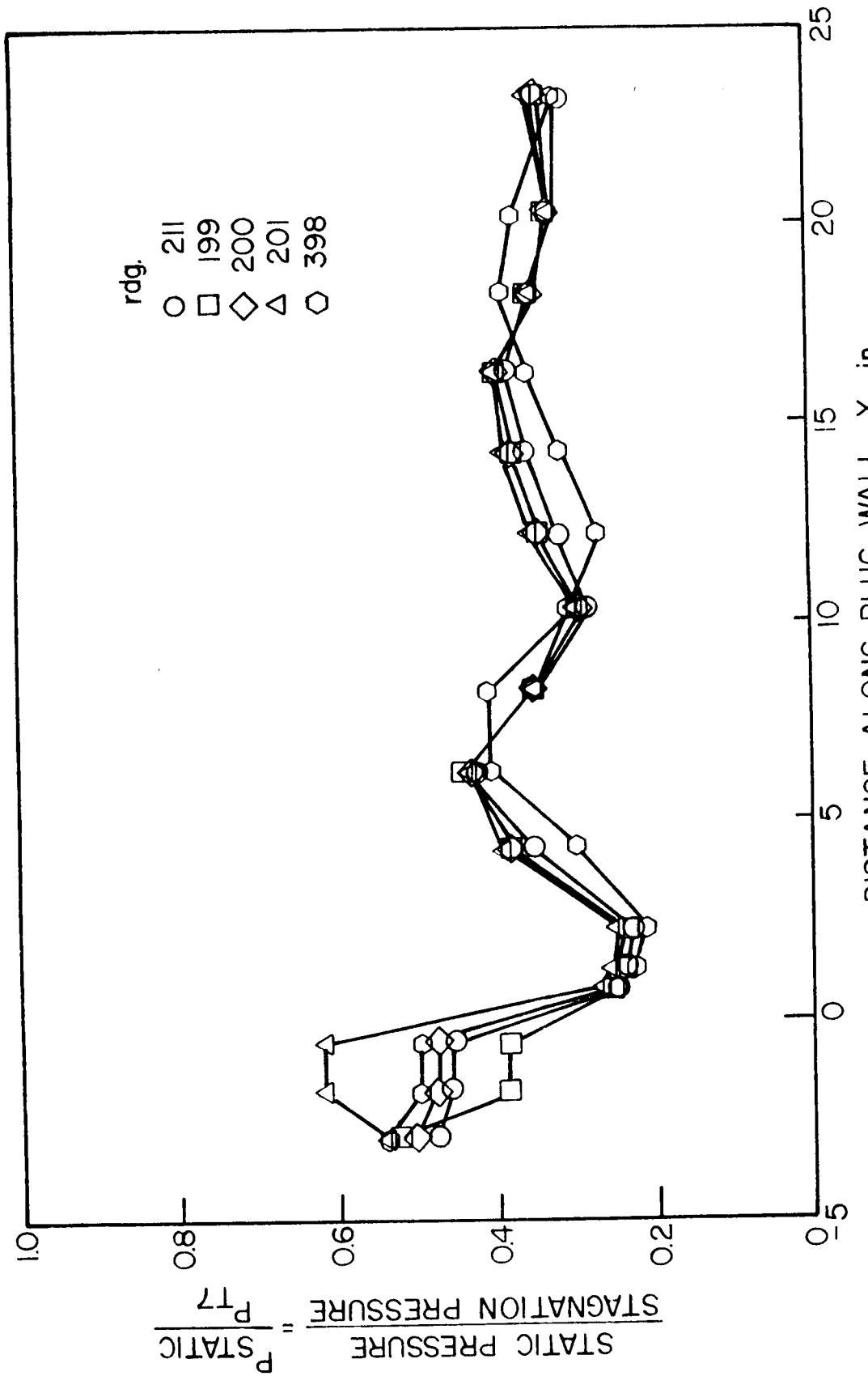

Figure IV.9. Distribution of static pressure along plug wall. NASA Test Data

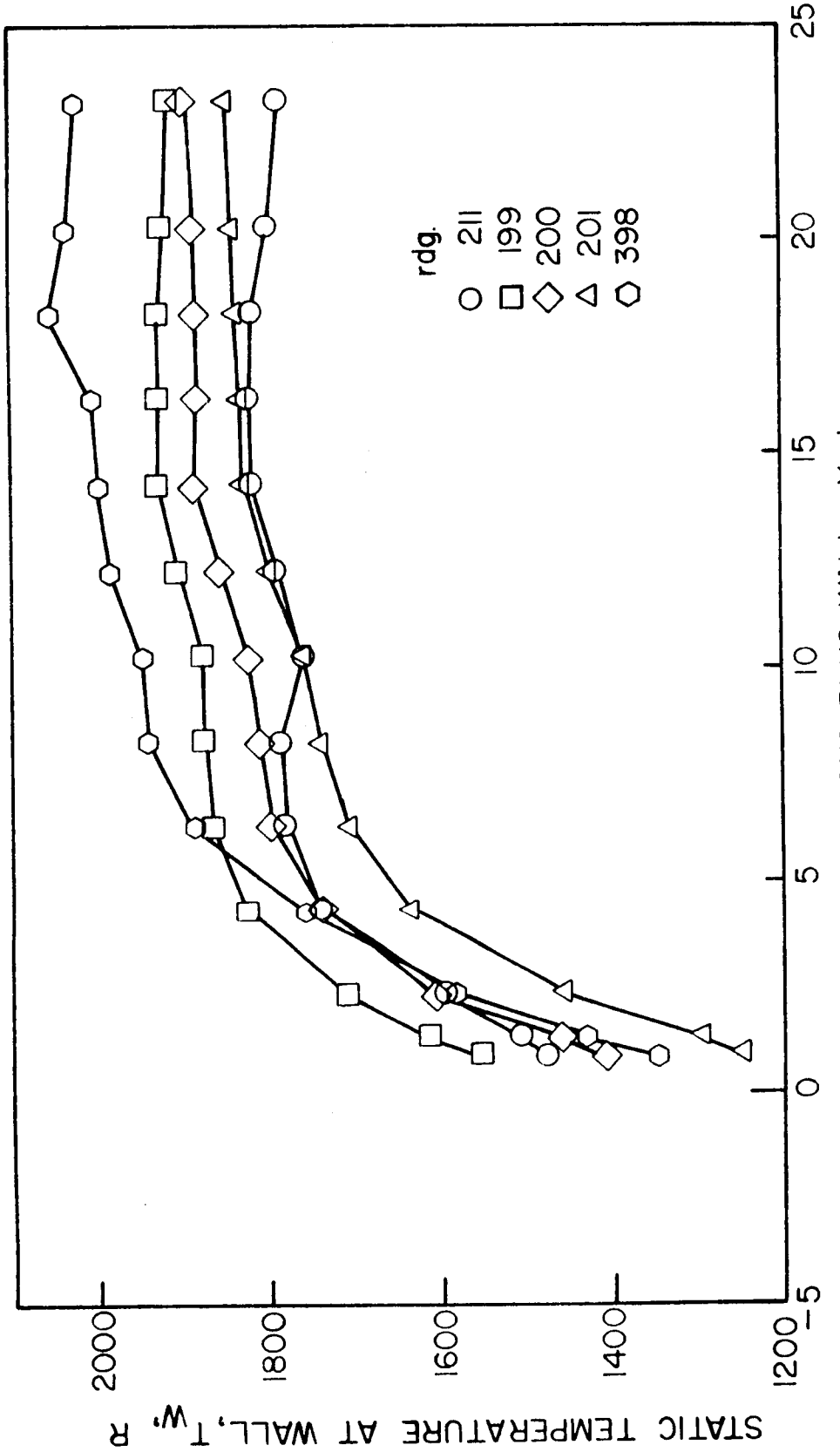

Figure IV.10. Distribution of static temperature along plug wall. NASA Test Data

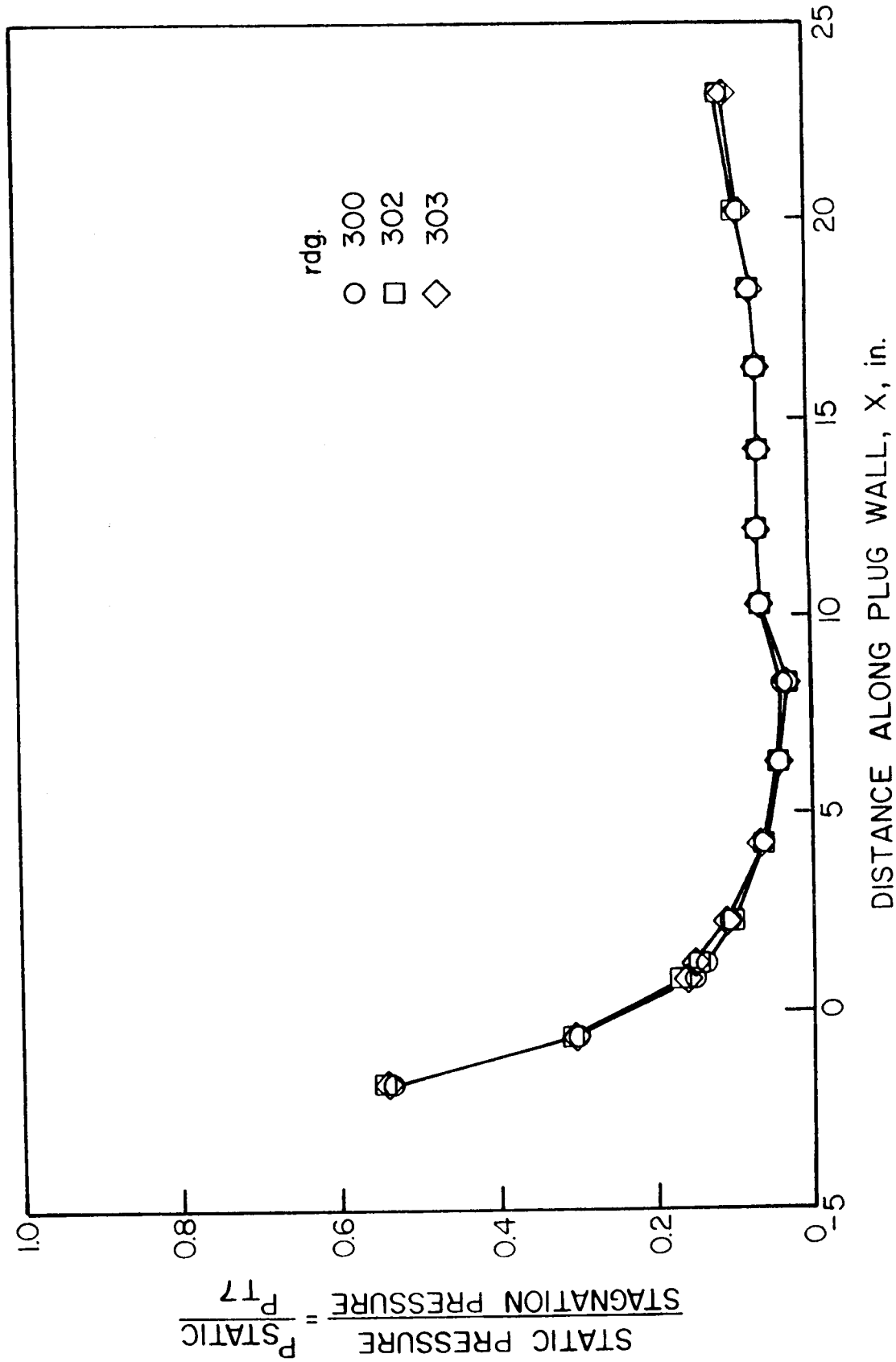

Figure IV.11. Distribtuion of static pressure along plug wall. NASA Test Data

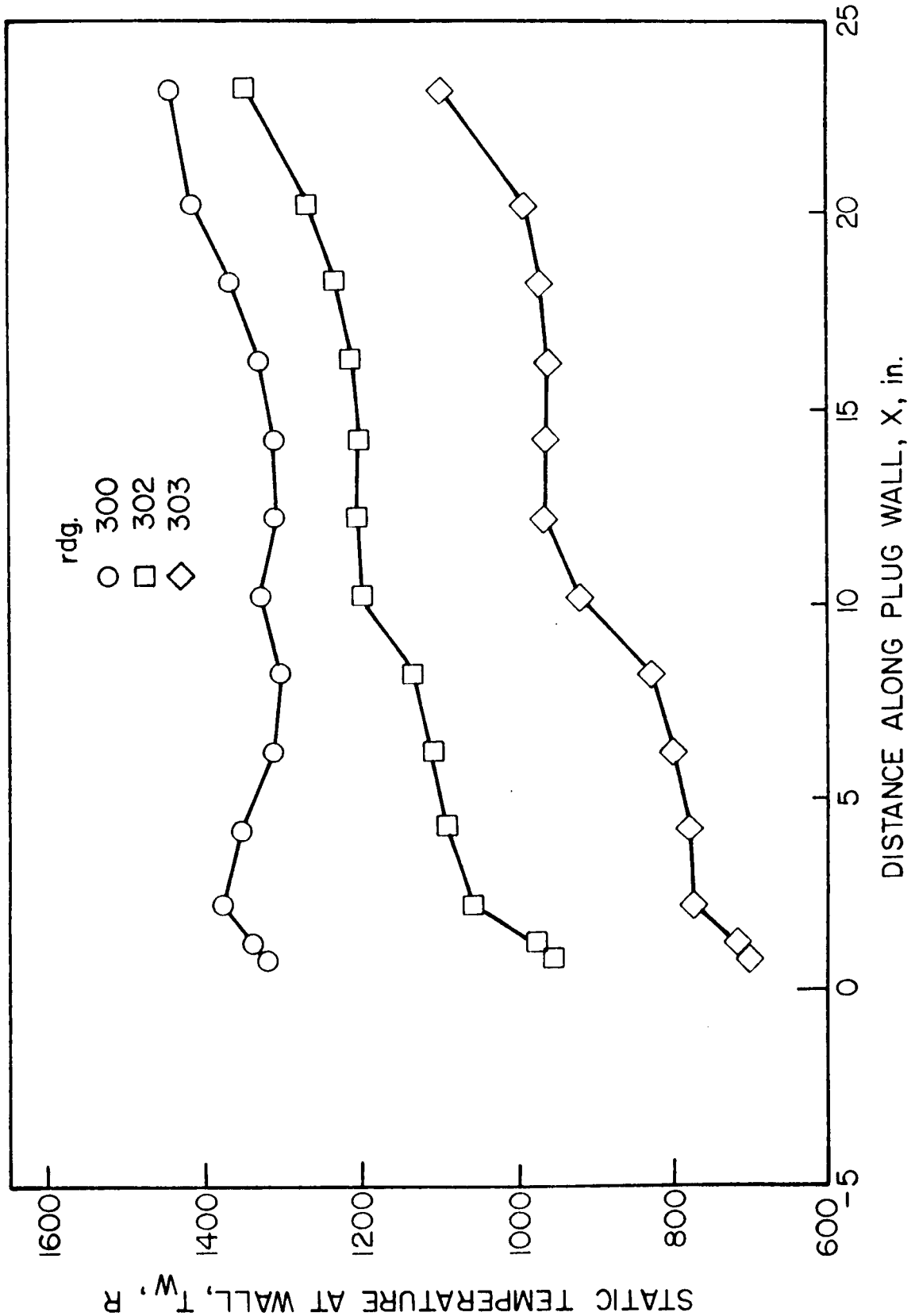

Figure IV.12. Distribution of static temperature along plug wall. NASA Test Data

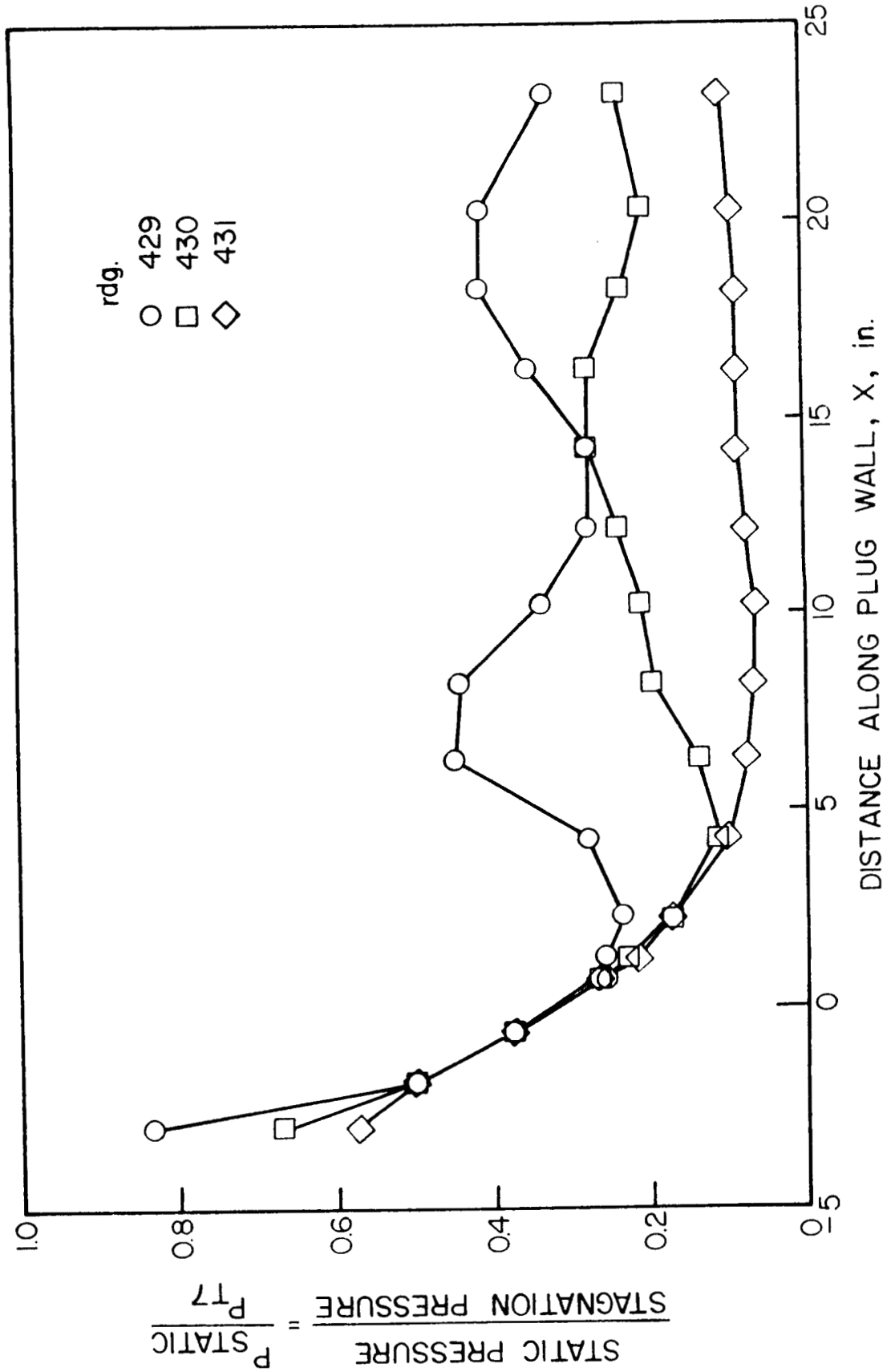

Figure IV.13. Distribution of static pressure along plug wall. NASA Test Data

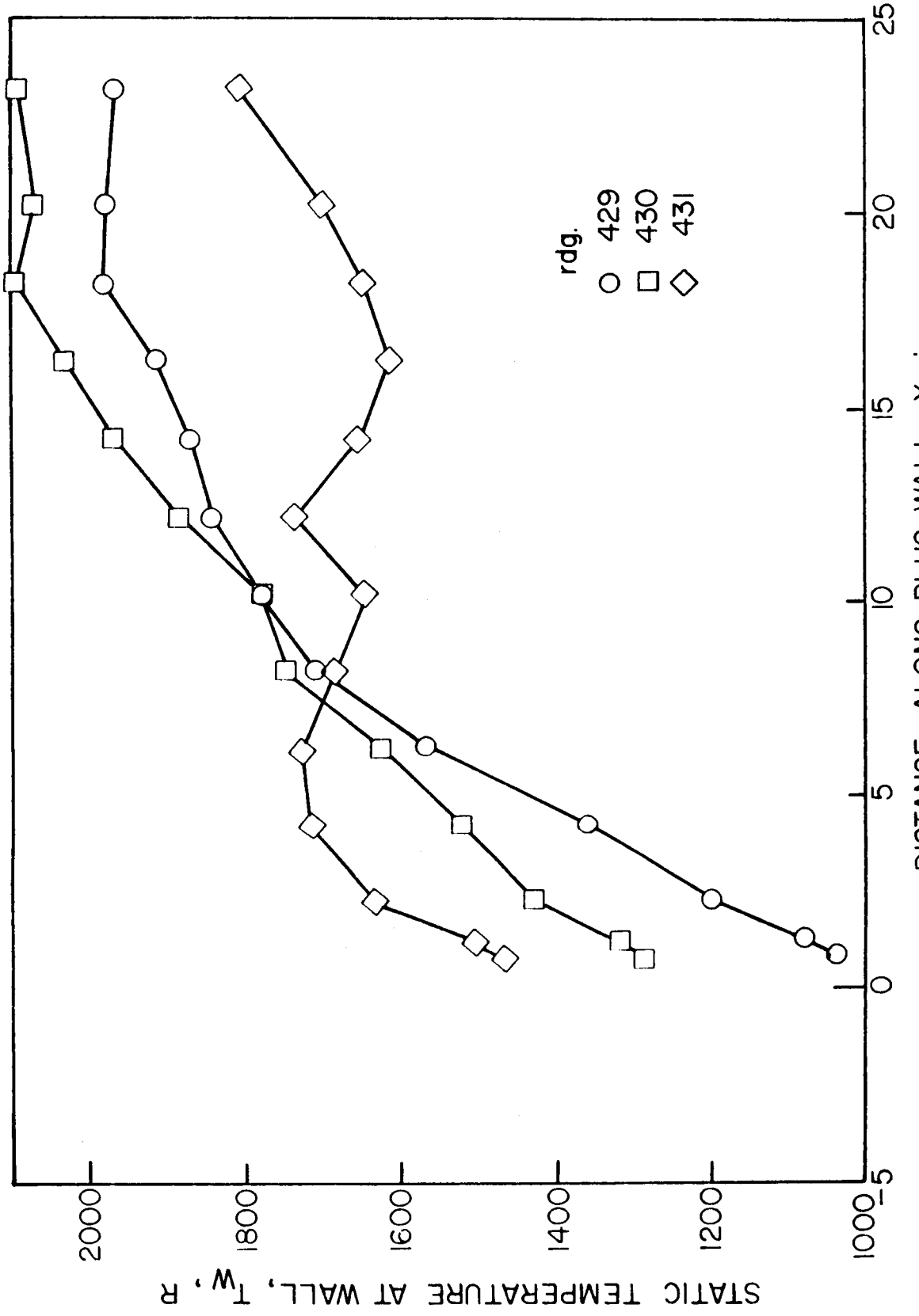

Figure IV.14. Distribution of static temperature along plug wall. NASA Test Data

APPENDIX V

TURBULENCE MODELING TO ESTIMATE HEAT TRANSFER IN SUPERSONIC FLOW IN A NOZZLE

The NASA Langley code (References V. 1-2) for the determination of heat transfer to the nozzle or plug wall utilizes a modified form for mixing length theory.

The turbulent shear stress and the rate of heat transfer are expressed in the forms, namely

$$\tau_T = \epsilon \frac{\partial \bar{u}}{\partial y} \quad \text{and} \quad \dot{q}_T = \frac{\epsilon}{Pr_T} \frac{\partial \bar{h}}{\partial y}$$

where the eddy viscosity is given by

$$\epsilon = \rho \ell_u^2 \left| \frac{\partial \bar{u}}{\partial y} \right|$$

and Pr_T is the turbulent Prandtl number. The mixing length for momentum transfer can be written as follows utilizing (Reference V.1) the Van Driest's damping function and modifying it for the effects of mass transfer on the viscous sublayer:

$$\frac{\ell_u}{\delta} = \left[1 - \exp\left(- \frac{y}{A} \right) \right] f\left(x, \frac{y}{\delta} \right)$$

The function f can be expressed in two parts:

near-wall region, $y/\delta \leq 0.1$: $f_n = K(y/\delta)$

far-wall region, $y/\delta \geq 0.3$: $f_f = f_f(H_{in}^*)$,

where, $f_f\left(H_{in}^*\right) = 0.265 - 0.196\, H_{in}^* + 0.0438\, H_{in}^{*2}$.

The latter is Prandtl's wall function and H_{in}^* is the incompressible form factor. The value of constant K utilized in the code is 0.4.

In order to utilize the mixing length concept when a finite coolant stream is present over the wall after being injected into the nozzle through a finite-thickness slot, it is necessary to obtain a mixing length distribution from the vicinity of the slot (in fact, from some upstream location on the wall forming the slot) to a location far downstream where the boundary layer may be approaching the classical structure. The entrance section of the slot presents various complications including the presence of a finite thickness "lip" in the dividing plate. A mixing layer is obviously formed between the coolant stream and the external fluid. The layer increases in thickness due to entrainment and diffusion. The wall layer at the "end of mixing" has to attain the standard wall boundary layer form. The NASA Langley code introduces an ad hoc distribution of mixing length in the coolant-affected region.

The initial conditions at the exit plane of the coolant jet are prescribed by means of distributions of temperature, concentration and velocity. The mixing length distribution at the slot exit is chosen in two parts: (i) in the near-wall region based on Prandtl's wall function, and (ii) in the center part of the coolant jet based on fully-developed channel flow (Reference V.2). At the same location in the boundary layer, a distribution of mixing length as in ordinary boundary layers (but up to a different value of y) is chosen. Thus four linear distributions of mixing length, two in the coolant flow and two in the main flow, are chosen for the slot exit plane.

The distribution of mixing length in the mixing layer between the coolant stream and the primary flow is chosen on the basis of experimental data available in the literature on jet mixing. The distribution of concentration mixing length is obtained simply by introducing a value of turbulent Schmidt number that varies linearly from a

high value (1.75) at the wall to a low value (0.5) at the boundary layer edge.

Finally, in the region, that may be called the relaxation region, between a location in the mixing layer to another where the effect of injection on the boundary layer has diminished sufficiently, the main consideration has been a smooth variation of mixing length such that the "transition" is smooth. It is postulated that the flowfield adjusts itself gradually form the outer edge to the wall and that both momentum and concentration diffusion can be modelled on that basis.

REFERENCES

V.1. Beckwith, I.E. and Bushnell, D.M., "Calculation by a finite-difference method of supersonic turbulent boundary layers with tangential slot injection", NASA Langley Research Center Report, March 1971.

V.2. Hixon, B.A., Beckwith, I.E., and Bushnell, D.M., " Computer Program for Compressible Laminar or Turbulent Nonsimilar Boundary Layers", NASA Technical Memorandum No. NASA TMX-2140, April 1971.

NASA
National Aeronautics and Space Administration

Report Documentation Page

1. Report No.	2. Government Accession No.	3. Recipient's Catalog No.
NASA CR-179554		

4. Title and Subtitle	5. Report Date
Analysis of Supersonic Plug Nozzle Flowfield and Heat Transfer	September 1988
	6. Performing Organization Code

7. Author(s)	8. Performing Organization Report No.
S.N.B. Murthy and W.H. Sheu	None
	10. Work Unit No. 505-62-91

9. Performing Organization Name and Address	11. Contract or Grant No.
Purdue University School of Mechanical Engineering West Lafayette, Indiana 47907	NAG3-281
	13. Type of Report and Period Covered Contractor Report Final

12. Sponsoring Agency Name and Address	14. Sponsoring Agency Code
National Aeronautics and Space Administration Lewis Research Center Cleveland, Ohio 44135-3191	

15. Supplementary Notes

Project Manager, Charles M. Spuckler, Propulsion Systems Division, NASA Lewis Research Center.

16. Abstract

A number of problems pertaining to the flowfield in a plug nozzle, designed as a supersonic thruster nozzle, with provision for cooling the plug with a coolant stream admitted parallel to the plug wall surface, have been studied, based on experimental data generated at the NASA Lewis Research Center. First, an analysis has been performed of the inviscid, non-turbulent, gas dynamic interaction between the primary hot stream and the secondary coolant stream. A numerical prediction code for establishing the resulting flowfield with a dividing surface between the two streams, for various combinations of stagnation and static properties of the two streams, has been utilized for illustrating the nature of interactions. A number of illustrative cases have been worked out, for which test results have been available from the NASA Lewis Research Center data sets. The code, while not described here in detail, has been made available to the NASA Lewis Research Center for verification of its operability. Secondly, skin friction coefficient, heat transfer coefficient and heat flux to the plug wall have been analyzed under smooth-flow conditions (without shocks or separation) for various coolant flow conditions. A numerical code, obtained from NASA Langley Research Center, has been suitably modified and utilized for the determination of heat transfer parameters in a number of cases for which experimental data have been available in the NASA Lewis Research Center test results. Thirdly and finally, an analysis has been initiated for modelling turbulence processes in transonic shock-boundary layer interaction without the appearance of flow separation. The model is based on a combination of the Reynolds stress balance equation coupled with dynamical equation for large eddy, and includes rapid distortion approximations. The model is suitable for use both under conditions of an adiabatic interaction as well as of heat transfer to the boundary wall, but in the presence of a single stream. A discussion is presented on future possibilities of each of the building block solutions, which in combination would be useful for the analysis of the flowfield in a plug nozzle and which can also serve individually to establish various types of interactions in wall-bounded multiple flows.

17. Key Words (Suggested by Author(s))	18. Distribution Statement
Plug nozzles Surface cooling Shock boundary layer interactions Nozzle flow fields	Unclassified – Unlimited Subject Category 02

19. Security Classif. (of this report)	20. Security Classif. (of this page)	21. No of pages	22. Price*
Unclassified	Unclassified	179	A09

NASA FORM 1626 OCT 86

*For sale by the National Technical Information Service, Springfield, Virginia 22161